NUCLEAR STRUCTURE OF TWO TRANSITION NUCLEI: $^{154}_{64}Gd_{90}$ AND $^{152}_{63}Eu_{89}$

NUCLEAR STRUCTURE OF TWO TRANSITION NUCLEI: $^{154}_{64}Gd_{90}$ AND $^{152}_{63}Eu_{89}$

By

OM PRAKASH JOLLY

A Thesis

Submitted to the School of Graduate Studies

in Partial Fulfilment of the Requirements

for the Degree

Dcotor of Philosophy

McMaster University

July 1976

DOCTOR OF PHILOSOPHY (1976) McMASTER UNIVERSITY
(Physics) Hamilton, Ontario

TITLE: Nuclear Structure of Two Transitional Nuclei: $^{154}_{64}Gd_{90}$ and $^{152}_{63}Eu_{89}$

AUTHOR: Om Prakash Jolly

SUPERVISOR: Dr. J. C. Waddington

NUMBER OF PAGES: xviii, 191

ABSTRACT

The nuclear structure of two transitional nuclei, $^{154}_{64}Gd_{90}$ (doubly-even) and $^{152}_{63}Eu_{89}$ (doubly-odd) has been investigated by single neutron and proton transfer reactions. In general, it was found that the unified nuclear model with the inclusion of pairing, Coriolis and $\Delta N=2$ interactions gives a good description of these nuclei. The reaction strengths to the many two-quasiparticle states have been predicted by the distorted wave Born approximation.

Experimentally deduced values of the splitting energies for the various two-quasiparticle configurations in ^{154}Gd and ^{152}Eu have been found to be in reasonable agreement with a calculation based upon a zero range interaction between the two unpaired particles.

ACKNOWLEDGEMENTS

It has been a great pleasure working with Dr. J. C. Waddington. I would like to express my sincere gratitude to him. He has provided me an informal and friendly atmosphere to complete this task. Due to his cheerful personality and humane approach, even the difficult physics and personal problems looked simple. I always enjoyed discussions with him and found him extremely relaxing. I am greatly in debt and amazed at his understanding and tolerance to a graduate student.

My special thanks are also due to all the other members of an unusually large supervisory committee, consisting of Drs. R. K. Bhaduri, C. E. Billigheimer, D. G. Burke, J. A. Cameron and M. W. Johns. All these members have spent a great deal of time in listening to my day-to-day progress and giving their remarks and suggestions. I acknowledge the help of Dr. D. G. Burke for suggesting this project and aiding in the initial stages of this work. My thanks are due to Dr. R. A. O'Neil for showing me the way to the 'quasi-world'. I appreciate the help of various colleagues, namely L. Buja-Bijunas, R. D. Gadsby, C. R. Hirning, K. Jan, J. P. Panar and W. Stott. Discussions with Drs. H. C. Cheung and O. Straumme have been quite stimulating. I am grateful for the assistance given by various accelerator staff members, including Messrs. P. G.Ashbaugh, H. Blanchard, W. Dunsmore, W. Froude (late), H. Harms, J. W. McKay, R. McNaught, J. Parkinson, J. Rosenthal

J. Stark, M. P. Vince and many student operators. I would like to thank the secretary of the accelerator laboratory, Mrs. E. Williams. Messrs. T. Noakes, J. O'Donnell and Dr. Y. Peng have contributed their efforts in constructing targets. I cannot escape without thanking the counting girls, namely Miss W. Cullis , Mrs. M. Dempsey, Mrs. J. Prestwich and Mrs. D. Vince for their contribution in scanning at least seven meters of the nuclear emulsion plates.

I would like to thank Drs. R. F. Casten and T. von Egidy for their unpublished ^{152}Eu results, Dr. T. L. Khoo for the discussions about splitting energies and Drs. J. W. Mihelich and R. L. West for the discussion of the ^{154}Gd structure.

During my stay at McMaster University, I have shared the company of Mr. N. Ramanathan and have spent several hours in discussing all the problems of physics and the world, and possibly have found the solutions.

A large number of friends and family members have given me constant encouragement, especially Savita who has shown her understanding and gone through all the pains and strains of being the wife of a poor graduate student.

I would like to thank Miss J. Balogh and Mrs. P. Petty for making a large number of diagrams. My special thanks are to Mrs. H. Kennelly for bringing to the present form the hand written manuscript. She not only showed her patience in typing but also has cheerfully corrected the mistakes. Mr. A. Khan has proof read a part of this thesis.

Finally, I wish to thank McMaster University for financial assistance in the form of a graduate scholarship and the work was supported by the National Research Council of Canada.

TABLE OF CONTENTS

			Page
CHAPTER 1		INTRODUCTION	1
CHAPTER 2		THEORETICAL ASPECTS AND CALCULATIONS	8
	2.1	The Nuclear Shell and Liquid Drop Models	8
	2.2	The Unified Model of the Nucleus	9
	2.3	Nuclear Deformation	10
	2.4	Quantum numbers and Coupling of Angular Momenta in Axially Symmetric Deformed Nuclei	13
	2.5	Separability of Nuclear Wave Functions	15
	2.6	Single Particle States in a Deformed Potential Well (Nilsson Model)	17
	2.7	Pairing Interaction	24
	2.8	Rotational Hamiltonian for Even Mass Nuclei	27
	2.9	Rotation-Particle Coupling (Coriolis Mixing)	32
	2.10	The $\Delta N=2$ Interaction	35
	2.11	Splitting Energy in Deformed Even Mass Nuclei	37
	2.12	Cross Section Calculations	39
	2.13	Identification and Assignment of Levels	45

			Page
CHAPTER 3		EXPERIMENTAL DETAILS	48
	3.1	FN Tandem Van de Graaff Accelerator	48
	3.2	The Enge Magnetic Spectrograph	49
	3.3	Target Preparation	53
	3.4	Monitoring and Detection of the Reaction Products	56
	3.5	Considerations for Obtaining Good Energy Resolution	57
		i) The Target Thickness Effects	58
		ii) Effect of the Beam Spot Size	59
		iii) Other Effects	62
	3.6	Calculation of Excitation Energies	63
CHAPTER 4		EXPERIMENTAL RESULTS	72
	4.1	Levels in ^{154}Gd	72
	4.2	Results for ^{152}Eu	87
		i) Q-values Measured in the $^{151}Sm(^{3}He,d)^{152}Eu$ and $^{151}Sm(\alpha,t)^{152}Eu$ reactions	87
		ii) Levels in ^{152}Eu	88
CHAPTER 5		NUCLEAR STRUCTURE OF ^{154}Gd	92
	5.1	The Ground State Band	92
		i) Population of the Ground State Band in the Neutron Transfer Reactions	92
		ii) Population of the Ground State Band in the Proton Transfer Reactions	96

		Page
5.2	Excited $K^{\pi} = 0$ Bands	98
	i) The Beta Band	98
	ii) The $K^{\pi} = 0^{+}$ Band at 1296 keV	100
5.3	The $K^{\pi} = 2^{+}$ Bands	101
	i) The Gamma Vibrational Band	101
	ii) Population of the Gamma Band in the Neutron Transfer Reactions	101
	iii) Population of the Gamma Band in the Proton Transfer Reactions	103
	iv) The Second $K^{\pi} = 2^{+}$ Band	104
5.4	Octupole Vibrational States	106
5.5	Levels at 1182 and 1576 keV Populated Weakly in the Neutron Transfer Reactions	110
5.6	$K^{\pi} = 1^{-}$ and 2^{-} Bands of the $\{3/2^{-}[521] \mp 1/2^{+}[400]\}_{\nu}$ and $\{3/2^{-}[521] \mp [1/2^{-}[600]\}_{\nu}$ Configurations	112
5.7	$K^{\pi} = 3^{-}$ and 0^{-} Bands of the $\{3/2^{-}[521] \pm 3/2^{+}[402]\}_{\nu}$ and $\{3/2^{-}[521] \pm 3/2^{-}[651]\}_{\nu}$ Configurations	118
5.8	$\Delta N=2$ and Coriolis Interactions	124

		Page
5.9	States Populated by High ℓ in the Neutron Transfer Reactions	127
	i) $K^{\pi} = 4^{+}$ and 7^{+} Bands of the $\{3/2^{-}[521] \mp 11/2^{-}[505]\}_{\nu}$ Configurations	128
	ii) Coriolis Coupled $i_{13/2}$ Nilsson States (Calculations)	131
5.10	The Transfer of the $1/2^{-}[530]$ Neutron	134
5.11	The Transfer of the $3/2^{+}[411]$ Proton	134
	i) The $K^{\pi} = 4^{+}$ Band	134
	ii) The $K^{\pi} = 1^{+}$ Band	137
5.12	The Transfer of the $1/2^{+}[411]$ Proton	140
	i) The $K^{\pi} = 2^{+}$ Band	140
	ii) The $K^{\pi} = 3^{+}$ Band	143
5.13	The Coriolis Mixed Negative Parity Band	144
5.14	Levels Above the Energy Gap Ppoulated in Reactions and the Decay of ^{154}Tb	147
5.15	The $K^{\pi} = 1^{+}$ Band at 2187.2 keV	147

			Page
CHAPTER 6		NUCLEAR STRUCTURE OF ^{152}Eu	152
	6.1	The Transfer of the $11/2^-[505]$ Neutron and the ground state band	152
	6.2	The Transfer of the $3/2^+[411]$ Proton	153
		i) The $K^\pi = 4^-$ Band	153
		ii) The $K^\pi = 1^-$ Band	154
	6.3	Levels at 65, 111 and 175 keV	156
	6.4	Isomeric State at 46 keV	157
	6.5	Other Levels	157
	6.6	Total Reaction Strength	158
CHAPTER 7		SUMMARY	161
	7.1	^{154}Gd	161
	7.2	^{152}Eu	175
	7.3	Splitting Energies	178
	7.4	Concluding Remarks	183
REFERENCES			185

LIST OF FIGURES

		Page
1.1	A part of the nuclear table near A~150	2
2.1	Coupling of angular momenta in axially symmetric nuclei	14
2.2	Nilsson diagram for proton orbitals	21
2.3	Nilsson diagram for neutron orbitals	22
2.4	Nilsson diagram for the $1/2^+[400]$, $1/2^+[660]$, $3/2^+[402]$ and $3/2^+[651]$ neutron orbitals	23
3.1	Outline of the Enge split-pole spectrograph	51
3.2	The effects of the target thickness and beam spot size on the resolution in the $^{153}Eu(\alpha,t)^{154}Gd$ reaction	60
3.3	The $^{155}Gd(d,t)^{154}Gd$ spectrum at $\theta=30°$ and the $^{155}Gd(^3He,\alpha)^{154}Gd$ spectrum at $\theta=45°$	67
3.4	The $^{155}Gd(d,t)^{154}Gd$ spectra at $\theta=7.5°$ and $\theta = 45°$	68
3.5	The $^{153}Eu(\alpha,t)^{154}Gd$ spectrum at $\theta=45°$ and the $^{153}Eu(^3He,d)^{154}Gd$ spectrum at $\theta = 30°$	69
3.6	The $^{151}Sm(^3He,d)^{152}Eu$ spectrum at $\theta=30°$ and the $^{151}Sm(\alpha,t)^{152}Eu$ spectrum at $\theta = 60°$	70
3.7	The $^{153}Eu(^3He,\alpha)^{152}Eu$ spectrum at $\theta=30°$	71
4.1	Cross section ratios for the $^{155}Gd(^3He,\alpha)^{154}Gd$ and $^{155}Gd(d,t)^{154}Gd$ reactions	85

		Page
4.2	Cross section ratios for the $^{153}Eu(^{3}He,d)^{154}Gd$ and $^{153}Eu(\alpha,t)^{154}Gd$ reactions	86
4.3	Cross section ratios for the $^{151}Sm(^{3}He,d)^{152}Eu$ and $^{151}Sm(\alpha,t)^{152}Eu$ reactions	90
5.1	The (d,t) angular distributions for the ground state members in ^{154}Gd	95
5.2	Predicted and observed cross sections of the ground state members of ^{154}Gd in the proton transfer reactions	99
5.3	Predicted and observed cross sections of the gamma band members of ^{154}Gd in the proton transfer reactions	105
5.4	The (d,t) angular distributions for the K_u=1 and 2 band members resulting from the ΔN=2 mixing between the $\{3/2^-[521]\mp 1/2^+[400]\}_\nu$ and $\{3/2^-[521]\mp 1/2^+[660]\}_\nu$ configurations in ^{154}Gd	113
5.5	The (d,t) angular distributions for the K_ℓ=1 and 2 band members resulting from the ΔN=2 mixing between the $\{3/2^-[521]\mp 1/2^+[400]\}_\nu$ and $\{3/2^-[521]\mp 1/2^+[660]\}_\nu$ configurations in ^{154}Gd	114

		Page
5.6	Predicted and observed cross sections in the $(d,t)_{45°}$ reactions for the members of the K_u and K_ℓ bands resulting from the $\Delta N=2$ mixing between $\{3/2^-[521]\mp 1/2^+[400]\}_\nu$ and $\{3/2^-[521]\mp 1/2^+[660]\}_\nu$ configurations in ^{154}Gd	119
5.7	The (d,t) angular distributions for the $K^\pi=3^-$ and 0^- band members resulting from the $\{3/2^-[521]\pm 3/2^+[402]\}_\nu$ configurations in ^{154}Gd	123
5.8	The (d,t) angular distributions to the levels in ^{154}Gd fitted to $\ell=5$ and 6 transitions	130
5.9	Calculated energies of yrast states arising from the $i_{13/2}$ orbitals coupled to the $3/2^-[521]$ orbital for ^{154}Gd	133
5.10	Predicted and observed cross sections to the members of the $K^\pi=4^+$ and 1^+ bands in ^{154}Gd, resulting from the $\{5/2^+[413]\pm 3/2^+[411]\}_\pi$ configurations	138
5.11	Predicted and observed cross sections to the members of the $K^\pi=2^+$ and 3^+ bands in ^{154}Gd, resulting from the $\{5/2^+[413]\mp 1/2^+[411]\}_\pi$ configurations	142

		Page
5.12	Predicted and observed cross sections for the negative parity levels in ^{154}Gd, resulting from the Coriolis mixed bands of the $\{5/2^+[413]+h_{11/2}\}_\pi$ configurations	146
7.1	Bands in ^{154}Gd, below 2000 keV	170
7.2	Bands in ^{154}Gd, above 2000 keV, populated in neutron transfer reactions	171
7.3	Bands in ^{154}Gd, populated mainly in proton transfer reactions	172
7.4	Five bands in ^{152}Eu	179
7.5	The splitting energies as a function of $(1-4\alpha)W$ for two quasi-particle configurations in ^{154}Gd	182

LIST OF TABLES

		Page
1.1	Various reactions leading to ^{154}Gd and ^{152}Eu	4
2.1	Optical model parameters used in DWBA calculations for the (d,t) and (^{3}He,α) reactions	43
2.2	Optical model parameters used in DWBA calculations for the (^{3}He,d) and (α,t) reactions	44
3.1	The isotopic composition (%) of targets	54
3.2	Estimated and experimental resolution	61
3.3	Q-values (MeV) of various reactions	66
4.1	Observed energies and cross sections of neutron transfer reactions to the levels in ^{154}Gd	73
4.2	Observed energies and cross sections of proton transfer reactions to the levels in ^{154}Gd	79
4.3	Levels in ^{152}Eu	89
5.1	Cross sections (μb/sr) to the ground state band members of ^{154}Gd	93
5.2	The $C^2_{j\ell}$ values for the $3/2^-$[521] neutron orbital	97
5.3	Cross sections (μb/sr) to the gamma band members of ^{154}Gd	102
5.4	Cross sections (μb/sr) to the octupole vibrational states of ^{154}Gd	107

		Page
5.5	Two-quasiparticle configurations of the octupole bands in ^{154}Gd (Soloviev, 1965)	108
5.6	The (d,t) cross sections to the levels in ^{154}Gd, populated by the transfer of the $1/2^+[400]$ and the $1/2^+[660]$ neutron orbitals	116
5.7	The (d,t) cross sections to the levels in ^{154}Gd, populated by the transfer of the $3/2^+[402]$ neutron orbital	120
5.8	$\Delta N=2$ and Coriolis mixed levels in ^{154}Gd	126
5.9	The (d,t) and (^{3}He,α) cross sections to the levels in ^{154}Gd, populated by $\ell=5$ or 6 transitions	129
5.10	Cross sections (μb/sr) to the levels in ^{154}Gd, populated by the transfer of the $3/2^+[411]$ proton orbital	136
5.11	Cross sections (μb/sr) to the levels in ^{154}Gd, populated by the transfer of the $1/2^+[411]$ proton orbital	141
5.12	Levels above the energy gap in ^{154}Gd populated in reactions and the decay of ^{154}Tb	148
5.13	$K^\pi = 1^+$ Band at 2187.2 keV	150

		Page
6.1	Expected total strength in the low lying levels of ^{152}Eu	159
7.1	Level structure of ^{154}Gd	162
7.2	Theoretical and experimental values of U^2 and V^2 (^{154}Gd)	176
7.3	Theoretical and experimental splitting energies (keV)	180

TO

AAVSBSVSRKOSSSP

CHAPTER 1

INTRODUCTION

The atomic nucleus is a very tiny object ($\sim 10^{-13}$ cm) and its main constituents are nucleons (protons and neutrons). The understanding of the structure of nuclei provides some information about the nature of the nuclear force. Ideally, if the precise nature of the nuclear force is known, then in principle it should be possible to estimate the mass of a given nucleus, its spin and magnetic moment, the binding energies of its nucleons and energies of its excited states. Lack of knowledge of the exact nature of the internucleon forces limits the understanding of the nuclear structure. One can attempt a microscopic approach to solve the many body problem by taking into account all the possible known interactions between the nucleons. But this approach is not very practical and to attempt this problem one takes a traditional and convenient approach, the formulation of a model. This is based upon the well established laws of physics. The experimental investigation of the nuclear structure of many nuclei should decide upon the validity of that model.

The present study of $^{154}_{64}Gd_{90}$ and $^{152}_{63}Eu_{89}$ nuclei is an attempt to understand nuclear structure in terms of the existing nuclear models. Figure 1.1 shows the location of these

Figure 1.1

A part of the nuclear table near A $\sim$ 150. In parentheses, the intrinsic quadrupole moments ($\frac{Q_o}{e}$, barns) of the ground states are shown.

Z	N = 88	89	90	91
64	^{152}Gd (3.8)	^{153}Gd ( )	^{154}Gd (6.2)	^{155}Gd (6.7)
63	^{151}Eu (3.2)	^{152}Eu (7.5)	^{153}Eu (8.0)	^{154}Eu (9.3)
62	^{150}Sm (3.7)	^{151}Sm (4.1)	^{152}Sm (5.9)	^{153}Sm (5.2)

nuclei in the nuclear periodic table. In this region, nuclei are known to be transitional, i.e. their shapes are different from those of the neighbouring nuclei. This aspect can be seen from figure 1.1, where the intrinsic quadrupole moment which measures the deviation from a spherical nuclear shape is given in parentheses. It can be seen that nuclei with neutron number N = 88, have a relatively smaller quadrupole moment than those with N = 90. It is also obvious that this change in the quadrupole moment is rather abrupt. Not only the quadrupole moments and shapes of the nuclei exhibit such effects, but there is a number of other nuclear properties where the manifestation of the transitional nature of these nuclei could be seen. The low lying excited states show a marked contrast between the N = 88 and 90 nuclei. In some of these nuclei, it has been found that properties which are otherwise typical of both spherical and deformed nuclei are present.

In the present study, the nuclear structure of two transitional nuclei $^{154}_{64}Gd_{90}$ and $^{152}_{63}Eu_{89}$ has been studied by single nucleon transfer reactions (see table 1.1). These reactions populate two-quasiparticle states at low excitation energies in a doubly-odd nucleus and above the energy gap in a doubly-even nucleus. In the latter case, collective states of the ground, beta, gamma and octupole bands could also be populated. These single nucleon transfer reactions are selective in the sense that one of the two-

Table 1.1

Various reactions leading to ^{154}Gd and ^{152}Eu

Reaction	Beam Energy (MeV)	θ (degrees)
$^{155}Gd(d,t)^{154}Gd$	12	7.5,17.5,25,30 45,60,100,120
$^{155}Gd(^{3}He,\alpha)^{154}Gd$	24	45,60
$^{153}Eu(^{3}He,d)^{154}Gd$	24	25,30,60
$^{153}Eu(\alpha,t)^{154}Gd$	27	45,60
$^{153}Eu(^{3}He,\alpha)^{152}Eu$	24	25,30,60
$^{151}Sm(^{3}He,d)^{152}Eu$	24	30,60
$^{151}Sm(\alpha,t)^{152}Eu$	27	60,90

quasiparticle orbitals is definitely the same orbital as the target ground state.

Most of the previous studies of ^{154}Gd have been done using the radioactive decay of ^{154}Eu and ^{154}Tb (Meyer, 1968, Meyer et al., 1968, Riedinger et al., 1970, 1971, Vylov et al., 1972, Sousa et al., 1975).

The decay energy of ^{154}Eu ($\sim$ 2 MeV) is much lower than that of ^{154}Tb ($\sim$ 3.8 MeV). Thus the information available from the decay of ^{154}Eu is limited to states below 1.9 MeV. However, Sousa et al. (1975) have observed more than 300 gamma rays in the decay of ^{154}Tb. They have established 50 new levels above 1.9 MeV along with 28 levels below this energy. In some of the cases the spin and parity assignments have been made conclusively and in most cases the two-quasiparticle configurations are not given. The Notre Dame group is still active in the study of ^{154}Gd by the (α,2n) reaction (West et al., 1976). The ground and beta bands have been investigated up to 18^+ states in ^{154}Gd by means of the (α,4n) reaction (Khoo et al., 1973).

Inelastic deuteron scattering experiments (d,d') by Bloch et al. (1967) have revealed the nature of some of the collective states in ^{154}Gd. Coulomb excitation experiments (Yoshizawa et al., 1966, Riedinger et al., 1969) have also been attempted. The present study of the proton and neutron transfer reactions leading to the residual nucleus ^{154}Gd is an attempt to provide additional nuclear structure information.

Various collective band members have been populated and also new two-quasiparticle configurations have been established for the levels populated above the energy gap in both the neutron and proton transfer reactions.

The doubly-odd nucleus ^{152}Eu is unstable (half life 12.4 years) and very little is known about its nuclear structure. Takahashi et al., 1965, gave an account of only four of the excited levels of ^{152}Eu. Of these two were isomers with half lives 9.3 h (50±15 keV) and 96±5 min (147.8 keV). This group was able to propose the structure for these levels. Recently unpublished results for ^{152}Eu by a group of investigators have become available (von Egidy et al., 1971, 1974, 1975, Breitig et al., 1973). This group has performed a large number of experiments such as (n,e), (n,γ), (n,$\gamma\gamma$), (n_{res},γ), (d,t), (d,p) and (p,d). Their work has allowed spin-parity assignments of many of the levels up to 500 keV.

In the present study, an attempt has been made to investigate the nuclear structure of ^{152}Eu via the (^{3}He,d) and (α,t) proton transfer reactions on a target of radioactive ^{151}Sm and also by the (^{3}He,α) reaction on an ^{153}Eu target. A large number of levels has been populated and the configurations of some of these levels have been given in terms of Nilsson orbitals. To interpret the data in this work, it has been necessary to rely very heavily on the unpublished results of von Egidy et al.,1975.

Apart from the nuclear structure of these nuclei,

additional information regarding the particle-particle interaction should be obtained from the energy difference of the two band head energies of those bands belonging to the same Nilsson orbitals. A comparison of these splitting energies may be made with the results of a theoretical calculation.

CHAPTER 2

THEORETICAL ASPECTS AND CALCULATIONS

2.1 The Nuclear Shell and Liquid Drop Models

The nuclear shell model has been found to be extremely good as a description of many general properties of nuclei. A few of these properties are the unusual stability of certain nuclei (magic numbers), the spin and parity of even and odd mass nuclei, the phenomenon of nuclear isomerism and the values of magnetic moments (Schmidt lines). These features are well predicted for the spherical (closed shell) or nearly spherical nuclei. It is worthwhile to mention the basic assumptions on which the shell model is based. Each nucleon is considered to move independently in its own quantized orbit inside a static, spherically symmetric potential generated as a result of the average force exerted by the remaining nucleons. Along with this, Mayer and Jensen (1955) introduced a strong spin-orbit force to reproduce the magic numbers and to give the correct ordering of the different shells. In this model, it is further assumed that most of the nucleons are paired off and thus the properties of a nucleus are determined by the last unpaired nucleons.

However for nuclei far from closed shells, the simple shell model does not properly describe the nuclear properties.

There are three regions in the nuclear table with mass numbers 18-28, 150-190 and 224-, where the nuclei are permanently deformed. The strong enhancement of E2 transition rates and the large quadrupole moments in these regions have shown that this deviation from sphericity corresponds to a deformation ($\Delta R/R_0$) as large as 30%.

On the other hand, the liquid drop model of the nucleus (Bohr, 1936) is a different approach to the explanation of the nuclear structure. This model was based upon the analogy of a nucleus with a liquid drop and was developed long before the formulation of a successful shell model. The liquid drop model had found a wide range of applications in the description of many nuclear properties, e.g. the binding energies, theory of nuclear reactions and fission. Both of these models are satisfactory to describe certain nuclear properties, but do have distinct limitations in their applications.

2.2 The Unified Model of the Nucleus

The unified model is a hybrid of the liquid drop model and the shell model, where attempts have been made to retain the main features of both models. Here, the static isotropic nuclear potential in which the nucleons move is replaced by another type of potential. This potential takes into account the variations in the nuclear field caused by oscillations in the shape of the nucleus.

Rainwater (1950) was the first to realize the importance

of the interaction of the individual particle and collective motions. Bohr (1952) and Bohr and Mottelson (1953) developed this model extensively. These three physicists have received the Nobel Prize for 1975, for this contribution to our understanding of nuclear structure.

For a closed shell configuration, the deforming effects of many nucleons cancel out because the orbitals are oriented equally in all directions. When a nucleus has only a few nucleons beyond a closed shell the nuclear equilibrium shape remains spherical. However, when there are many particles outside the closed shell, the spherical shape becomes unstable and the nucleus assumes a spheroidal equilibrium shape. Under these conditions the collective motion of the nuclear system appears in the form of rotational and vibrational modes. The unified model then consists of considering the last nucleons to be moving in the deformed potential of all of the other paired nucleons and has been useful as an explanation of the properties of deformed nuclei.

2.3 Nuclear Deformation

The most common way of describing the shape (or the deformation) of a nucleus is by the use of spherical harmonics, with the assumption that shape oscillations preserve the nuclear volume. The nuclear radius is written as (Bohr, 1952):

$$R(\theta,\phi) = R_0\{1 + \sum_{\lambda\mu} \alpha_{\lambda\mu} Y_\mu^\lambda(\theta,\phi)\} , \qquad (2.3.1)$$

where R_0 is the equilibrium radius,

$\alpha_{\lambda\mu}$ are the coefficients which define the deformation of the nucleus,

$Y^{\lambda}_{\mu}(\theta,\phi)$ are the normalized spherical harmonics of order λ and μ is the projection of λ on a space fixed axis, of which there are $(2\lambda+1)$ values ranging from $-\lambda$ to $+\lambda$.

The shape oscillations are classified according to their multipole order λ. These excitation quanta, called phonons, have total angular momentum λ and parity $(-1)^{\lambda}$. The lowest frequency of collective vibrations is expected to be of quadrupole type corresponding to $\lambda=2$. With the assumption that the co-ordinate system coincides with the principal axes of the ellipsoidal nucleus, only two coefficients are required, viz. α_{20} and α_{22} along with three angular coordinates specifying the orientation of the ellipsoid in space. Furthermore, with the introduction of two parameters β and γ such that

$$\begin{aligned} \alpha_{2,1} &= \alpha_{2,-1} = 0 \\ \alpha_{20} &= \beta \cos\gamma \\ \alpha_{2,2} &= \alpha_{2,-2} = \frac{1}{\sqrt{2}} \beta \sin\gamma, \end{aligned} \qquad (2.3.2)$$

the nuclear radius can be written as

$$R = R_0[1 + \sqrt{\frac{5}{16\pi}} \beta\{\cos\gamma(3\cos^2\theta-1) + \sqrt{3}\ \sin\gamma\sin^2\theta\cos2\phi\}]. \qquad (2.3.3)$$

Here, the parameter β measures the total deformation from sphericity and the angular parameter γ is the deviation from

the rotational symmetry about the principal axis of the ellipsoid. In general, β can take any value from zero to infinity and $0° \leq \gamma \leq 60°$.

The collective motion of the nucleons in a deformed nucleus may be of a rotational or vibrational character. In beta vibrations axial symmetry of the nucleus is preserved, while in gamma vibrations it relinquishes this symmetry.

Although there is some evidence that permanent gamma deformation exists for some nuclei, the majority of deformed nuclei have $\gamma = 0$. However, since there is no evidence for large permanent gamma deformation near A=154, the following discussion will be limited to considering the case of $\gamma = 0$.

Nilsson (1955) has defined another deformation δ related to β and the intrinsic quadrupole moment by:

$$\delta = 3\sqrt{\frac{5}{16\pi}}\,\beta$$

$$\approx 0.95\,\beta\,, \qquad (2.3.4)$$

and

$$Q_0 \approx 0.8\ Ze\ R^2\delta\left(1 + \frac{2}{3}\,\delta\right)\,, \qquad (2.3.5)$$

where Ze is the charge of the nucleus of mass number A and $R = 1.2\times10^{-13}\ A^{1/3}$ cm.

The intrinsic quadrupole moment Q_0 is related to the measured quadrupole moment Q, of an axially symmetric deformed nucleus by,

$$Q = \frac{3K^2 - I(I+1)}{(I+1)(2I+3)}\,Q_0\,, \qquad (2.3.6)$$

where K is the projection of the nuclear spin I on the symmetry axis (see figure 2.1).

The sign of the quadrupole moment or of the deformation parameter gives the shape of the nucleus, e,g.

for $Q_0 > 0$, the nucleus is prolate,

$Q_0 = 0$, the nucleus is spherical,

$Q_0 < 0$, the nucleus is oblate.

2.4 Quantum Numbers and Coupling of Angular Momenta in Axially Symmetric Deformed Nuclei

Most deformed nuclei are known to be axially symmetric. For these nuclei, the angular momentum vector $\vec{R}$, associated with the rotation, is perpendicular to the symmetry axis z (see figure 2.1). The angular momentum $\vec{j}(=\vec{\ell}+\vec{s})$ resulting from the particle motion is not a conserved quantity. Thus, for a deformed nucleus additional quantum numbers are required than those used for a spherical nucleus. The component of $\vec{j}$ on the symmetry axis is Ω and is a constant of motion. The nuclear spin vector $\vec{I} = \vec{j}+\vec{R}$, and its projections M and K on the space fixed and nuclear symmetry axes respectively, are constants of motion for these nuclei. Furthermore, the projection of $\vec{\ell}$ and $\vec{s}$ on the nuclear symmetry axis are Λ and Σ, respectively. This gives $\Omega = \Lambda+\Sigma$, where $\Sigma = \pm 1/2$.

The single particle states for deformed nuclei (Nilsson, 1955) are usually denoted by $\Omega^{\pi}[Nn_z\Lambda]$ where the quantities inside the brackets are called the asymptotic quantum numbers.

Figure 2.1

Coupling of angular momenta in an axially symmetric a) odd A nucleus and b) of two-quasiparticle states in a doubly-odd or even nuclei.

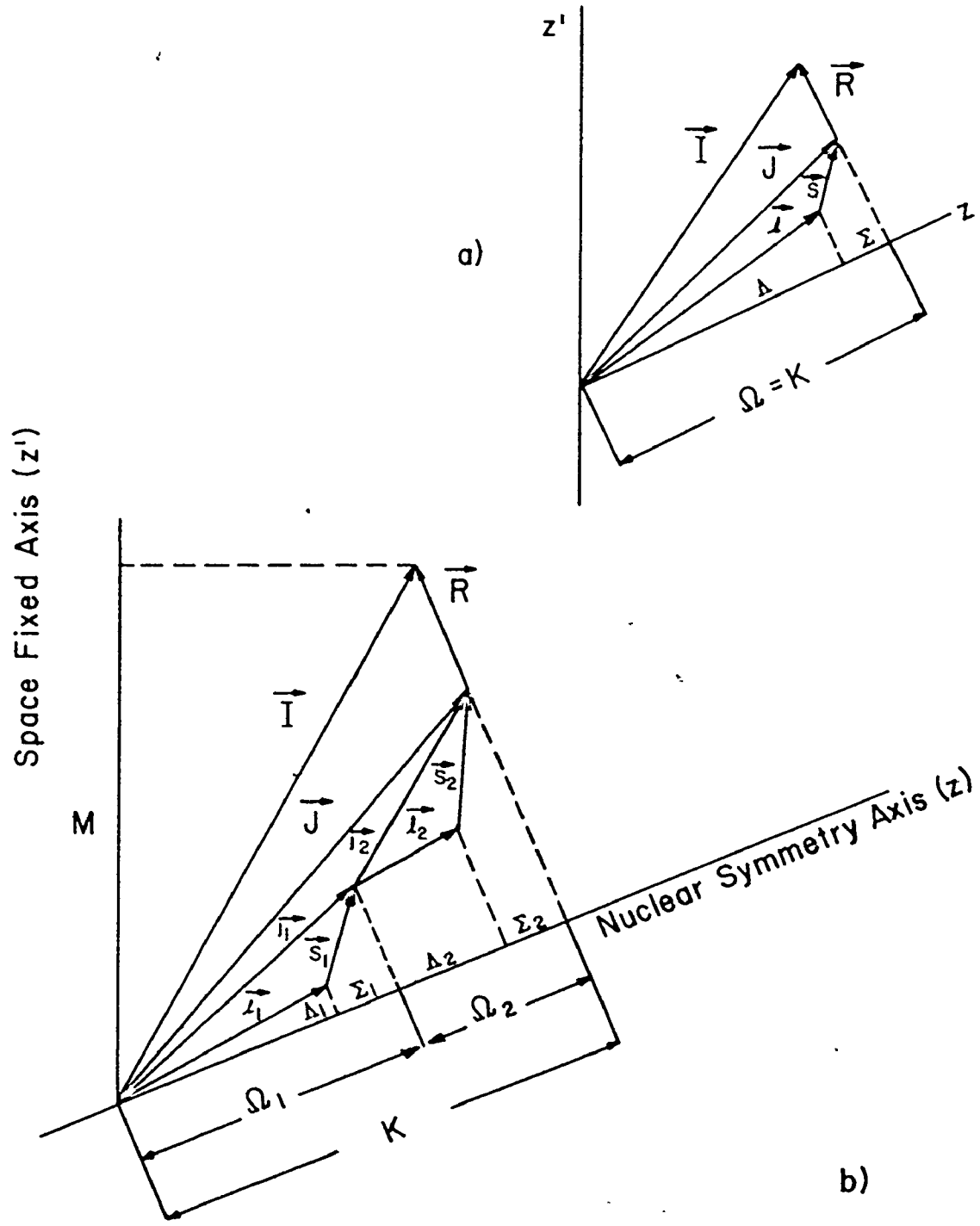
z'
R
I
J
s
l
Σ
z
Λ
Ω = K
a)
Space Fixed Axis (z')
M
R
I
J
s2
l2
l2
l1
s1
l1
Λ1
Σ1
Λ2
Σ2
Nuclear Symmetry Axis (z)
Ω2
Ω1
K
b)

N is the principle quantum number, n_z the number of oscillator quanta along the nuclear symmetry axis and the parity π is given by $(-1)^N$.

The coupling of angular momenta in a doubly-odd or even nuclei is shown in figure 2.1b. Two Nilsson states which are denoted by $\{\Omega^\pi[Nn_z\Lambda]\}_1$ and $\{\Omega^\pi[Nn_z\Lambda]\}_2$, represent proton and neutron orbitals respectively in the case of a doubly-odd nucleus. For a doubly-even nucleus 1 and 2 refer to either protons or neutrons. In these cases, the two-quasiparticle states result from either the parallel coupling $\{\Omega^\pi[Nn_z\Lambda]\}_1 + \{\Omega^\pi[Nn_z\Lambda]\}_2$ or the anti-parallel coupling $\{\Omega^\pi[Nn_z\Lambda]\}_1 - \{\Omega^\pi[Nn_z\Lambda]\}_2$ of the two unpaired particles. Thus two values of K are possible, i.e.

$$K_1 = ||\Omega_1| - |\Omega_2|| \qquad (2.4.1)$$

(for anti-parallel coupling)

and

$$K_2 = |\Omega_1| + |\Omega_2| \qquad (2.4.2)$$

(for parallel coupling)

with the parity given by $(-1)^{N_1+N_2}$.

Each intrinsic configuration thus gives rise to two bands separated in energy by the interaction between the two unpaired nucleons. This splitting of bands in even mass nuclei will be discussed in section 2.11.

2.5 Separability of Nuclear Wave Functions

For a strongly deformed nucleus, the frequencies of the vibrational and especially of the rotational motion are slower than those of the intrinsic particle excitations. Thus it can be thought that the particle motion does not disturb

the collective rotation and vibration of the entire system and vice versa. Under these circumstances, the total nuclear wave function in general form is

$$\psi = \phi_{Vib} D_{Rot} \chi_{part} \qquad (2.5.1)$$

where ϕ_{vib} describes the vibration of the nucleus around the equilibrium shape, D_{Rot} represents the collective rotational motion of the system as a whole and the χ_{Part} represents the intrinsic motion of nucleons which is expressed as the independent motion of the individual nucleons in the deformed potential field. The separability of the nuclear wave function into this product form is usually called the 'adiabatic assumption'.

In the following discussion only the rotational and intrinsic wave functions and their interplay with each other will be discussed.

The rotational D-functions are the transformation functions for the spherical harmonics under finite rotations. The normalized rotational wave functions are given by Edmonds (1957),

$$|IMK\rangle = \left(\frac{2I+1}{8\pi^2}\right)^{1/2} D^{I}_{MK} \, . \qquad (2.5.2)$$

The following relations are satisfied by the angular momentum operator for these rotational wave functions

$$\vec{I}^2 D^I_{MK} = I(I+1) D^I_{MK}$$

$$I_z, D^I_{MK} = M D^I_{MK}$$

$$I_z D^I_{MK} = K D^I_{MK} \quad . \qquad (2.5.3)$$

2.6 Single Particle States in a Deformed Potential Well (Nilsson Model)

The interaction of a nucleon with a deformed potential field has been considered by Nilsson (1955). In that work the single particle energy levels and wavefunctions for deformed nuclei have been calculated. Nilsson has considered a Hamiltonian of the following type,

$$H = H_0 + C\ \vec{\ell}\cdot\vec{s} + D\ \vec{\ell}\cdot\vec{\ell} \qquad (2.6.1)$$

where

$$H_0 = -\frac{\hbar^2}{2m}\nabla^2 + V(\vec{r})$$

$$= -\frac{\hbar^2}{2m}\nabla^2 + \frac{1}{2}m(\omega_1^2 x_1^2 + \omega_2^2 y_1^2 + \omega_3^2 z_1^2) \quad . \qquad (2.6.2)$$

Here, Nilsson has introduced a term proportional to $\vec{\ell}\cdot\vec{\ell}$ in the Hamiltonian of an isotropic harmonic oscillator. The effect of this term is to increase the binding energy of high ℓ orbitals. C and D are proportionality constants. x_1, y_1 and z_1 are the co-ordinates of a particle in a system fixed in the nucleus.

For the axially symmetric case, the following conditions are used

$$\omega_1 = \omega_2 = \omega_0 \left(1 + \frac{2}{3}\delta\right)^{1/2}$$

$$\omega_3 = \omega_0 \left(1 - \frac{4}{3}\delta\right)^{1/2} . \qquad (2.6.3)$$

The restriction to constant volume gives

$$\omega_1\omega_2\omega_3 = \text{constant}$$

and leads to

$$\omega_0(\delta) = \omega_0^0 \left(1 - \frac{4}{3}\delta^2 - \frac{16}{27}\delta^3\right)^{-1/6} . \qquad (2.6.4)$$

ω_0^0 is the value of $\omega_0(\delta)$ for $\delta = 0$ and

$$\hbar\omega_0^0 = 41\ A^{-1/3}\ \text{MeV} . \qquad (2.6.5)$$

With the conditions given by (2.6.3), the $V(\vec{r})$ can be written as:

$$V(\vec{r}) = \frac{1}{2} m\omega_0^2 r^2 [1 - 2\beta Y_{20}(\theta,\phi)] , \qquad (2.6.6)$$

where β is related to δ by the relation (2.3.4). The spherical harmonic, Y_{20}, corresponds to the quadrupole deformation of the nucleus. Furthermore a new set of co-ordinates were introduced:

$$\rho^2 = \frac{m\omega_0}{\hbar} r^2$$

$$H_0 = H_0^0 + H_\delta \qquad (2.6.7)$$

$$H_0^0 = \frac{1}{2}\hbar\omega_0[-\nabla^2 + \rho^2] \qquad (2.6.8)$$

$$H_\delta = -\beta\hbar\omega_0\rho^2 Y_{20}(\theta,\phi) . \qquad (2.6.9)$$

Here, H_0^0 is a spherically symmetric term and

H_δ is a deformed Hamiltonian.

Thus the total Hamiltonian H can be written as:

$$H = H_0^0 + H_\delta + C\ \vec{\ell}\cdot\vec{s} + D\ \vec{\ell}\cdot\vec{\ell}\ . \qquad (2.6.10)$$

Two more well parameters were introduced:

$$\kappa = -C/2\hbar\omega_0$$

and

$$\mu = 2D/C \qquad (2.6.11)$$

and their values were chosen to reproduce the shell model ordering of the different orbitals.

The values of the κ and μ used in the present study are those which are recommended by Lamm (1969) for the rare earth region.

$\kappa = 0.0637$ and $\mu = 0.600$ (for protons) (2.6.12)

$\kappa = 0.0637$ and $\mu = 0.42$ (for neutrons) (2.6.13)

Using relations (2.6.7-10), the total Hamiltonian H, can be written as:

$$\frac{H}{\hbar\omega_0} = \frac{1}{2}[-\nabla^2 + \rho^2] - \beta\rho^2 Y_{20}(\theta,\phi) - 2\kappa\ \vec{\ell}\cdot\vec{s} - \mu\kappa\ \vec{\ell}\cdot\vec{\ell}\ . \qquad (2.6.14)$$

Nilsson (1955) used $|N\ell\Lambda\Sigma\rangle$ as basis vectors to solve this Hamiltonian. But the basis vectors $|N\ell j\Omega\rangle$ have the advantage that all the terms except the H_δ term in the Hamiltonian H are such that:

$$\frac{1}{2}(-\nabla^2+\rho^2)\,|N\ell j\Omega\rangle = (N+3/2)\,|N\ell j\Omega\rangle, \quad N = 0,1,2\ldots$$

$$\ell^2|N\ell j\Omega\rangle = \ell(\ell+1)\;|N\ell j\Omega\rangle, \quad \ell = N,(N-1)\ldots 1 \text{ or } 0$$

$$j^2|N\ell j\Omega\rangle = j(j+1)\;|N\ell j\Omega\rangle, \quad j = \ell \pm 1/2$$

$$j_z|N\ell j\Omega\rangle = \Omega\;|N\ell j\Omega\rangle, \quad \Omega = -j, -(j-1), \ldots(j-1), j\ . \qquad (2.6.15)$$

Non-zero matrix elements of H_δ arise between the states differing by $\Delta N = 0,\pm 2$. Usually the shells differing by two units are far apart and are neglected. As will be discussed later, there exists a situation in the present study where such effects are important.

For deformation $\delta=0$, the Hamiltonian (2.6.14) should give rise to the spherical energy levels.

$$E_{N\ell j} = \hbar\omega_0[(N+3/2)-\kappa(2\vec{\ell}\cdot\vec{s} + \mu\vec{\ell}\cdot\vec{\ell})]. \qquad (2.6.16)$$

For very small deformations, the energy shifts ΔE from the spherical energy levels are given approximately by the diagonal matrix elements of the operator H_δ, (using (2.6.14) and (2.6.16)).

$$\Delta E_{N\ell j\Omega} = -\hbar\omega_0\beta(N+3/2)\langle N\ell j\Omega|Y_{20}(\theta,\phi)|N\ell j\Omega\rangle$$

$$= -\sqrt{\frac{5}{\pi}}\;\frac{j(j+1)-3\Omega^2}{8j(j+1)}\;\hbar\omega_0\beta\;(N+3/2). \qquad (2.6.17)$$

This expression is used to find the slope of the energy levels at $\delta=0$ and also for the construction of the so-called Nilsson diagrams. These diagrams are shown in figures 2.2 (for proton states) and 2.3 and 2.4 (for neutron states). Each Nilsson orbital is labelled with $\Omega^\pi[Nn_z\Lambda]$ and can accomodate

Figure 2.2

Nilsson diagram for proton orbitals.

(κ = 0.0637 and μ = 0.600)

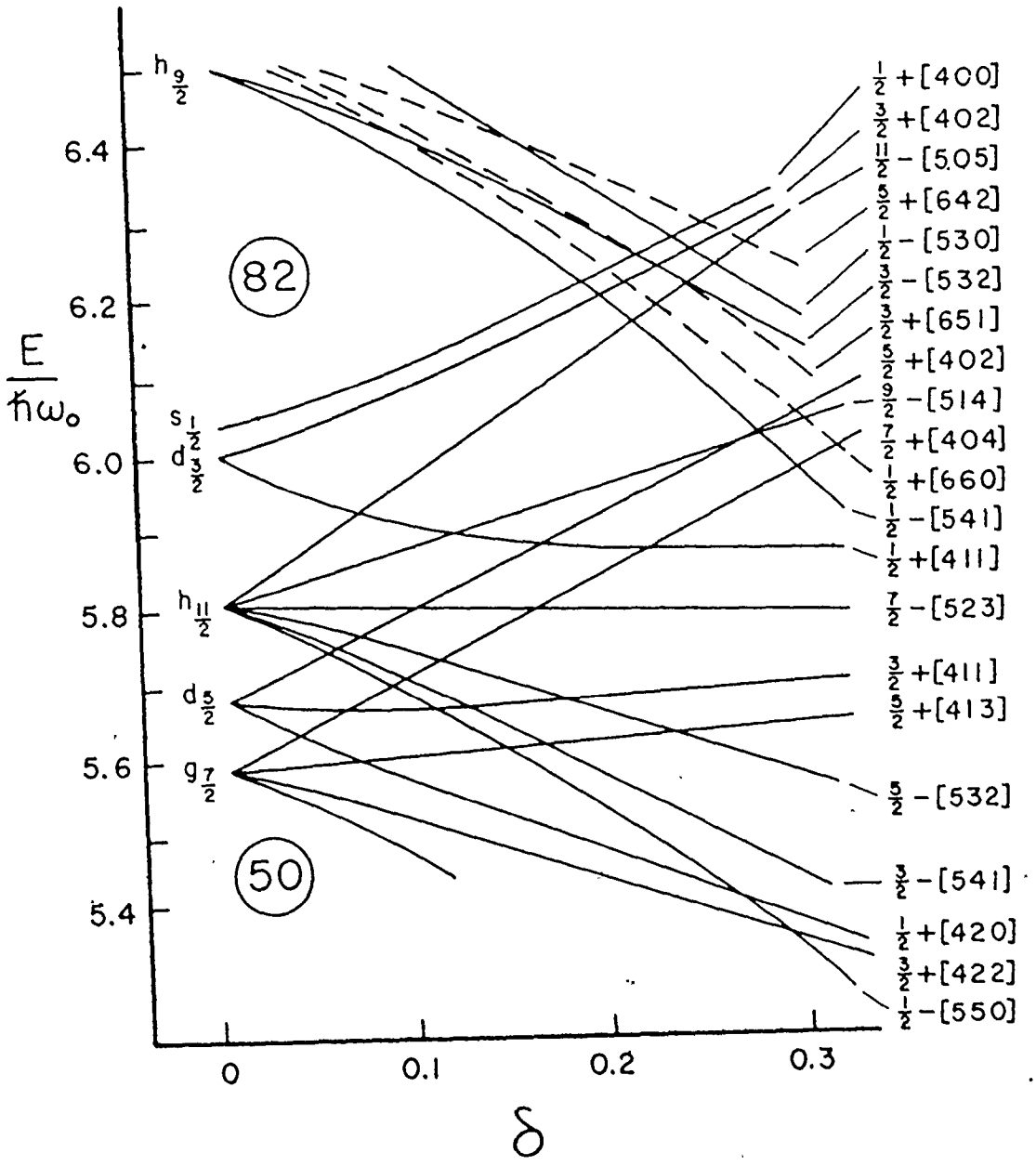
$h_{\frac{9}{2}}$
$s_{\frac{1}{2}}$
$d_{\frac{3}{2}}$
$h_{\frac{11}{2}}$
$d_{\frac{5}{2}}$
$g_{\frac{7}{2}}$
82
50
6.4
6.2
6.0
5.8
5.6
5.4
$\frac{E}{\hbar\omega_o}$
0
0.1
0.2
0.3
δ
$\frac{1}{2}$ +[400]
$\frac{3}{2}$ +[402]
$\frac{11}{2}$ −[505]
$\frac{5}{2}$ +[642]
$\frac{1}{2}$ −[530]
$\frac{3}{2}$ −[532]
$\frac{3}{2}$ +[651]
$\frac{5}{2}$ +[402]
$\frac{9}{2}$ −[514]
$\frac{7}{2}$ +[404]
$\frac{1}{2}$ +[660]
$\frac{1}{2}$ −[541]
$\frac{1}{2}$ +[411]
$\frac{7}{2}$ −[523]
$\frac{3}{2}$ +[411]
$\frac{5}{2}$ +[413]
$\frac{5}{2}$ −[532]
$\frac{3}{2}$ −[541]
$\frac{1}{2}$ +[420]
$\frac{3}{2}$ +[422]
$\frac{1}{2}$ −[550]

Figure 2.3

Nilsson diagram for neutron orbitals.

(κ = 0.0637 and μ = 0.42)

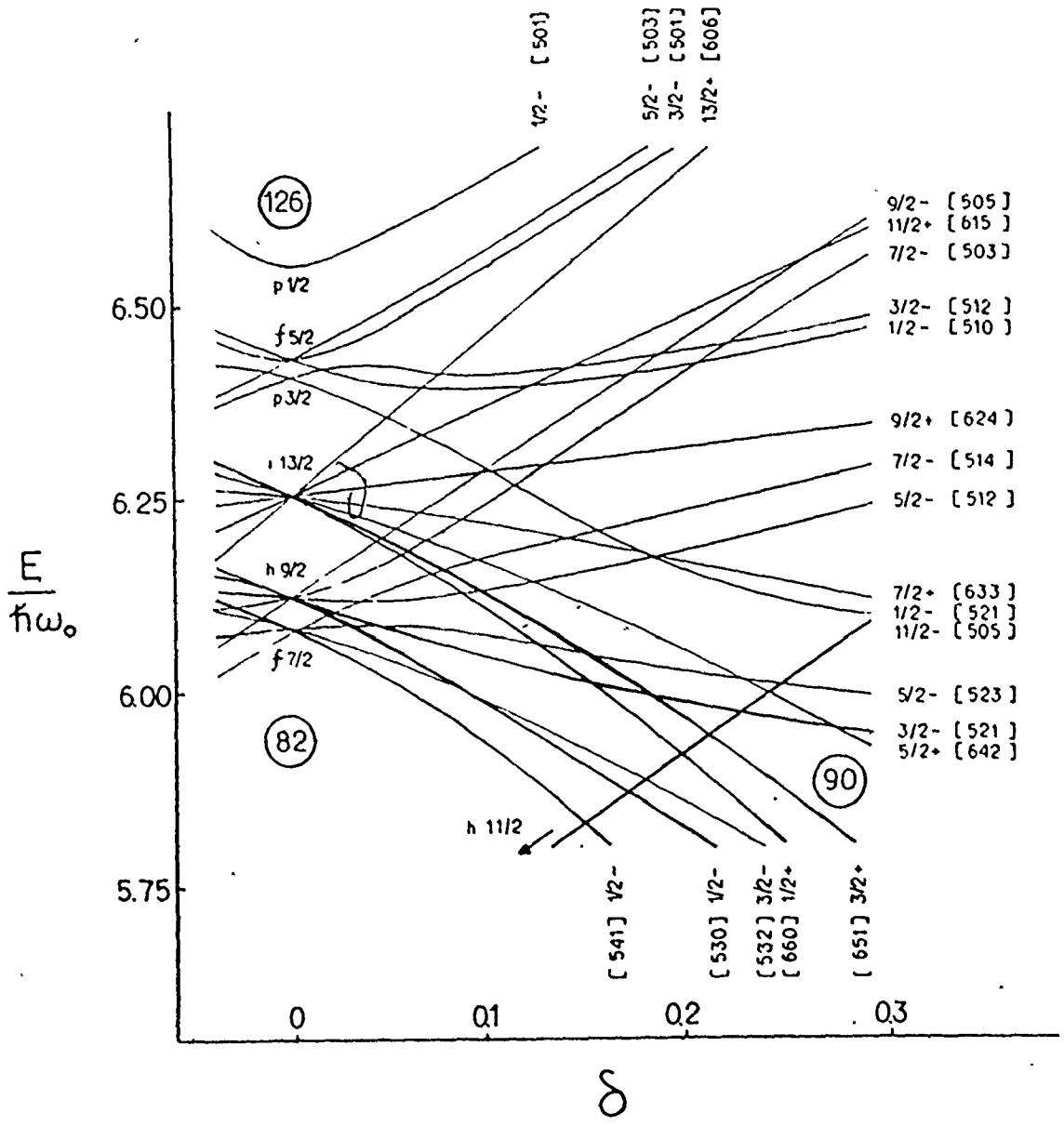
1/2- [501]
5/2- [503]
3/2- [501]
13/2+ [606]
126
p 1/2
f 5/2
p 3/2
i 13/2
h 9/2
f 7/2
82
90
h 11/2
9/2- [505]
11/2+ [615]
7/2- [503]
3/2- [512]
1/2- [510]
9/2+ [624]
7/2- [514]
5/2- [512]
7/2+ [633]
1/2- [521]
11/2- [505]
5/2- [523]
3/2- [521]
5/2+ [642]
[541] 1/2-
[530] 1/2-
[532] 3/2-
[660] 1/2+
[651] 3/2+
6.50
6.25
6.00
5.75
E/ħω₀
0
0.1
0.2
0.3
δ

Figure 2.4

Intersection of the $1/2^+[400]$ and $1/2^+[660]$ orbitals in the Nilsson diagram. A similar situation is found for the $3/2^+[402]$ and $3/2^+[651]$ orbitals in the beginning of the rare earth region (adopted from Elbek and Tjøm, 1969).

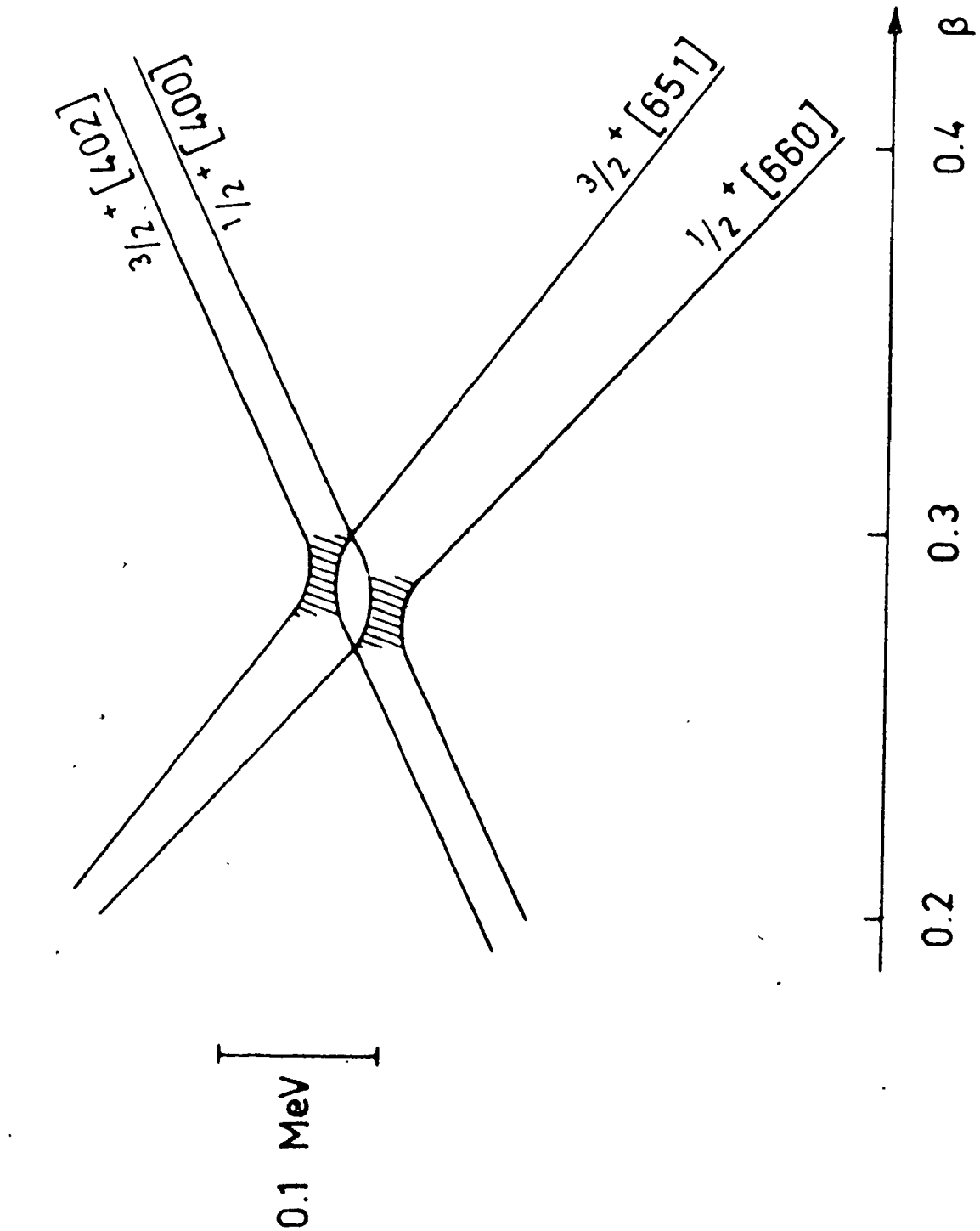
3/2 + [402]
1/2 + [400]
3/2 + [651]
1/2 + [660]
0.1 MeV
0.2
0.3
0.4
β

two particles corresponding to $\pm\Omega$. It can be seen from these diagrams that as deformation sets in, each shell model state splits into $(j + \frac{1}{2})$ levels. These Nilsson diagrams have been very successful in determining the nuclear spins of many deformed nuclei.

The deformed single particle wave functions $\chi_{N\Omega}$ are expressed as a sum of spherical harmonic oscillator functions $|N\ell j\Omega>$,

$$\chi_{N\Omega} = \sum_{j} C_{j\ell}(N\Omega)\,|N\ell j\Omega>. \qquad (2.6.18)$$

The summation extends over the range $\Omega \leq j \leq (N + \frac{1}{2})$. The square of the $C_{j\ell}$ expansion coefficients gives the fractions of the spherical states contained in a Nilsson orbital. There are many forms of these coefficients available. In the present study, the $C_{j\ell}$ values were obtained from a modified version of a computer program originally due to Chi (1967,1966). In these calculations, a term $-\frac{1}{2}DN(N+3)$ is added to the Hamiltonian (2.6.1), in order to keep the energy difference between the centres of gravity of different N-shells constant (Lamm, 1969).

2.7 Pairing Interaction

The increased stability of the doubly-even nuclei over the doubly-odd or odd mass nuclei has been attributed to the pairing interaction. Nathan and Nilsson (1965) have used the mathematical techniques of the BCS theory of superconduc-

tivity (Bardeen et al., 1957) to describe the pairing phenomena applied to the nuclear case. In this section, the effect of pairing on the excitation energies as well as on the single nucleon transfer cross sections will be discussed.

A quantity V^2, the fullness factor, gives the probability for a state ν being occupied by a pair of nucleons. Similarly the probability for the state ν being empty is given by U^2 with

$$U^2 + V^2 = 1 \ . \qquad (2.7.1)$$

These factors U^2 and V^2 have a great influence on the stripping and pick-up reaction cross sections. In the simple shell or unified models, states up to the Fermi energy λ are filled. Under the influence of the pairing force, the pairs of particles are subjected to scattering to higher lying levels beyond λ. This scattering modifies the Fermi surface so that it no longer remains sharp, but becomes diffuse. An energy gap parameter Δ provides the measure of the strength of the pairing force and also represents the extent of diffuseness of the Fermi surface.

The ground state of an odd mass nucleus is a quasiparticle state while for a doubly-odd nucleus it is a two-quasiparticle state made by the coupling of the last unpaired proton and neutron states. Two-quasiparticle states in a doubly-even nucleus are due to two unpaired protons or neutrons and occur above the energy gap, 2Δ.

For an odd mass nucleus, the ground state particle energy is given as (Elbek and Tjøm, 1969)

$$E_\nu = \sqrt{(\varepsilon_\nu - \lambda)^2 + \Delta^2} \qquad (2.7.2)$$

where ε_ν is the single particle energy.

The excitation energy of a quasiparticle occupying the level ν' is given by

$$E = E_{\nu'} - E_\nu$$

$$= \sqrt{(\varepsilon_{\nu'}-\lambda)^2 + \Delta^2} - \sqrt{(\varepsilon_\nu-\lambda)^2 + \Delta^2} \ .$$

As the $(\varepsilon_\nu - \lambda)^2$ is very small compared to Δ^2, this expression simplifies to

$$E = \sqrt{(\varepsilon_{\nu'} - \lambda)^2 + \Delta^2} - \Delta. \qquad (2.7.3)$$

The general effect of pairing is that the states near the Fermi level are compressed near to the ground state.

The quantities U^2 and V^2 can be calculated provided the ε_ν, ,λ and Δ are known, from the expressions

$$U^2 = \frac{1}{2}\left(1 + \frac{(\varepsilon_\nu - \lambda)}{\sqrt{(\varepsilon_\nu - \lambda)^2 + \Delta^2}}\right) \qquad (2.7.4)$$

and

$$V^2 = \frac{1}{2}\left(1 - \frac{(\varepsilon_\nu - \lambda)}{\sqrt{(\varepsilon_\nu - \lambda)^2 + \Delta^2}}\right) \ . \qquad (2.7.5)$$

The energy gap parameter can be calculated from the binding energies of the neighbouring nuclei. Nilsson (1961) has given a relationship between Δ_p and the separation energies ($S_p(Z,N)$),

$$\Delta_p(Z,N) \approx \frac{1}{4}[2S_p(Z,N)-S_p(Z+1,N)-S_p(Z-1,N)]. \qquad (2.7.6)$$

Similarly the neutron gap energy parameter (Δ_n) can be calculated from a knowledge of neutron separation energies in the neighbouring nuclei.

Values of the proton and neutron separation energies were obtained from the compilation of Meredith and Barber (1972). For the doubly-even ^{154}Gd nucleus the values of the energy gap parameter thus calculated are

$$\Delta_p = 1.125 \text{ MeV}$$

and

$$\Delta_n = 1.275 \text{ MeV}. \qquad (2.7.7)$$

In general, it is impossible to calculate U^2 and V^2 exactly from such a simple theory of pairing phenomenon.

2.8 Rotational Hamiltonian for Even Mass Nuclei

Jones (1969) has derived explicitly the various terms of the nuclear Hamiltonian for a doubly-odd nucleus. The development of this section is based along essentially the same lines.

For a deformed nucleus, the rotational kinetic energy

is given by

$$T_{ROT} = A\vec{R}^2 \ , \qquad (2.8.1)$$

where $A(=\hbar^2/2\mathcal{J})$ is the rotational parameter and $\mathcal{J}$ is the moment of inertia.

The rotational angular momentum $\vec{R}$ is related to the total angular momentum $\vec{I}$ (figure 2.1) by

$$\vec{R} = \vec{I} - \vec{j}$$

where

$$\vec{j} = \vec{j}_1 + \vec{j}_2 .$$

$\vec{j}_1$ and $\vec{j}_2$ refer to the proton and neutron angular momentum respectively for a doubly-odd nucleus and either to both protons or to neutrons for a doubly-even nucleus.

As discussed in section 2.4, for an axially symmetric nucleus, the angular momentum vector $\vec{R}$ is always perpendicular to the nuclear symmetry axis z, i.e. its component R_z along this axis is zero.

Thus

$$\begin{aligned} \vec{R}^2 &= R_x^2 + R_y^2 \\ &= (I_x - j_x)^2 + (I_y - j_y)^2 \\ &= (\vec{I}^2 - I_z^2) + (\vec{j}^2 - j_z^2) - 2(I_x j_x + I_y j_y) \ . \end{aligned} \qquad (2.8.2)$$

The $(\vec{j}^2 - j_z^2)$ can be written as a function of the particles angular momenta and their components, i.e.

$$\vec{j}^2 - j_z^2 = \vec{j}_1^2 + \vec{j}_2^2 - j_{1z}^2 - j_{2z}^2 + 2(j_{1x}j_{2x} + j_{1y}j_{2y}) \ . \qquad (2.8.3)$$

Using relations (2.8.1-3), the rotational Hamiltonian can be written as

$$T_{ROT} = H_R + H_1 + H_2 + H_{PP} + H_{RPC} \tag{2.8.4}$$

where

$$H_R = A[\vec{I}^2 - I_z^2 - j_{1z}^2 - j_{2z}^2] \tag{2.8.5}$$

$$H_1 = A\,\vec{j}_1^2 \tag{2.8.6}$$

$$H_2 = A\,\vec{j}_2^2 \tag{2.8.7}$$

$$H_{PP} = 2A[j_{1x}j_{2x} + j_{1y}j_{2y}] \tag{2.8.8}$$

$$H_{RPC} = -2A[I_x j_x + I_y j_y] \tag{2.8.9}$$

The matrix elements of H_R, H_1, H_2 and H_{PP} have contributions only from the diagonal elements and the matrix elements of the H_{RPC} are between states differing in K.

Under the adiabatic assumption (section 2.5), the nuclear wave functions can be written as

$$\psi = D_{Rot}\chi_1\chi_2 \tag{2.8.10}$$

χ_1 and χ_2 refer to proton and neutron single particle wave functions for a doubly-odd nucleus, and are either both protons or neutrons for a doubly-even nucleus. Normalized rotational wave functions are defined in eq. (2.5.3). The single particle wave functions χ_1 and χ_2 may be expanded as

$$\chi_1 = \sum_{j_1} C_{j_1}^{\Omega_1}\, \chi_{j_1}^{\Omega_1} \tag{2.8.11}$$

and

$$\chi_2 = \sum_{j_2} C_{j_2}^{\Omega_2} \chi_{j_2}^{\Omega_2} . \qquad (2.8.12)$$

For the-Ω orbital, the phase relation between the expansion coefficients is

$$C_j^{-\Omega} = (-1)^{N+j-1/2} C_j^{\Omega} . \qquad (2.8.13)$$

For the doubly-odd case, the wave function can be written as

$$|IMK\Omega_1\Omega_2\rangle = \sqrt{\frac{2I+1}{16\pi^2}} \sum_{j_1,j_2} C_{j_1}^{\Omega_1} C_{j_2}^{\Omega_2} [D_{MK}^I \chi_{j_1}^{\Omega_1} \chi_{j_2}^{\Omega_2} + (-)^{I-j_1-j_2} D_{M-K}^I \chi_{j_1}^{-\Omega_1} \chi_{j_2}^{-\Omega_2}] . \qquad (2.8.14)$$

For the doubly-even case, because of the identical particles, the wave functions are further anti-symmetrized and can be written as

$$|IMK\Omega_1\Omega_2\rangle = \sqrt{\frac{2I+1}{16\pi^2}} \sum_{j_1,j_2} C_{j_1}^{\Omega_1} C_{j_2}^{\Omega_2} D_{MK}^I [\chi_{j_1}^{\Omega_1}(1)\chi_{j_2}^{\Omega_2}(2) - \chi_{j_2}^{\Omega_2}(1)\chi_{j_1}^{\Omega_1}(2)] + (-1)^{I-j_1-j_2} D_{M-K}^I [\chi_{j_1}^{-\Omega_1}(1)\chi_{j_2}^{-\Omega_2}(2) - \chi_{j_2}^{-\Omega_2}(1)\chi_{j_1}^{-\Omega_1}(2)] . \qquad (2.8.15)$$

Using these wave functions, the matrix elements of various parts of T_{ROT} are:

$$E_R = \langle IMK\Omega_1\Omega_2|H_R|IMK\Omega_1\Omega_2\rangle$$

$$= A[I(I+1)-K^2-\Omega_1^2-\Omega_2^2] . \qquad (2.8.16)$$

$$E_1 = \langle IMK\Omega_1\Omega_2|H_1|IMK\Omega_1\Omega_2\rangle$$

$$= A \sum_{j_1} |C_{j_1}^{\Omega_1}|^2 \; j_1(j_1+1). \qquad (2.8.17)$$

$$E_2 = \langle IMK\Omega_1\Omega_2|H_2|IMK\Omega_1\Omega_2\rangle$$

$$= A \sum_{j_2} |C_{j_2}^{\Omega_2}|^2 \; j_2(j_2+1). \qquad (2.8.18)$$

With the application of the properties of the raising and lowering operators $I_\pm = I_x \pm iI_y$, the H_{PP} and H_{RPC} terms can be written as

$$H_{PP} = A(j_{1+}j_{2-} + j_{1-}j_{2+}) . \qquad (2.8.19)$$

$$H_{RPC} = -A(I_+j_- + I_-j_+) . \qquad (2.8.20)$$

H_{PP} has matrix elements connecting states with the same K. For the doubly-odd case,

$$E_{PP} = \langle I'M'K'\Omega_1'\Omega_2'|H_{PP}|IMK\Omega_1\Omega_2\rangle$$

$$= \langle I'M'K'\Omega_1'\Omega_2'|A(j_{1+}j_{2-} + j_{1-}j_{2+})|IMK\Omega_1\Omega_2\rangle$$

$$= A \sum_{j_1,j_2} C_{j_1}^{\Omega_1'} C_{j_1}^{\Omega_1} C_{j_2}^{\Omega_2'} C_{j_2}^{\Omega_2} \{\sqrt{(j_1-\Omega_1)(j_1+\Omega_1+1)(j_2+\Omega_2)(j_2-\Omega_2+1)}$$

$$[\delta_{\Omega_1'\Omega_1+1}\delta_{\Omega_2'\Omega_2-1} + (-1)^{I-j_1-j_2}\delta_{KO}\delta_{\Omega_1'-\Omega_1-1}\delta_{\Omega_2'-\Omega_2+1}]$$

(cont'd)

$$+ \sqrt{(j_1+\Omega_1)(j_1-\Omega_1+1)(j_2-\Omega_2)(j_2+\Omega_2+1)}$$

$$[\delta_{\Omega_1'\Omega_1-1}\delta_{\Omega_2'\Omega_2+1} + (-1)^{I-j_1-j_2}\delta_{KO}\delta_{\Omega_1'-\Omega_1+1}\delta_{\Omega_2'-\Omega_2-1}]\}. \quad (2.8.21)$$

For the doubly-even case,

$$E_{PP} = A \sum_{j_1,j_2} C_{j_1}^{\Omega_1'} C_{j_1}^{\Omega_1} C_{j_2}^{\Omega_2'} C_{j_2}^{\Omega_2} \{\sqrt{(j_1-\Omega_1)(j_1+\Omega_1+1)(j_2+\Omega_2)(j_2-\Omega_2+1)}$$

$$[\delta_{\Omega_1'\Omega_1+1}\delta_{\Omega_2'\Omega_2-1} - (-)^{I-j_1-j_2}\delta_{KO}\delta_{\Omega_1'-\Omega_2+1}\delta_{-\Omega_1-1\Omega_2'}]$$

$$+ \sqrt{(j_1+\Omega_1)(j_1-\Omega_1+1)(j_2-\Omega_2)(j_2-\Omega_2)(j_2+\Omega_2+1)}$$

$$[\delta_{\Omega_1'\Omega_1-1}\delta_{\Omega_2'\Omega_2+1} + (-1)^{I-j_1-j_2}\delta_{KO}(\delta_{\Omega_1'-\Omega_1+1}\delta_{\Omega_2'-\delta_{\Omega_2+1}}$$

$$\delta_{\Omega_1'-\Omega_2-1}\delta_{\Omega_2'-\Omega_1+1})]\} \quad (2.8.22)$$

2.9 Rotation-Particle Coupling (Coriolis Mixing)

In section 2.5, it was mentioned that the nuclear wave functions are separable, i.e. there is no interplay between the rotational and particle motion. But, for rotation-particle coupling (RPC) (commonly called Coriolis mixing), the adiabatic assumptions no longer remain valid. The result of this interaction is to change the rotational parameter and also to change the energy spacings between the various states from the I(I+1) interval rule. In single nucleon transfer reactions, the spectroscopic strength of the states populated is also affected. The quantum number K no longer remains exact.

The H_{RPC} term of the rotational Hamiltonian (equation (2.8.20) connects states differing in K by ±1. It will be seen below that the mixing is strongest for high spin states and when the Nilsson orbitals involved are from the same spherical shell model state.

The matrix elements of the H_{RPC} are

$$E_{RPC} = \langle I' M' K' \Omega_1' \Omega_2' | H_{RPC} | IMK\Omega_1\Omega_2 \rangle \delta_{K',K\pm1}$$

$$= -A\langle I' M' K' \Omega_1' \Omega_2' | I_+ j_- + I_- j_+ | IMK\Omega_1\Omega_2 \rangle \delta_{K',K\pm1} \quad (2.9.1)$$

where all the terms have been defined in section 2.8.

For the doubly-odd case, the following expressions for E_{RPC} can be derived. For $K' = (K-1)$ or $-(K-1)$,

$$E_{RPC} = A_K \sqrt{(I+K)(I-K+1)} \quad (2.9.2)$$

$$A_K = -A \sum_{j_1,j_2} C^{\Omega_1'}_{j_1} C^{\Omega_1}_{j_1} C^{\Omega_2'}_{j_2} C^{\Omega_2}_{j_2} \{(\delta_{\Omega_1'\Omega_1-1}\delta_{\Omega_2'\Omega_2}$$

$$+ (-1)^{I-j_1-j_2}\delta_{\Omega_1'-\Omega_1+1}\delta_{\Omega_2'-\Omega_2}) \sqrt{(j_1+\Omega_1)(j_1-\Omega_1+1)}$$

$$+ (\delta_{\Omega_1'\Omega_1}\delta_{\Omega_2'\Omega_2-1} + (-1)^{I-j_1-j_2}\delta_{\Omega_1'-\Omega_1}\delta_{\Omega_2'-\Omega_2+1})$$

$$\sqrt{(j_2+\Omega_2)(j_2-\Omega_2+1)} \; . \quad (2.9.3)$$

For $K' = (K+1)$,

$$E_{RPC} = A_K \sqrt{(I-K)(I+K+1)} \tag{2.9.4}$$

$$A_K = - A \sum_{j_1, j_2} C^{\Omega_1'}_{j_1} C^{\Omega_1}_{j_1} C^{\Omega_2'}_{j_2} C^{\Omega_2}_{j_2} \{\delta_{\Omega_1'\Omega_1+1}\delta_{\Omega_2'\Omega_2+1} \delta_{\Omega_2'\Omega_2} \sqrt{(j_1-\Omega_1)(j_1+\Omega_1+1)}$$

$$+ \delta_{\Omega_1'\Omega_1}\delta_{\Omega_2'\Omega_2+1} \sqrt{(j_2-\Omega_2)(j_2+\Omega_2+1)}. \tag{2.9.5}$$

Similar expressions for the doubly-even case may be derived.

For $K' = (K-1)$ or $-(K-1)$,

$$E_{RPC} = A_K \sqrt{(I+K)(I-K+1)} . \tag{2.9.6}$$

$$A_K = - A \sum_{j_1, j_2} C^{\Omega_1'}_{j_1} C^{\Omega_1}_{j_1} C^{\Omega_2'}_{j_2} C^{\Omega_2}_{j_2} \{[(\delta_{\Omega_1'\Omega_1-1}\delta_{\Omega_2'\Omega_2} - \delta_{\Omega_1'\Omega_2}\delta_{\Omega_2'\Omega_1-1})$$

$$+(-1)^{I-j_1-j_2}(\delta_{\Omega_1'-\Omega_1+1}\delta_{\Omega_2'-\Omega_2} - \delta_{\Omega_1'-\Omega_2}\delta_{\Omega_2'-\Omega_1+1}) \sqrt{(j_1+\Omega_1)(j_1-\Omega_1+1)}$$

$$+(\delta_{\Omega_1'\Omega_1}\delta_{\Omega_2'\Omega_2-1} - \delta_{\Omega_1'\Omega_2-1}\delta_{\Omega_2'\Omega_1-1}(-1)^{I-j_1-j_2}\delta_{\Omega_1'-\Omega_2+1}\delta_{\Omega_2'-\Omega_1})$$

$$\sqrt{(j_2+\Omega_2)(j_2-\Omega_2+1)}\} . \tag{2.9.7}$$

For $K' = (K+1)$,

$$E_{RPC} = A_K \sqrt{(I-K)(I+K+1)} \tag{2.9.8}$$

$$A_K = -A \sum_{j_1, j_2} C^{\Omega_1'}_{j_1} C^{\Omega_1}_{j_1} C^{\Omega_2'}_{j_2} C^{\Omega_2}_{j_2} \{(\delta_{\Omega_1'\Omega_1+1}\delta_{\Omega_2'\Omega_2} - \delta_{\Omega_1'\Omega_2}\delta_{\Omega_2'\Omega_1+1})$$

$$\sqrt{(j_1-\Omega_1)(j_1+\Omega_1+1)} + (\delta_{\Omega_1'\Omega_1}\delta_{\Omega_2'\Omega_2+1} - \delta_{\Omega_1'\Omega_2+1}\delta_{\Omega_2'\Omega_1})$$

$$\sqrt{(j_2-\Omega_2)(j_2+\Omega_2+1)}\} . \tag{2.9.9}$$

From these expressions, it can be seen that matrix elements connect bands which differ by ±1 in K. In addition, other restrictions are:

i) there should be a common quasiparticle and

ii) the Ω's of the other two particles should differ by unity.

Pairing as discussed in the section 2.7 also affects the Coriolis and the particle-particle matrix elements (Brockmeier et al., 1965). This pairing correction is known to be very small (O'Neil, 1972). It has also been found necessary to reduce the Coriolis strength by a factor (η) to reproduce the experimental results (Løvhøiden and Kanestrøm, 1972, Løvhøiden and Burke, 1973). A computer program GREATER (O'Neil, 1972) may be used to calculate the matrix elements between the various bands and the eigenfunctions, which are in turn used to calculate the perturbed cross sections (section 2.12).

2.10 The ΔN=2 Interaction

The Nilsson model, with the inclusion of the pairing and Coriolis interactions, has found application in describing the low energy excitations of many deformed nuclei. In the beginning of the rare-earth mass region (near A∿155) it was also found necessary to include the ΔN=2 interaction which mixes states from different principal harmonic oscillator shells. In section 2.6, the assumption was made that the matrix elements of the operator H_δ between states differing

in N by 2 are small compared to the average energy spacings between N and (N+2) shells. However, this assumption is not always valid. This coupling has been observed in the odd mass Sm, Gd, Dy and Er nuclei between the $1/2^+[400]$ and $1/2^+[660]$ Nilsson orbitals and the $3/2^+[402]$ and $3/2^+[651]$ Nilsson orbitals (Sheline et al., 1967, Tjøm and Elbek, 1967 and Nelson et al., 1973).

From two observable quantities, the difference in the energy of two states (ΔE) and ratio of the intensities in the single nucleon transfer reactions, the strength of the $\Delta N=2$ interaction can be calculated. Two states with unperturbed energies E_1 and E_2 interact with the matrix element V which gives rise to the difference ΔE in the energy,

$$\Delta E = \sqrt{(E_2-E_1)^2 + 4V^2} \qquad (2.10.1)$$

with

$$|V| = \frac{a}{1+a^2}\,\Delta E \ . \qquad (2.10.2)$$

The parameter a is the mixing amplitude of the two states and the square of it corresponds to the ratio of intensities in the single nucleon transfer reaction of the two states.

Anderson (1968) has deduced the values of the $\Delta N=2$ interaction $|V|$ from the experimental data of Tjøm and Elbek, (1967) and has found that these values are an order of magnitude larger than those calculated from the Nilsson model. In order to explain this discrepancy, Anderson has used a Woods-Saxon type potential well to calculate the $\Delta N=2$ matrix

elements. These calculations show that for a quadrupole deformation, the calculated magnitude of the $\Delta N=2$ matrix elements is of the same order as has been observed experimentally in ^{159}Gd. Later Kanestrøm et al. (1971) have shown that the strength of $\Delta N=2$ interaction depends strongly on the hexadecapole deformation of the Woods-Saxon potential.

2.11 Splitting Energy in Deformed Even Mass Nuclei

In section 2.4, it was stated that the two bands based upon the parallel and anti-parallel coupling between two-quasiparticle configurations in an even mass nucleus would be separated in energy by the interaction between the two unpaired nucleons. There are certain empirical rules which may be used to decide which of the two bands should lie lower in energy. The Gallagher and Moszkowski rule (1958) for a doubly-odd nucleus predicts that a 'deuteron type' of coupling of spins between a proton and neutron is favoured. Symbolically these rules are that the band which has $\Sigma = (\Sigma_1 + \Sigma_2) = 1$ would lie lower in energy than the other band which has $\Sigma = (|\Sigma_1 - \Sigma_2|) = 0$. These rules have been used successfully for predicting the ground state of many doubly-odd deformed nuclei. However, ^{166}Ho is a violation of these rules (Struble et al., 1965).

For doubly-even nuclei, Gallagher (1962) has laid down the same type of rules for identical particles, either two protons or two neutrons. These rules are applicable to the two-quasiparticle states in doubly-even nuclei. In this

case the band for which $\Sigma = (|\Sigma_1 - \Sigma_2|) = 0$ would lie lower in energy than the other band for which $\Sigma = (\Sigma_1+\Sigma_2) = 1$.

The success of these empirical rules is based upon the fact that these even mass deformed nuclei have two valence nucleons moving outside an inert tightly bound deformed core. The interaction between these two nucleons could provide information regarding the nature of the nuclear force between these fundamental particles. For a doubly-odd nucleus, this interaction is between an odd proton and an odd neutron, which is similar to the case of the deuteron, where it provides information about the short range, attractive nuclear force. In addition it is known that this force is spin dependent. Pyatov (1963) has considered a spin-dependent central potential for the nucleon-nucleon interaction in a zero range approximation of the form

$$H_{int} = -4\pi g\delta(\vec{r}_1-\vec{r}_2)[1-\alpha+\alpha\vec{\sigma}_1\cdot\vec{\sigma}_2] \quad . \qquad (2.11.1)$$

Here α determines the contribution of the spin forces. $\vec{\sigma}_1$ and $\vec{\sigma}_2$ are the nucleon spin operators, the interaction parameter g is dimensionless and is related to another commonly used parameter, W, which has dimensions of energy

$$W = g\sqrt{\frac{2\nu^3}{\pi}} \quad . \qquad (2.11.2)$$

The quantity ν is a parameter that enters into the expressions for the radial wave functions (Talmi, 1952).

The expressions for splitting energy are

$$\Delta E = -2\alpha\{A[1+(-1)^{I+N_1+N_2}\delta_{K,O}]+B\} \quad \text{(for a doubly-odd nucleus)} \quad (2.11.3)$$

and

$$\Delta E = (1-4\alpha)\{A[1+(-1)^{I+N_1+N_2}\delta_{K,O}]+B\} \quad \text{(for a doubly-even nucleus)}. \quad (2.11.4)$$

The explicit expressions for A and B are given by Pyatov (1963). In these expressions for A and B, the W is a common factor of all the terms. As a consequence, the splitting energies are proportional to αW and $(1-4\alpha)W$ for doubly-odd and doubly-even nuclei, respectively. The remaining parts of A and B are thus dependent only on the nature of two-quasiparticle states. For a doubly-odd nucleus, only the spin forces contribute to the splitting energy, whereas for a doubly-even nucleus, the splitting energy is due to Wigner forces, while the spin forces act only to decrease its magnitude.

The program SPLIT (Cheung, 1975) has been used for the calculation of the splitting energies for various two-quasiparticle configurations in ^{154}Gd and ^{152}Eu. In this program the parameters α, W and the expansion coefficients, $C_{j\ell}$ are required.

2.12 Cross Section Calculations

Elbek and Tjøm (1969) have given an expression for the calculation of a single nucleon transfer reaction cross section from an odd target with the ground state I_i, K_i leading to a level I, K:

$$\frac{d\sigma}{d\Omega} = \sum_{j,\ell} \langle I_i j K_i \Delta K | IK\rangle^2 g^2 P^2 C_{j\ell}^2 N \sigma_{j\ell}(0). \quad (2.12.1)$$

Here j and ℓ are the total and orbital angular momenta respectively, and ΔK is the projection quantum number of the transferred particle. The factor $g^2 = 2$ only when two particles in an identical orbital combine to $K = 0$, e.g. the ground state band in a doubly-even nucleus, otherwise it is unity. For a general case P^2 is U^2 (emptiness factor) for a stripping reaction or V^2 (fullness factor) for a pick-up reaction. For the ground state band, however, these factors are V^2 and U^2 for stripping and pick-up reactions respectively. The reasoning for this has been discussed by Burke and Elbek (1967). The $C_{j\ell}$'s are expansion coefficients and are obtained from the Nilsson model (section 2.6). The normalization factor N and the single particle cross sections $\sigma_{j\ell}$, are discussed in the next section.

DWBA Calculations

The single particle cross sections $\sigma_{j\ell}(\theta)$ contain all the kinematics and angular dependence of the cross sections. These cross sections have been obtained from DWBA calculations using the computer code DWUCK (Kunz, 1969).

These single particle cross sections have been calculated under the following basic assumptions:

1) The interaction of the reaction is direct, i.e. the core nucleons are undisturbed in this process.
2) The projectile is moving in the average potential generated by the nucleons in the target. An optical model potential is considered which reproduces the elastic scattering of

the incident particle from the target nucleus.

3) A particle is transferred to a single particle orbital in the target; the rest of the target is assumed to be unaffected by this interaction. Finally, the scattered particle moves away from the residual nucleus.

In addition to the effects of the optical potential, the projectiles and the scattered particles are also influenced by the Coulomb potential of the form:

$$V_c = \frac{Ze^2}{2R}\left[3 - \left(\frac{r}{R}\right)^2\right] \qquad r \leq R$$

$$= \frac{Ze^2}{r} \qquad r > R$$

and $$R = r_{oc} A^{1/3} , \qquad (2.12.2)$$

where r_{oc} is the Coulomb charge radius. Z and A are the nuclear charge and mass number respectively and e is the electronic charge.

The optical potential used is of the form

$$V_{opt} = V_0 f(r,r_0,a) + i\{W_0 f(r,r_0',a') + 4W_D \frac{d}{dr} f(r,r_0',a')\}$$

where $f(r,r_0,a)$ stands for a Woods-Saxon well shape:

$$f(r,r_0,a) = \left[1 + \exp\left(\frac{r - r_0 A^{1/3}}{a}\right)\right]^{-1} . \qquad (2.12.3)$$

The parameter a is the diffuseness of the nuclear surface at radius $r_0 A^{1/3}$, where r_0 is the well radius. V_0 and W_0 are the volume potential terms for the maximum depth of the real and imaginary parts of the Woods-Saxon potentials. W_D is

the surface imaginary potential term.

The bound particle is further affected by the spin-orbit force and the potential for the particle is

$$V_{bound} = V_{opt} + V_{SO}$$

$$V_{SO} = - V_0 \frac{\lambda}{45.2} \frac{1}{r} \frac{d}{dr} f(r,r_0,a) \vec{\ell} \cdot \vec{s} \ . \qquad (2.12.4)$$

λ is a parameter used to describe the nuclear spin-orbit splitting.

In some of the calculations the non-local correction factors suggested by Kunz (1969) were used. The optical model parameters employed in the DWBA calculations for the neutron and proton transfer reactions are shown in tables 2.1 and 2.2, respectively. The normalization constants (N) used for various reactions are also included in these tables. These parameters are very similar to those used in the study of the neighbouring mass nuclei by these reactions (Christensen et al., 1969, Burke et al., 1973, Burke and Waddington, 1972).

The effects of indirect processes in the single nucleon transfer reactions have been considered by some authors (Ascuitto et al., 1972). These effects are known to be very serious only for those cases where the transitions involved are rather weak. In the present study no attempt has been made to consider these multi-step processes.

The cross sections are greatly modified when mixing effects, either in the target ground state or in the final states, are present. In such cases the theoretical cross

Table 2.1

Optical model parameters used in DWBA calculation for the (d,t) and (^{3}He,α) reactions

		V_o (MeV)	r_o (fm)	a (fm)	W_o (MeV)	$4W_D$ (MeV)	r_o' (fm)	a' (fm)	λ	r_{oc} (fm)
				(d,t) (Beam Energy = 12 MeV, N = 3.33)						
	d	- 91.48	1.15	0.925	0.	99.2	1.344	0.579	0.	1.15
	t	-154.	1.1	0.75	0.	48.	1.4	0.65	0.	1.10
bound neutron		a	1.25	0.65					8.	
				(^{3}He,α) (Beam Energy = 24 MeV, N = 26)						
	^{3}He	-175.	1.14	0.723	-17.5	0.	1.6	0.81	0.	1.4
	α	-206.	1.41	0.519	-25.8	0.	1.41	0.519	0.	1.3
bound neutron		a	1.25	0.65					8.	

: adjusted to reproduce the neutron separation energy.

Table 2.2

Optical model parameters used in DWBA calculations for the (^{3}He,d) and (α,t) reactions

	V_o(MeV)	r_o(fm)	a(fm)	W_o(MeV)	$4W_D$(MeV)	r'_o(fm)	a'(fm)	λ	r_{oc}(fm)	β [b]
				(^{3}He,d) (Beam Energy = 24 MeV, N = 4.42)						
^{3}He	-175.	1.14	0.723	-17.5	0.	1.6	0.81	0.	1.4	0.25
d	-111.	1.05	0.859	0.	70.8	1.24	0.794	0.	1.25	0.54
bound proton	a	1.24	0.65					6.	1.25	0.85
				(α,t) (Beam Energy = 27 MeV, N = 57)						
α	-200.	1.4	0.6	-20.	0.	1.4	0.6	0.	1.3	0.2
t	-200.	1.4	0.6	-50.	0.	1.4	0.6	0.	1.3	0.25
bound proton	a	1.25	0.65					8.	1.25	0.85

a: adjusted to reproduce the proton separation energy

b: non-local parameter (Kunz, 1969).

sections were calculated using the modified form of equation (2.12.1):

$$\left(\frac{d\sigma}{d\Omega}\right)_{-} = \sum_{j,\ell} N\{\sum_{n} a_n g_n \langle I_i j K_i \Lambda K^{(n)} | I K^{(n)} \rangle P_n C_{j\ell}^{(n)} \sqrt{\sigma_{j\ell}(0)}\}^2 \quad (2.12.5)$$

where the a_n's are the appropriate mixing amplitudes.

2.13 Identification and Assignment of Levels

Since the number of levels populated in these reactions was very large, identification and assignments have not been very straightforward. In some cases identification has been aided by knowledge from previous studies of these nuclei. However, many of the levels populated in the present work have not been previously studied. In the present case, the following general scheme for assignments has been used. Additional details have been discussed in sections 5 and 6.

1) In the identification of two-quasiparticle states, one of the orbitals involved must be that of the target ground state and the other one is the transferred orbital. Only those Nilsson orbitals have been considered for which the states have been well established in the neighbouring odd mass nuclei.

2) If the Nilsson orbital has a large expansion coefficient $C_{j\ell}$ for a given j and ℓ value, the reaction cross sections to a state based upon that orbital, should show the characteristic ℓ-value. The ℓ-value of the transferred particle could be obtained from the angular distribution

to that level. The other method for deduction of the ℓ-value is from the ratio of cross sections of a level in the (^{3}He,α) to (d,t) reactions for a neutron state and a similar ratio for the (^{3}He,d) to (α,t) reactions for a proton state.

3) By using the Nilsson model and single particle cross sections, the relative intensities to the various members in a band follow a definite pattern or 'finger-print', which is characteristic of the intrinsic states on which the rotational band is based. Comparison of these calculated finger-prints with the population of the observed levels leads to the identification and thus the assignment of these levels to a band.

4) The energies of the various members of a band are compared with the I(I+1) energy rule, to check for the rotational nature.

5) For a well behaved rotational band, the cross sections to all the states in a band are summed and compared with a similar summation in the other band based upon the same configuration. If the mixing is negligible then these two values should be the same. Further, in some of the cases, the total strength in the two bands could be related to the total observed strength in the odd mass nuclei studied by the same reactions.

6) When both the bands belonging to the same Nilsson configurations are identified, the validity of these assign-

ments is checked with the Gallagher-Moszkowski (1958) and Gallagher (1962) rules for coupling of spins in doubly-odd and doubly-even nuclei, respectively. On a quantitative basis, this is further checked on the basis of splitting energy calculations.

7) The independent assignments thus made are checked with any previous results for the same nucleus.

CHAPTER 3

EXPERIMENTAL DETAILS

The basic equipment required for the nuclear reactions studies were: i) an accelerator capable of producing stable beams of high energy deuterons, ^{3}He and ^{4}He particles, ii) thin, enriched targets of ^{155}Gd, ^{153}Eu and ^{151}Sm, iii) a high resolution spectrograph and (iv) nuclear emulsion plates.

The experiments were done at the Tandem Accelerator Laboratory of McMaster University which is well equipped with a 9 MV FN tandem Van de Graaff accelerator and a split-pole Enge magnetic spectrograph with large solid angle and high resolving power (Spencer and Enge, 1967).

3.1 FN Tandem Van de Graaff Accelerator

The FN tandem Van de Graaff accelerator is capable of producing stable beams, controllable over a wide range of particle energies, being intense and homogeneous in energy. The main components of the accelerator are the negative ion source, the high voltage system and the beam transport system. The negative ion source is comprised of a duoplasmatron which generates positive ions that are focused into a beam and passed through an electron-adder canal. The negatively charged

ions emerging from the canal pass through a magnetic field to remove unwanted ions and are focused, steered and injected into the high voltage section. The high voltage system is situated inside a large tank containing a pressurized insulator gas, SF_6. The negative ions are accelerated to the high voltage terminal which can be maintained at a positive potential of up to 9 MV. At the terminal the negative ions lose their electrons by stripping collisions with a thin carbon foil. Thus the beams of negative ions become positively charged and the ions experience an additional acceleration away from the terminal. The beam is then defined by a set of object slits and analyzed by a 90° magnet which selects the positive ions of a particular mass, energy, and charge for transmission through a set of image slits. The beam currents on the image slits together with an improved feed back mechanism are used to stabilize the terminal voltage (Cairns 1972).

A multi-port switching magnet is used to direct the beam to one of the experimental areas, in the present case to an Enge magnetic spectrograph.

3.2 The Enge Magnetic Spectrograph

The details of the Enge spectrograph have been described by Spencer and Enge (1967). The features of such a spectrograph are summarized as follows: a fairly large solid angle of acceptance $\sim$ 9 msr, second order focussing over a large momentum range of $p_{max}/p_{min} \approx 2.8$ (corresponding to the energy range of

$E_{max}/E_{min} \gtrsim 8$) and ability to compensate for kinematic broadening. Figure 3.1 shows the paths of the reaction products in the magnetic field of this spectrograph.

This spectrograph has two separate pole pieces enveloped by a single coil. The purpose of the split between the poles is to provide second order focussing over a broad range of energies. The split pole pieces and the non-normal entry and exit angles of the trajectories into the magnetic fields provide enough design parameters that second order aberrations are eliminated, while the desired dispersion and magnifications are maintained. The Enge spectrograph at McMaster University has a maximum radius of curvature of $\sim$ 90 cm, the energy dispersion is approximately 1 keV/mm/MeV of particle energy. The horizontal magnification at the focal plane is about one half. Vertical focussing also exists, the main purpose of this is to increase the solid angle. In the vertical direction the particles are focussed over about a centimeter at the focal plane, making tracks easy to count in nuclear emulsions. The spectrograph as a whole can be easily rotated about the target chamber such that the reaction products from the angles 0° to 150° may be analyzed. When a large solid angle spectrograph is used the energy of a particle entering one side of the aperture is different from the energy of the particle entering on the opposite side. This difference is due to the recoil energy of the target nucleus. This gives rise to the so called kinematic broadening

Figure 3.1

Outline of the Enge Split-pole Spectrograph, showing the magnet pole faces, and some particle trajectories.

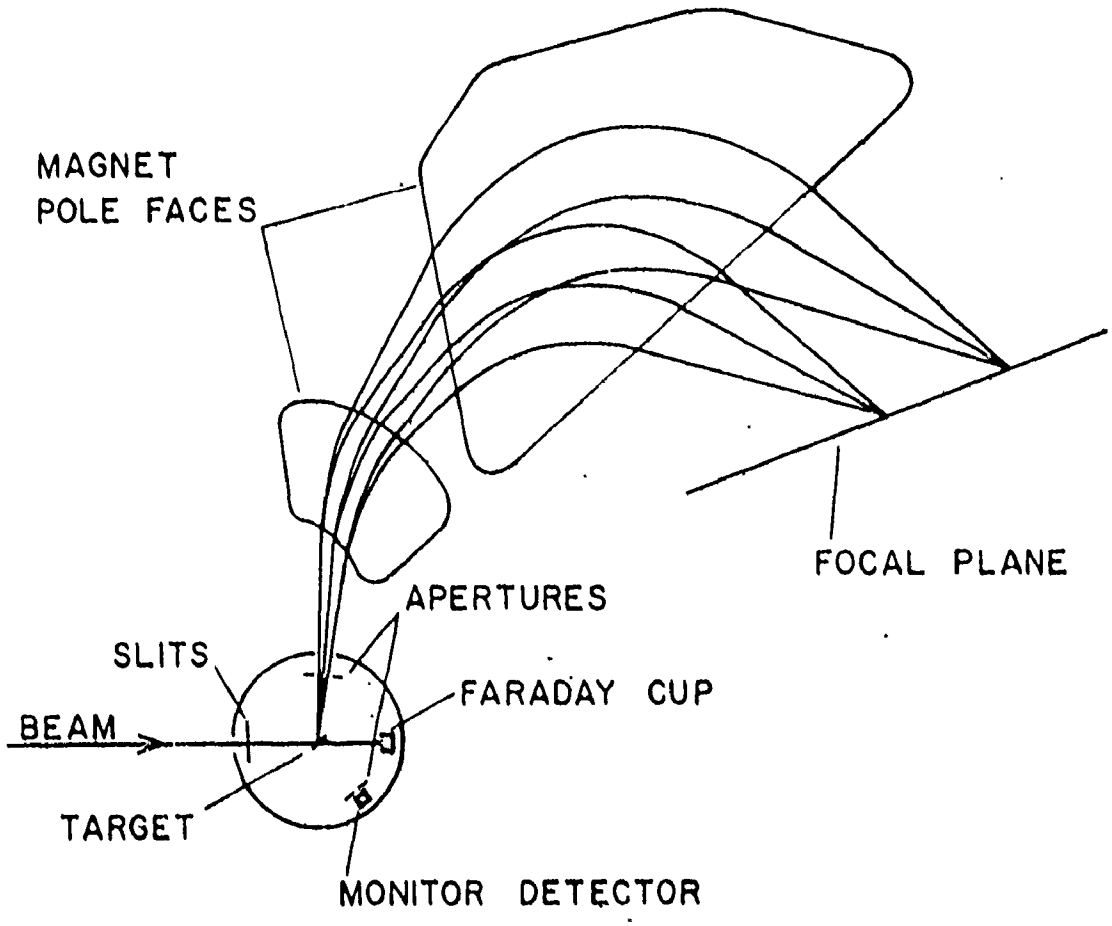
MAGNET
POLE FACES
FOCAL PLANE
APERTURES
SLITS
FARADAY CUP
BEAM
TARGET
MONITOR DETECTOR

of the peaks. By shifting the focal plane along the particle trajectories, the Enge spectrograph may be used to correct for the kinematic broadening. The shift may be calculated using the known kinematics for the reaction (Spencer and Enge, 1967). If there are any light mass impurities in the target, the peaks due to these impurities are broader than those for the target nucleus, as the corrections for kinematic broadening are made only for the target nucleus. In many of the spectra, broader peaks due to lighter nuclei like carbon, oxygen, etc. can easily be recognized.

In the Enge spectrograph dispersion compensation at the focal plane may be achieved. The beam entering the analyzing magnet has an energy spread which is the product of the effects of the ion source, the straggling in the stripper foil and the voltage fluctuations of the terminal. Thus the dispersive effects of the analyzing and the switching magnets combine to produce a gradient of particle energies across the beam spot on the target. The spectrograph is located relative to the switching and the analyzing magnets such that this dispersive effect could be compensated by the spectrograph and results in a narrow image at the focal plane.

Charged particles of given mass, charge and energy have a fixed radius of curvature in a magnetic field and thus are focussed to a definite position on the focal plane. The spectrograph has been pre-calibrated to obtain a function

of plate position versus the radius of curvature of the particles in the magnetic field. Alpha particles of known energy from a thorium source are used for the calibration and the magnetic field is measured with the help of a nuclear magnetic resonance fluxmeter. Thus with a knowledge of the beam energy, ground state Q-value, type of particles, the position of the peak on the focal plane can be directly related to the excitation energy of the levels populated in a particular reaction.

3.3 Target Preparation

The technique for target preparation was similar to that described by Westgaard and Bjørnholm (1966). In this method the metallic oxides are reduced with a suitable agent and metal is collected on thin carbon foils. For the present reaction studies, targets of ^{155}Gd, ^{153}Eu and ^{151}Sm were prepared by this technique. The oxides of these enriched metals were obtained from Oak Ridge National Laboratory. Lists of the isotopic impurities in these targets are given in table 3.1. The method of preparation of these targets varied slightly in each case.

The ^{155}Gd targets

A 10 mg sample of gadolinium oxide enriched in ^{155}Gd was mixed with 18 mg of thorium metal in a small tantalum crucible. This crucible was heated in a vacuum evaporator to a temperature of 2150°C by electron bombardment. In this

Table 3.1

The isotopic composition (%) of targets

Mass Number	Targets		
	Gadolinium	Europium	Samarium[a]
147			0.89
148			0.04
149			0.16
150			2.95
151		1.24	88.86
152	<0.005		6.84
153		98.76	
154	0.01		0.25
155	99.82		
156	0.10		
157	0.07		
158	<0.01		
159			
160	<0.005		

a: also contains ^{151}Eu impurity as the decay product of ^{151}Sm

manner the oxide was reduced and the evaporated gadolinium metal was condensed onto carbon foils mounted on aluminum frames. These frames, which were 1" square with a one cm hole in the centre, were suitable for mounting in the scattering chamber. In the $^{155}Gd(d,t)^{154}Gd$ experiments, the peaks due to thorium impurities occurred in some of the spectra.

The ^{153}Eu targets

These targets were prepared by reducing the europium oxide by lanthanum metal. As the ^{153}Eu metal is easily oxidized in air, special care was taken to protect these targets. They were stored in a vacuum sealed dessicator.

The ^{155}Gd and ^{153}Eu line targets

Line targets of ^{155}Gd and ^{153}Eu were prepared with the idea to reduce the effective beam spot size at the target site and thus to improve the resolution. These targets were made by putting a mask with a $\frac{1}{2}$ mm opening, between the crucible and the carbon foils, so that the metal should only be deposited on a $\frac{1}{2}$ mm wide line.

The radioactive targets of ^{151}Sm

^{151}Sm is a radioactive isotope (half life $\simeq$ 90 years). These targets have already been made and used in this laboratory (Nelson, 1972, Gadsby, 1972). Nelson has discussed in detail the preparation of these radioactive targets. Those targets used in the present study were about 60 $\mu g/cm^2$ thick

deposited on a carbon backing of 100 μg/cm^2. Thicker backings were used in order to provide more strength and thus avoid breaking and radioactive contamination of the scattering chamber.

3.4 Monitoring and Detection of the Reaction Products

The reaction takes place in a scattering chamber and the number of charged particles entering a Faraday cup gives the intensity of the incident beam and is monitored remotely in the control room. A Si(Li) particle detector is also placed to detect elastically scattered particles from the target. The particle detector spectrum is monitored on an oscilloscope during the exposures.

The (Z=1) reaction products, the tritons from the (d,t) and (α,t) reactions and the deuterons from the (^{3}He,d) reaction were momentum analyzed by the Enge magnetic spectrograph and detected with 50 μm thick Kodak NTB nuclear emulsions. The alpha particles from the (^{3}He,α) reaction were recorded with the less sensitive Ilford K minus 1 emulsions. This emulsion avoids a large background due to deuterons with the same magnetic rigidity $\sqrt{2M}/Z$ as the alphas.

These nuclear emulsions were on a glass backing about 10" in length and 1" in width. As the dispersion in the (d,t) reaction was less than the other reactions, two plates were required to record the spectrum up to 2.8 MeV. The charged particles produced in the other competing reactions

were stopped from reaching the emulsion by covering these plates with suitable absorbers. Aluminum absorbers of thicknesses 0.05 to 0.1 mm were used in the (d,t) reaction. In the (^{3}He,α) and (^{3}He,d) exposures, the emulsions were covered with 0.25 and 0.55 mm thick aluminum absorbers respectively, to stop the tritons produced in the (^{3}He,t) reaction. While in the (α,t) exposures a 0.1 mm aluminum absorber was used so that the emulsion should not be exposed to recoiling carbon ions from the target or to singly charged ^{4}He$^+$ particles.

The exposed NTB plates were developed for 10 minutes in the freshly prepared Kodak D-19 developer and fixed for 40 minutes in the fixer at 20°C. K minus 1 plates were developed and fixed for a somewhat longer time. The plates were scanned in $\frac{1}{4}$ mm wide strips across the plate width under a specially constructed travelling microscope with a magnification of 400 times. The number of particle tracks per strip were recorded. The position of the peak corresponds to the energy of the particle group or in turn to the energy of a level in the final nucleus. The integrated number of tracks in the peak gives the intensity by which the level is populated in that reaction.

3.5 Considerations for Obtaining Good Energy Resolution

In the rare earth region, the density of the levels populated in the single nucleon transfer reaction is quite large. Since the energy spectra obtained in these reactions are rather complex, there is a very genuine demand for a good

resolution experiment. In the following sections, the factors which contribute to the resolution will be discussed.

The target thickness, the beam spot size, the spread in the energy of the incident beam and the aberrations of the spectrograph are the main factors which contribute to the energy spread of the peaks in a spectrum. Any improvement in the resolution would require optimum control of all these factors.

i) The Target Thickness Effects

The thickness of the target plays a very important role in the broadening of the peaks. The effect due to target thickness can further be sub-divided: (i) the differential energy loss of the incoming and the outgoing charged particles in the target material, and (ii) straggling from electronic scattering of the charged particles. The energy loss of a charged particle in a material depends upon its mass, charge and energy. The first effect is due to the difference in the stopping power of the incoming and outgoing particles. Thus the differential energy loss by various kinds of charged particles should be calculated using the difference in the stopping power of the incoming and outgoing particles and the depth at which the reaction has occurred. The statistical nature of the slowing down process is responsible for the straggling which is a manifestation of the fact that identical particles of the same energy have different losses. In such a case the energy distribution is found to be a Gaussian and contributes to the width as $\Delta E \approx 18\ zt^{1/2}$ (keV) where z

is the charge of the particle and t is the thickness in mg/cm^2 (Enge, 1966). This expression brings out two important features: this contribution to the width is independent of the energy of the particles and is very sensitive to the charge of the particles, e.g. a doubly charged particle, say $^3He^{++}$ will contribute twice the energy spread of a singly charged triton in the same target. Since the straggling depends on the square root of the thickness, this demands an appreciable reduction in its value in order to achieve modest gains in the resolution. The effect of the target thickness on the resolution is illustrated in figure 3.2, for the $^{153}Eu(\alpha,t)^{154}Gd$ reaction. It can be seen that the straggling of the α-particles is the major contribution to the total resolution.

ii) Effect of the Beam Spot Size

The Enge magnetic spectrograph has a magnification of $\frac{1}{2}$ (Spencer and Enge, 1967). For a monoenergetic beam a spot of $\frac{1}{2}$ mm at the target site will yield a peak width of $\frac{1}{4}$ mm on the focal plane, where the reaction products are detected. Even with this advantage, the effect of the beam spot size is especially very important for the $(^3He,\alpha)$ and the $(^3He,d)$ reactions where the out going particles are emitted with fairly large energies. Thus even a $\frac{1}{4}$ mm width contributes to the resolution in a very significant way (table 3.2).

Figure 3.2

The effects of the target thickness and beam spot size on the resolution in the $^{153}Eu(\alpha,t)^{154}Gd$ reaction.

A: The differential energy loss due to incoming and outgoing particles.

B: Straggling due to the outgoing particle in the carbon backing of 10 $\mu g/cm^2$.

C: Straggling due to the incoming particle in the target material.

D: Contribution to the resolution due to the target effects A, B and C.

E: Effect of beam spot size on the resolution corresponding to $\frac{1}{2}$ mm size at the target position.
The total energy spread was obtained by adding the individual contributions in quadrature.

F: The effect of the target thickness on the exposure time.

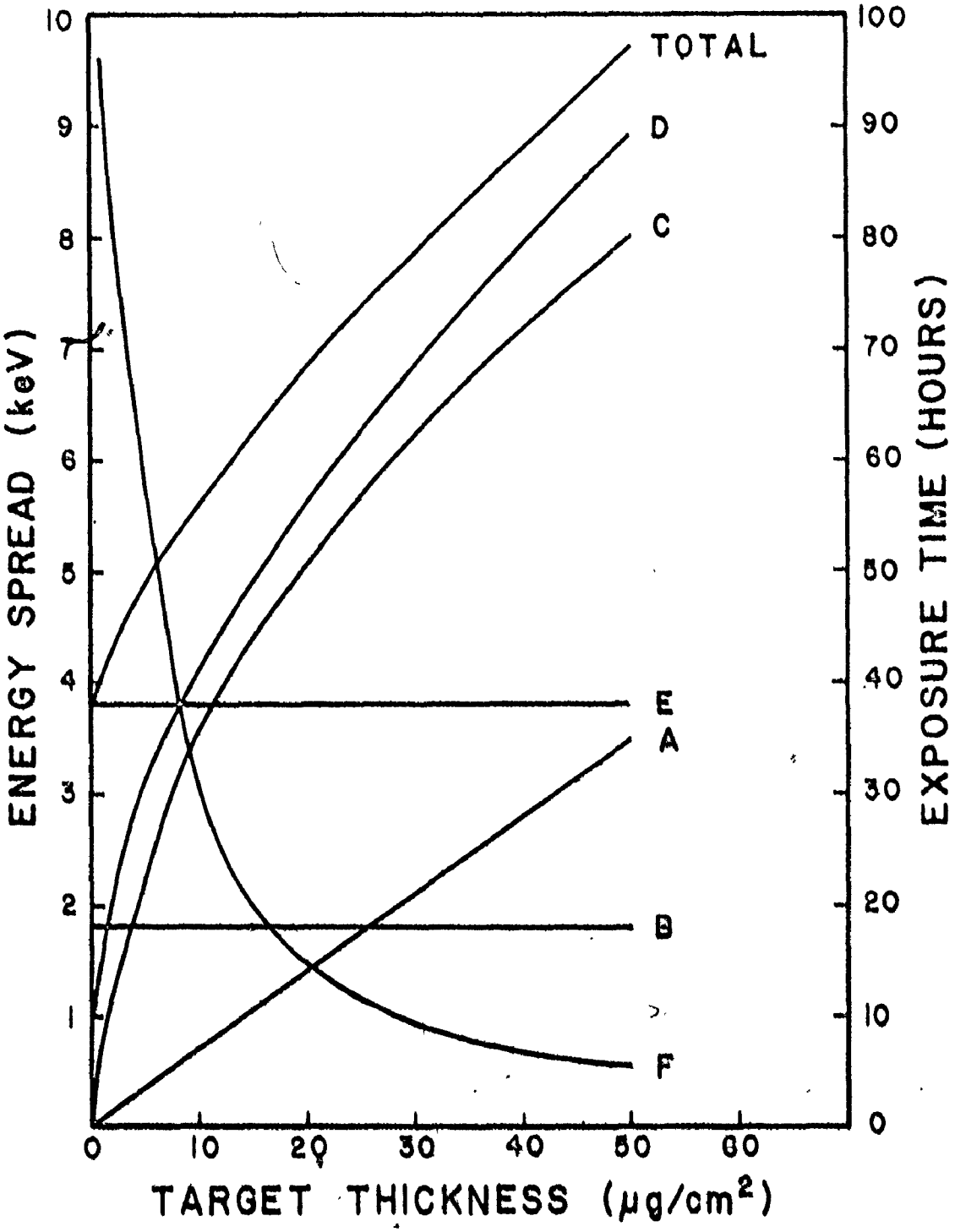
ENERGY SPREAD (keV)
EXPOSURE TIME (HOURS)
TARGET THICKNESS (μg/cm²)
TOTAL
D
C
E
A
B
F
0
10
20
30
40
50
60
1
2
3
4
5
6
7
8
9
10
70
80
90
100

Table 3.2

Estimated and experimental resolution

Reaction	Thickness ($\mu g/cm^2$) Target	Carbon backing	keV[a] A	B	C	D	E	Total	Experimental
$^{155}Gd(d,t)^{154}Gd$	20	10	0.2	1.8	2.5	3.1	3.0	3.5	5
$^{153}Eu(\alpha,t)^{154}Gd$	25	10	1.8	1.8	5.7	6.3	3.8	7.4	9
$^{153}Eu(^3He,d)^{154}Gd$	25	10	1.8	1.8	5.7	6.3	6.5	9.1	11
$^{155}Gd(^3He,\alpha)^{154}Gd$	30	50[b]	0.3	8.0	6.2	10.1	9.5	13.9	18
$^{151}Sm(\alpha,t)^{152}Eu$	60	100	4.2	5.7	8.8	11.3	3.2	11.7	14
$^{151}Sm(^3He,d)^{152}Eu$	60	100	4.4	5.7	8.8	11.3	6.0	12.8	16
$^{153}Eu(^3He,\alpha)^{152}Eu$	25	10	0.3	3.6	5.7	6.7	9.0	11.2	18

a: Meaning of various symbols is given in the caption of figure 3.2

b: These targets used in the ($^3He,\alpha$) and (d,t) reactions at 45° and 60° had only 94.4% enrichment in ^{155}Gd (Løvhøiden and Burke, 1973).

Thus it was thought that in addition to a thin target and backing, the size of the beam spot should also be reduced. The beam spot at the target is defined by a set of slits of dimensions $\frac{1}{2}$ mm by 2 mm in front of the scattering chamber, the $\frac{1}{2}$ mm dimension being in the primary focussing plane (the horizontal plane) of the spectrograph. As these slits were about 20 cm in front of the target, the spot width on the target might be larger than $\frac{1}{2}$ mm. In order to eliminate this effect a new set of horizontal slits with a separation of $\frac{1}{2}$ mm, were put at the target position. Once the beam was focussed, these slits were removed and the target was placed in this position and the beam optics were left unchanged during the exposure time. This method worked and there was a definite improvement in the resolution.

The other approach, namely the use of line targets, was also tried to reduce the effective beam spot size. In this method the active material was only $\frac{1}{2}$ mm wide in a vertical line. Even if the beam spot size was more than $\frac{1}{2}$ mm, the reaction would take place only at the active material. Thus the peak width at the focal plane would not be more than $\frac{1}{4}$ mm. Although it was quite possible that there might be some improvement in the resolution due to the beam spot size, these targets were thicker than the previous (broad targets) and no net improvement in the resolution was obtained.

iii) Other Effects

Other factors such as the stability of the beam energy are also important. The high voltage t[illegible] of the tan

accelerator at McMaster University has been improved. A stability of 1-2 KeV in the beam energy is usually achieved. This effect is relatively smaller than the previous ones (table 3.2).

The spectrograph aberrations could also affect the resolution. The Enge magnetic spectrograph corrects for the second order aberrations (Spencer and Enge, 1967). For most of the experiments the aperture sizes at the entrance to the spectrograph were kept quite small, $\sim$.8 mm, compared to the 9 mm available for this spectrograph. Although these effects are relatively quite small, they should still be taken into account. In figure 3.2 the effect of the target thickness on the exposure time is also shown. The exposure time is calculated for a typical 1 μamp incident beam on targets of different thicknesses. From the figure it is quite obvious that a thinner target definitely leads to better resolution, but on the other hand it seriously affects the rate of data collection. The selection of the target thickness is chosen in such a way as to obtain good resolution within a reasonable exposure time. For an exposure time of 10 to 15 hours and a desired resolution of 7 to 8 KeV in the (α,t) reaction, figure 3.2 suggests that the target thickness should be $\sim$ 25 $\mu g/cm^2$.

3.6 Calculation of Excitation Energies and Cross sections

The position of the peak on the plate may be used to calculate the energy of the level and the total number of

tracks in that peak corresponds to the intensity with which it is populated in a nuclear reaction. This procedure is simple only for those cases where the peaks are well resolved. For a complex spectrum, in which peaks are not completely resolved, the above method cannot be applied directly to determine the excitation energy and the intensity of the levels. A computer program called 'SPECTR' (O'Neil, 1972) was used for the determination of the centroid and the intensity of the peaks. This program fits all the peaks in the spectrum to a standard peak shape, namely a Gaussian with an exponential tail on the high excitation energy side. Using the spectrograph calibration, beam energy, ground state Q-value, the plate position is directly related to the excitation energy of the various levels populated in a reaction.

The absolute cross-sections to the levels are obtained from the intensities by normalizing to the elastically scattered particles detected in a Si(Li) detector placed in the scattering chamber at 30° to the beam direction. The output of this detector is recorded on a multi-channel analyzer during the exposure. From the solid angles of the monitor detector and of the spectrograph the elastic cross-section of the incident particles and the integrated number of counts in the detector, one may obtain the absolute cross section. The elastic cross sections were obtained from DWBA calculations which gave 105% and 116% of the Rutherford value for 24 MeV ^{3}He and 27 MeV ^{4}He particles, respectively. For the (d,t)

reaction, the value from Christensen et al. (1969) for the elastic cross section has been used, which is in excellent agreement with the DWBA calculations.

The Q-values of the various reactions leading to the final ^{154}Gd and ^{152}Eu nuclei are given in table 3.3. These Q-values are calculated from the recent atomic mass compilation data of Kayser and Johnson Jr. (1975) and also from the neutron and proton separation energy data of Meredith and Barber (1972). A comparison of the two sets of Q-values shows that the agreement is good. For ^{152}Eu, the Q-values in the (^{3}He,d) and (α,t) reactions were measured and are also shown in the same table.

Typical spectra for the various reactions are shown in figure 3.3-5 for ^{154}Gd and 3.6-7 for ^{152}Eu nuclei respectively.

Table 3.3

Q-values (MeV) of Various Reactions

Reaction	Kayser and Johnson Jr. (1975)	Meredith and Barber (1972)	Present
$^{155}Gd(d,t)^{154}Gd$	-0.1865(35)	-0.1845(25)	
$^{155}Gd(^{3}He,\alpha)^{154}Gd$	14.1351(35)	14.1366(25)	
$^{153}Eu(^{3}He,d)^{154}Gd$	2.1262(39)	2.1276(29)	
$^{153}Eu(\alpha,t)^{154}Gd$	-12.1953(39)	-12.1940(29)	
$^{153}Eu(^{3}He,\alpha)^{152}Eu$	12.010 (4)	12.019 (4)	
$^{151}Sm(^{3}He,d)^{152}Eu$	0.1055(39)	0.1039(34)	0.112(5)
$^{151}Sm(\alpha,t)^{152}Eu$	-14.2160(39)	-14.2177(34)	-14.212(4)

Figure 3.3

The spectra obtained from the $^{155}Gd(d,t)^{154}Gd$ reaction at $\theta = 30°$ and the $^{155}Gd(^{3}He,\alpha)^{154}Gd$ reaction at $\theta = 45°$. Note the change in the energy scale beyond 2100 keV. Peaks labelled G_1, G_2 and G_4 are 361, 428 and 838 keV levels respectively in ^{157}Gd, and peaks G_3 and G_4 are 119 and 214 keV levels in ^{155}Gd in the $(^{3}He,\alpha)$ spectrum.

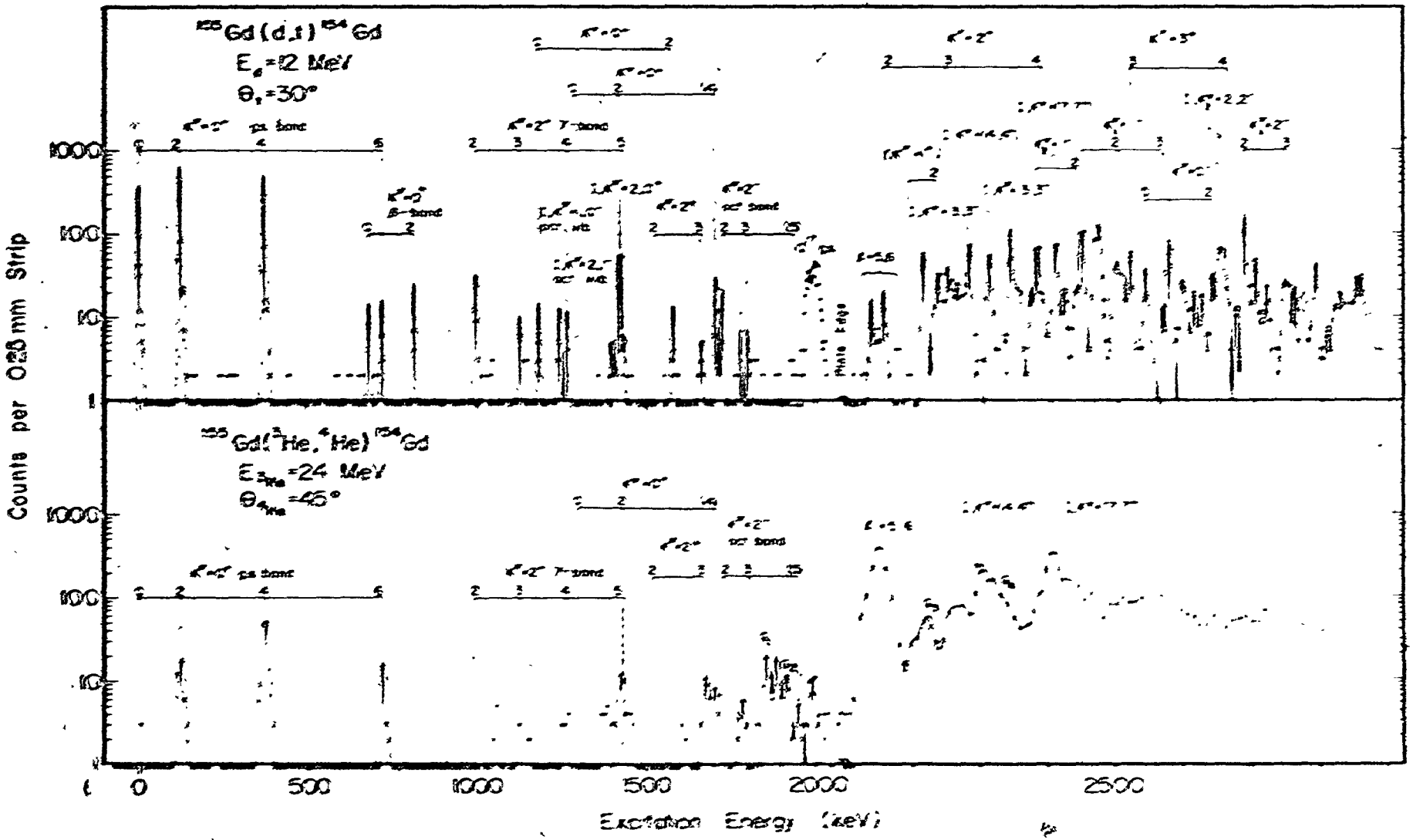
^{155}Gd(d,t)^{154}Gd
E_d=12 MeV
θ_t=30°
^{155}Gd(^{3}He,^{4}He)^{154}Gd
$E_{^3He}$=24 MeV
$\theta_{^4He}$=46°
Counts per 0.25 mm Strip
1000
100
10
1
0
500
1000
1500
2000
2500
Excitation Energy (keV)

Figure 3.4

The spectra obtained from the $^{155}Gd(d,t)^{154}Gd$ reaction at $\theta = 7.5°$ and 45°. The number of levels populated at $\theta = 7.5°$ is small compared to $\theta = 45°$. Note the change in scale beyond 2100 keV. The peaks labelled by 'G' are populated due to isotopic impurities of gadolinium.

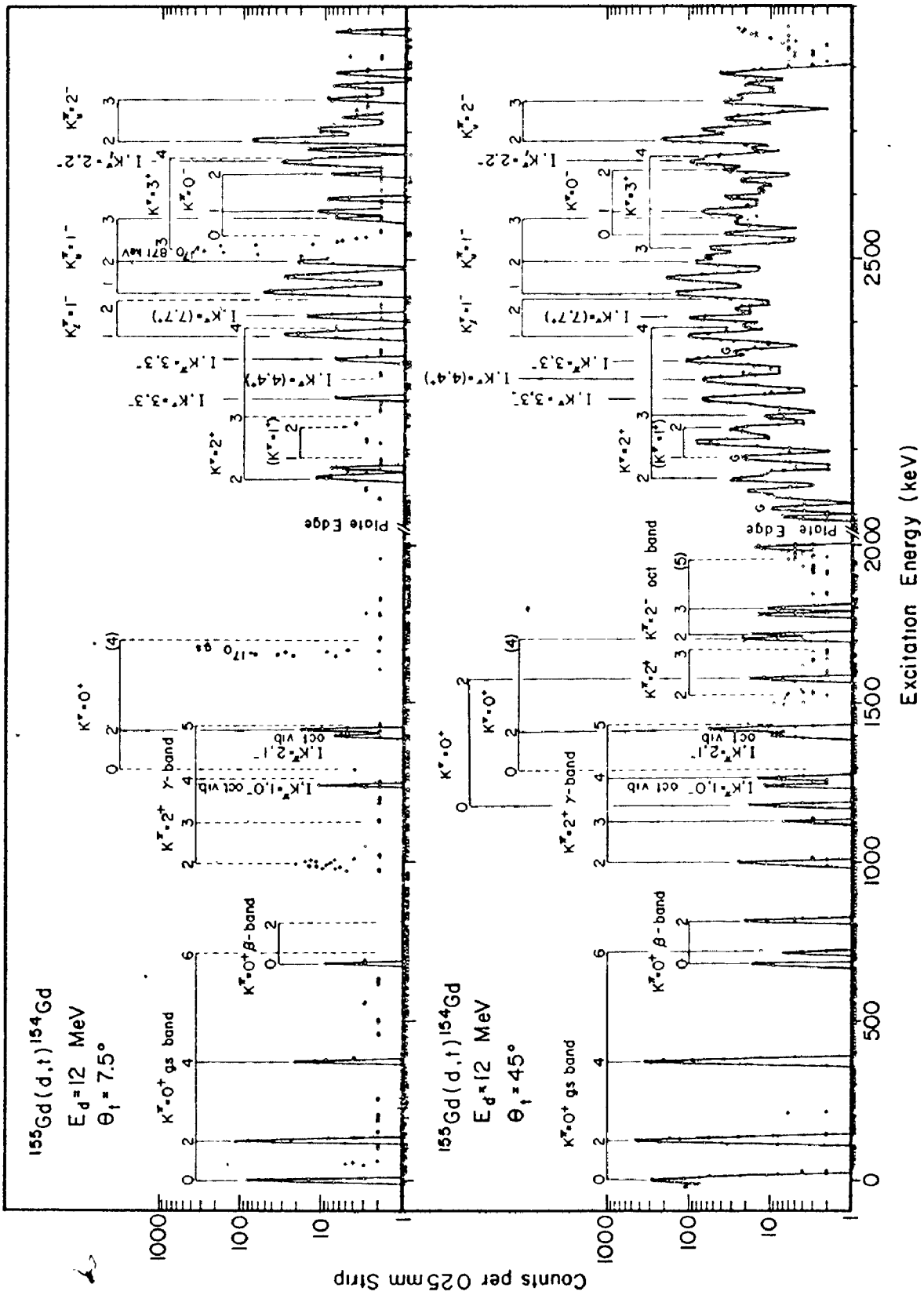

^{155}Gd(d,t)^{154}Gd
E_d=12 MeV
θ_t=7.5°
^{155}Gd(d,t)^{154}Gd
E_d=12 MeV
θ_t=45°
Counts per 0.25 mm Strip
Excitation Energy (keV)
Plate Edge

Figure 3.5

The spectra obtained in the $^{153}Eu(\alpha,t)^{154}Gd$ reaction at $\theta = 45°$ and the $^{153}Eu(^{3}He,d)^{154}Gd$ at $\theta = 30°$. Note the change in the energy scale beyond 2000 keV.

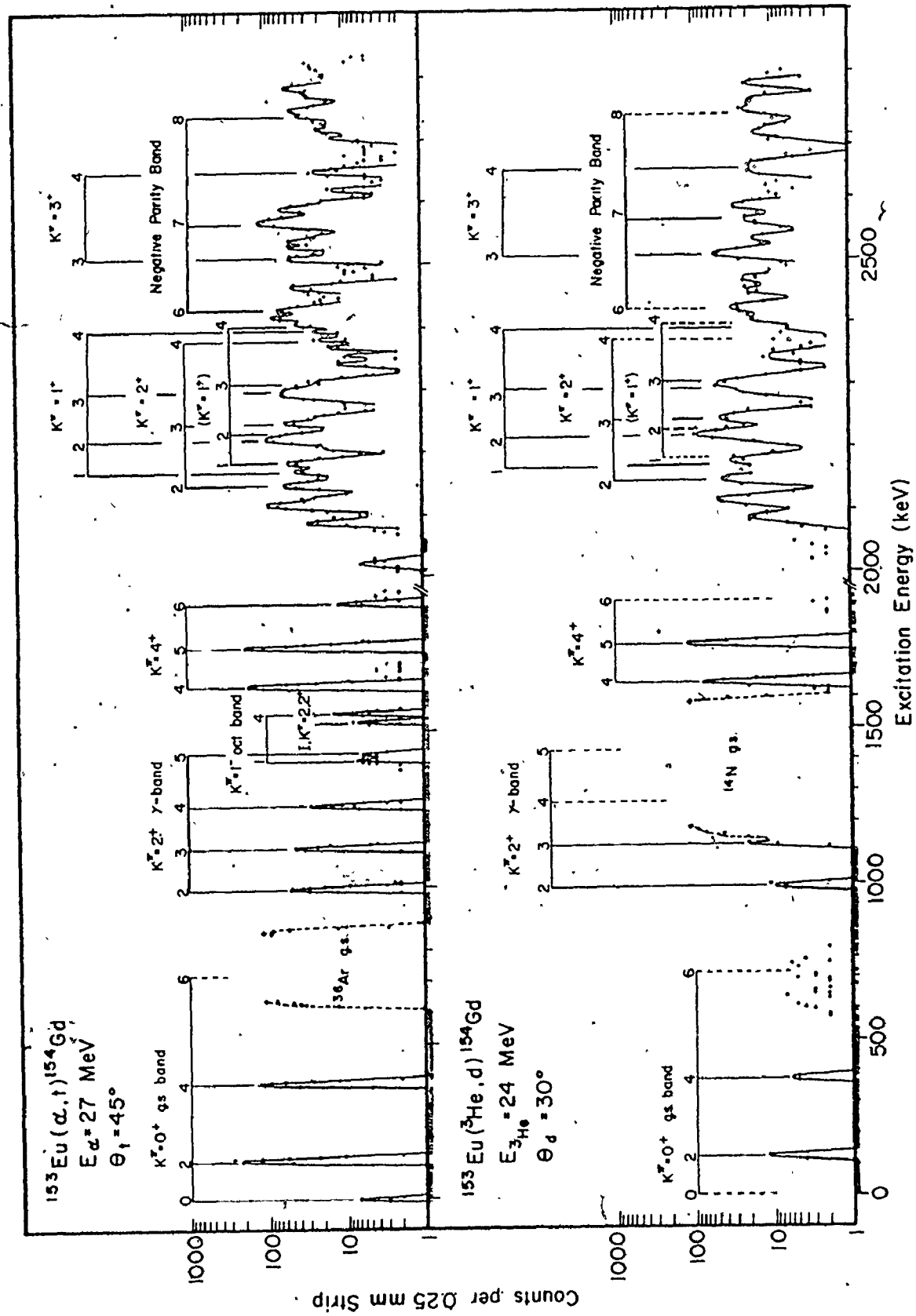
153Eu(α,t)154Gd
Eα=27 MeV
θt=45°
153Eu(3He,d)154Gd
E3He=24 MeV
θd=30°
Kπ=0+ gs band
Kπ=2+ γ-band
Kπ=1- oct band
I.Kπ=2-
Kπ=4+
Kπ=1-
Kπ=2-
(Kπ=1-)
Kπ=3-
Negative Parity Band
36Ar gs.
14N gs.
Counts per 0.25 mm Strip
Excitation Energy (keV)

Figure 3.6

The spectra obtained from the $^{151}Sm(^{3}He,d)^{152}Eu$ reaction at $\theta = 30°$ and the $^{151}Sm(\alpha,t)^{152}Eu$ reaction at $\theta = 60°$. The peak labelled 'C' is contaminated by the 700 keV level in ^{153}Eu.

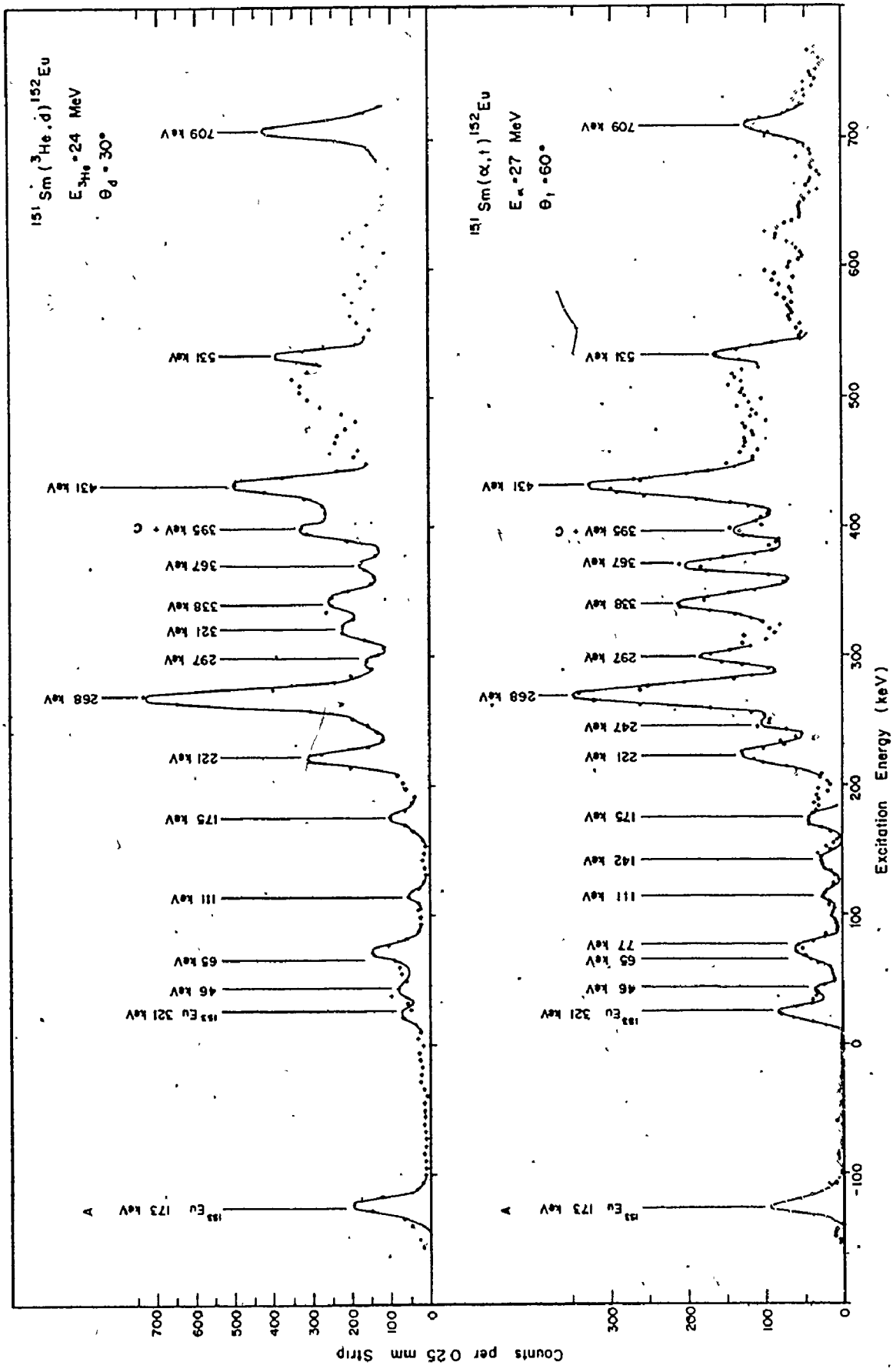
$^{151}Sm(^3He,d)^{152}Eu$
$E_{^3He}$ = 24 MeV
θ_d = 30°
$^{151}Sm(\alpha,t)^{152}Eu$
E_α = 27 MeV
θ_t = 60°
709 keV
531 keV
431 keV
395 keV + C
367 keV
338 keV
321 keV
297 keV
268 keV
247 keV
221 keV
175 keV
142 keV
111 keV
77 keV
65 keV
46 keV
^{152}Eu 321 keV
^{152}Eu 173 keV
Counts per 0.25 mm Strip
Excitation Energy (keV)

Figure 3.7

The $^{153}Eu(^{3}He,\alpha)^{152}Eu$ spectrum at $\theta = 30°$.

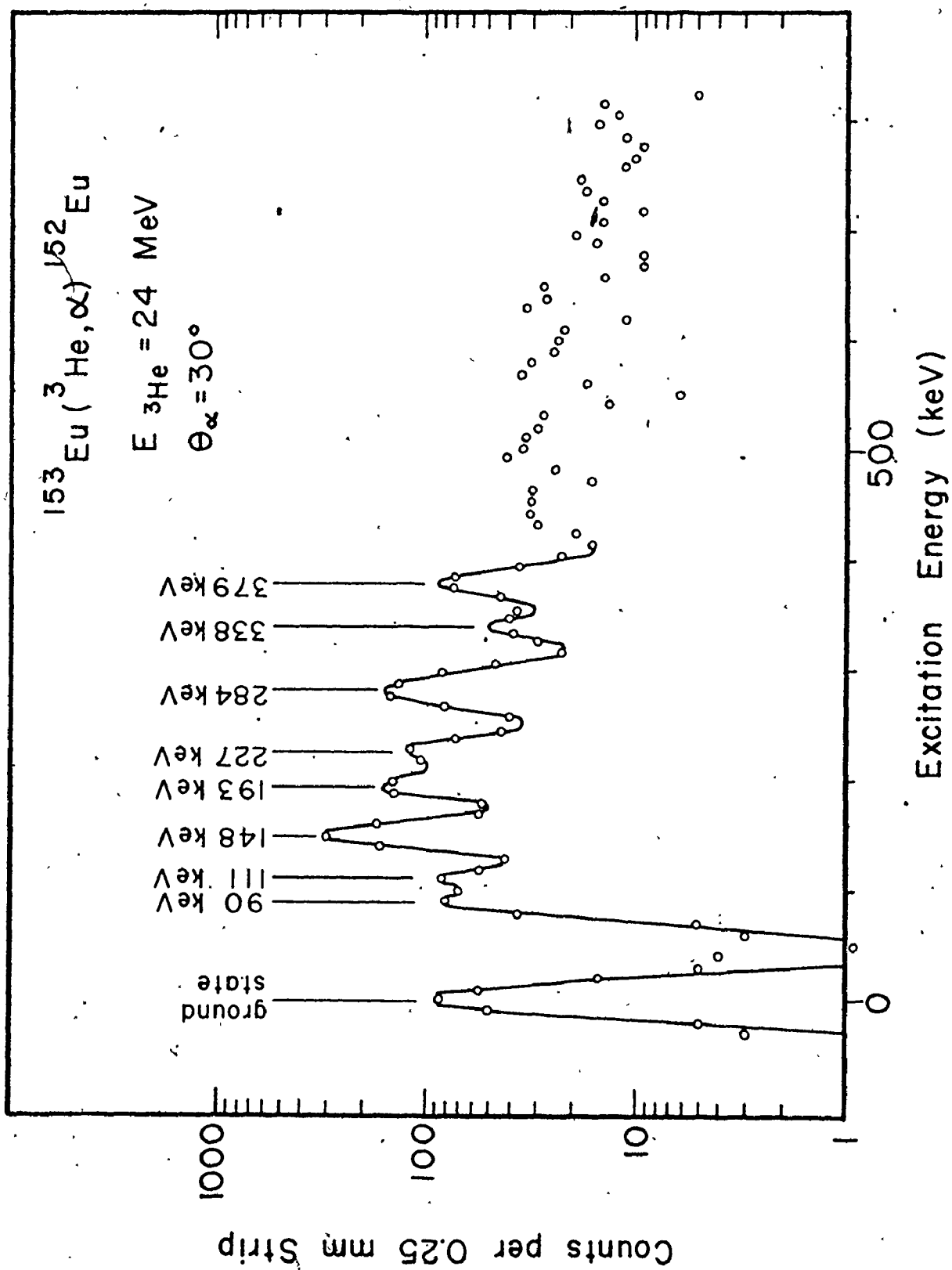
153Eu(3He,α)152Eu
E 3He = 24 MeV
θα = 30°
ground state
90 keV
111 keV
148 keV
193 keV
227 keV
284 keV
338 keV
379 keV
Counts per 0.25 mm Strip
1000
100
10
1
0
500
Excitation Energy (keV)

CHAPTER 4

EXPERIMENTAL RESULTS

4.1 Levels in ^{154}Gd

Tables 4.1 and 4.2 list the excitation energies and cross sections of the levels of ^{154}Gd populated in the neutron and proton transfer reactions respectively. The average values of the excitation energies are shown in these tables. In the (d,t) reaction, the energies of the levels below 1.5 MeV agreed within a keV with the energies obtained previously (Sousa et al., 1975). At somewhat higher excitation energies, it was noticed that the (d,t) energies are systematically higher than reported by Sousa et al. A linear correction in the (d,t) excitation energies between 1.5 and 2.8 MeV was made. This correction was 4 keV at 2.8 MeV. The excitation energies agree with the decay data within 4 keV for the well resolved peaks in the (α,t), (^{3}He,d) and (^{3}He,α) reactions.

The error in the relative values of cross sections, for the strong well resolved peaks, is less than 10% while the absolute error is about 20%. For weak peaks, cross sections $\leq$ 2 μb/sr or so, the errors in the cross sections may be as

Table 4.1

Observed energies and cross sections of neutron transfer reactions to the levels in ^{154}Gd

Excitation Energy (keV)		Cross sections (μb/sr) (d,t)								(^{3}He,α)	
(d,t)	(^{3}He,α)	7.5°	17.5°	25°	30°	45°	60°	100°	120°	45°	60°
0	0	14	33	30	38	58	58	19	11	0.2	
123	122	22	44	54	69	113	118	62	28	2	2
371	371	4	14	31	49	77	98	63	55	5	5
680		1	2	2	1	3	ob	5	ob		
718	721		1	1	1	2	ob	8	9	1	0.8
816		0.2	2	1	2	4	ob	2	1		
996		ob	3	3	4	5	6	2	1		
1049	1052	0.3	0.4	0.1	0.2		1	0.6		0.3	
1128	1128	0.3	0.3	0.8	1	1	3	0.6	0.6	0.2	0.3
1182		0.3	1	1	1	1	2	0.6	0.5		
1242		1	1	1	1	2	3	1	0.3		
1264	1260	0.3	0.6	1	1	2	3	4	5	0.4	0.3
1295		0.5	1	0.2				3			

(continued next page)

Table 4.1 (continued)

Excitation Energy (keV)		Cross sections (μb/sr)									
(d,t)	(^{3}He,α)	7.5°	17.5°	25°	(d,t) 30°	45°	60°	100°	120°	(^{3}He,α) 45°	60°
1399		2		2	0.4	2	3	3	2		
1417	1425	4	5	5	6	15	18	15	7	1	1
1432		0.3		0.5	1	0.4	0.7	un	1		
1532			0.6	0.5	0.1	1	1				
1576			1	1	1	3	3	3	0.2		
1662	1677(?)	ob	0.4	1	0.4	0.4	0.5		0.5	1	0.
1704	1705	0.3	0.3	1	3	4	5		4	1	1
1719			ob	1	2	2	6		un		
1777	1785	0.5	ob	1	1	2	2		0.6	1	0.6
1797		0.2	ob	0.3	1	3	3	1	1		
1950	1949	0.3	pe	0.2	ob	1	0.2	pe	pe	1	0.
1988	1991	pe	pe		ob	3	3	pe	pe	1	0.
2082			0.3	0.3	pe	1	ob	0.8	pe		
2122		0.3	2	0.2	0.2	2	1	2	0.3		

(continued next page)

Table 4.1 (continued)

Excitation Energy (keV)		Cross sections (μb/sr) (d,t)								(^{3}He,α)	
(d,t)	(^{3}He,α)	7.5°	17.5°	25°	30°	45°	60°	100°	120°	45°	60°
2131	2135	0.5	un	1	1	4	9	6	4	8	11
2150	2153	3	2	2	2	7	14	23	16	35	17
2169		1	1	4[d]	0.4	un	un	2	1		
2189		0.3	1	8[d]	0.3	un	3	1	un		
2209		0.3	6	6	7	20[c]	30[c]	22	10		
2230		0.6	2	2	4	7	12	10	5		
2247		2	2	1	4	3[c]	5[c]	4	un		
2266	2267	0.3	2	2	2	3	8	8	4	7	6
2277		1	6	8	9	19	37	45	27		
2299			un	2	un	6	un	12	9		
2306	2310	0.3	5	6	7	15[c]	33[c]	36	17	18	10
2322		0.3	1	1	1	un	8	13	7		
2336		1	7	12	13	30	58	65	39		
2349		0.3	2	2	3	7	un	un	6		

(continued next page)

Table 4.1 (continued)

Excitation Energy (keV)		Cross sections (μb/sr)									
		(d,t)								(^{3}He,α)	
(d,t)	(^{3}He,α)	7.5°	17.5°	25°	30°	45°	60°	100°	120°	45°	60°
2376		6	4	5	7	21	29	35	22		
2386		1	1	un	2	6	un	12	un		
2404	2406	2	8	7	9	24	32	41	28	34	20
2417		0.3	2	3	2	6	12	12	9		
2434		0.5	1	3	3	6	10	un	10		
2443		12	6	8	13	40	59	70	40		
2461		0.7	2	5	9	50^d	85^d	41	11		
2467		6	10	10	14			71	54		
2489				3	4	21	20	un	20		
2496		4	4	4	4	15	26	41	15		
2503		ob	1	un	4	6	19	un	un		
2514		ob	6	6	6	13	26	33	21		
2536		0.3	3	2	3	9	18	20	13		
2561		1	1	4	1	5	9	8	un		

(continued next page)

Table 4.1 (continued)

Excitation Energy (keV)		Cross sections (μb/sr) (d,t)								(^{3}He,α)	
(d,t)	(^{3}He,α)	7.5°	17.5°	25°	30°	45°	60°	100°	120°	45°	60°
2571		2	7	5	9	12	32	29	16		
2590		1	2	3	2	9	11	18	10		
2595		un	2	un	2	un	7	un	4		
2606		0.3	3	2	2	4	un	7	5		
2618		0.3	2	2	2	6	9	7	7		
2632		1	3	3	3	9	un	11	un		
2648		7	4	5	8	27	40	37	26		
2656		2	3	un	3	un	12	un	un		
2669		2	un	un	1	4	8	9	4		
2683		18	7	8	18	57	82	94	63		
2691		un	2	un	2	un	16	un	un		
2699		3	3	4	6	17	22	25	20		
2713		un	2	4	2	8	14^d	11	un		
2717		1	2	un	un	2		9	9		

(continued next page)

Table 4.1

Excitation Energy (keV) (d,t)	(^{3}He,α)	Cross sections (μb/sr) (d,t) 7.5°	17.5°	25°	30°	45°	60°	100°	120°	(^{3}He,α) 45°	60°
2741		1	3	6	3	9	17	19[d]	11		
2749		1	2	3	3	6	10		11		
2757		un	1	un	2	2	8	un	6		
2768		1	1	1	2	4	8	8	8		
2780			1	un	1	un	3	10	4		
2786		1	3	3	4	9	15	6	8		

c: contaminated

d: doublet

ob: obscured by impurity

pe: plate edge

un: unresolved

Table 4.2

Observed energies and cross sections of proton transfer reactions to the levels in ^{154}Gd

Excitation Energy (keV)		Cross sections (μb/sr)				
		(α,t)		(^{3}He,d)		
(α,t)	(^{3}He,d)	45°	60°	25°	30°	60°
0	0	0.9	0.4	0.1		0.1
123	123	30	18	4	5	3
371	371	18	10	2	2	1
718	718	ob		0.8	0.3	0.2
815	816	ob	0.8	ob	0.4	0.3
997	996	7	3	ob	4	2
1128	1128	6	4	ob	ob	2
1263	1264	2	2	2	ob	1
1412	1415	1	1		ob	un
1429	1429	1	un	2	ob	un
1533	1531	1	1	1	ob	un
1559	1560	1	un	0.3	ob	un
1645	1646	27	22	19	30	14

(continued next page)

Table 4.2 (continued)

Excitation Energy (keV)		Cross sections (μb/sr)				
		(α,t)		(^{3}He,d)		
(α,t)	(^{3}He,d)	45°	60°	25°	30°	60°
1770	1770	28	22	25	39	16
1913	1912	1	2	1	1	1
2025		1				
2089	2091	3	2	4	8	
2117	2116	12	13	11	18	8
2148	2146	6	6	10	15	6
2175	2177	4	7	6	12	7
2186		6	5			
2210		3				
2223	2224	12	15	16	31	13
2234		5				
2250	2250	8	9	11	17	8
2262		2	3			

(continued next page)

Table 4.2 (continued)

Excitation Energy (keV)		Cross sections (μb/sr)				
		(α,t)		(^{3}He,d)		
(α,t)	(^{3}He,d)	45°	60°	25°	30°	60°
2294	2293	8	11	14	16	12
2304	2304	6	8		13	
2317		2				
2344	2346	1		4	5	2
2373		2	2			
2386		2				
2400	2403	3		6	6	4
2411		6	15			
2420	2424	10		6	12	8
2432		8	pe			
2466	2467	5	pe	8	10	5
2513	2512	7	pe	10	20	9
2531	2535	6	pe	5	6	4
2541		4	pe			
2570	2566	15	13	6	9	7

(continued next page)

Table 4.2

Excitation Energy (keV)		Cross sections (μb/sr)				
		(α,t)		(^{3}He,d)		
(α,t)	(^{3}He,d)	45°	60°	25°	30°	60°
2578		6	7			
2594	2591	6	6	4	9	5
2605		1				
2622		1				
2652	2649	2	3	7	6	4
2707	2703	2	3		5	
2718		3				
2739		4	4			
2749	2752	5	6		6	8
2773		4	7			
2785	2782	7	8		7	
2797		3				

ob: obscured by impurity

pe: plate edge

un: unresolved

large as 50%.

The angular distributions of the reaction products have been used for the determination of the transferred ℓ-value in the (d,t) reaction. At the beam energies used (Table 1.1) the angular distributions of the (α,t) and (^{3}He,α) reactions are not very characteristic of the transferred ℓ-values. With the exception of the ℓ=0 transition, the (^{3}He,d) angular distributions show little structure for the different ℓ-values. The discussion of the (d,t) angular distributions will be presented later with the discussion of the individual levels. It should also be noted that in the study of single nucleon transfer reactions on the targets with I≠0, the transition amplitude to a particular state may have contributions from several different ℓ-values. The lack of fine structure in the angular distributions between θ = 30° and 60° has often been used to advantage by calculating a quantity R which is the ratio of the differential cross section in the (^{3}He,α) reaction to that in the (d,t) reaction or the ratio of the differential cross sections in the (^{3}He,d) and (α,t) reactions (Burke et al., 1971, O'Neil et al., 1971). The (d,t) reaction preferentially populates states by low ℓ-transfer while the (^{3}He,α) reaction populates states with high ℓ-transfer. A similar situation exists with the (^{3}He,d) and (α,t) reactions, whereas the former populates states by low ℓ-transfer, the (α,t) reaction is not very selective. Although the observed cross section ratio for targets with I≠0 gives only a weighted average of the transferred

ℓ-values, in certain cases where the contribution to the cross sections is mainly due to a single ℓ-value, this ratio could provide information regarding the transferred ℓ.

Cross section ratio plots are shown in figures 4.1 and 4.2 for the neutron and proton transfer reactions respectively. In figure 4.1 the solid lines are the calculated cross section ratios from the single particle cross sections for the $(^3He,\alpha)_{45°}$ and $(d,t)_{60°}$ reactions. These single particle cross sections were determined by DWBA calculations. For the (d,t) reaction, the most common value for the normalization constant, N = 3.33 has been used, while for the $(^3He,\alpha)$ reaction the normalization constant used is 26, very similar to that suggested by Elbek and Tjøm (1969) and Burke et al.,(1973). The observed cross section ratios to the various levels are shown with their excitation energies in figure 4.1.

In figure 4.2 the calculated cross section ratios for the $(^3He,d)_{30°}$ and $(\alpha,t)_{45°}$ reactions are shown by the solid lines for different ℓ-values. The calculated cross section ratios are obtained by DWBA calculations with the customary value of 4.42 used as the normalization constant for the $(^3He,d)$ reaction. For the (α,t) reaction a value of 57 has been used. This value is very similar to that obtained from Tippett's data for ^{153}Eu (1972). Details about the (α,t) reaction normalization constant will appear in the discussion of ^{152}Eu (section 4.2).

These plots will be used only to estimate the major

Figure 4.1

Ratios of the differential cross sections for the $(^3He,\alpha)_{45°}$ and $(d,t)_{60°}$ reactions as a function of excitation energies in keV. The solid lines represent the predicted ratio for the transfer of a neutron with a single ℓ value. The points are the observed ratios for the levels in ^{154}Gd and the numbers indicate the excitation energies.

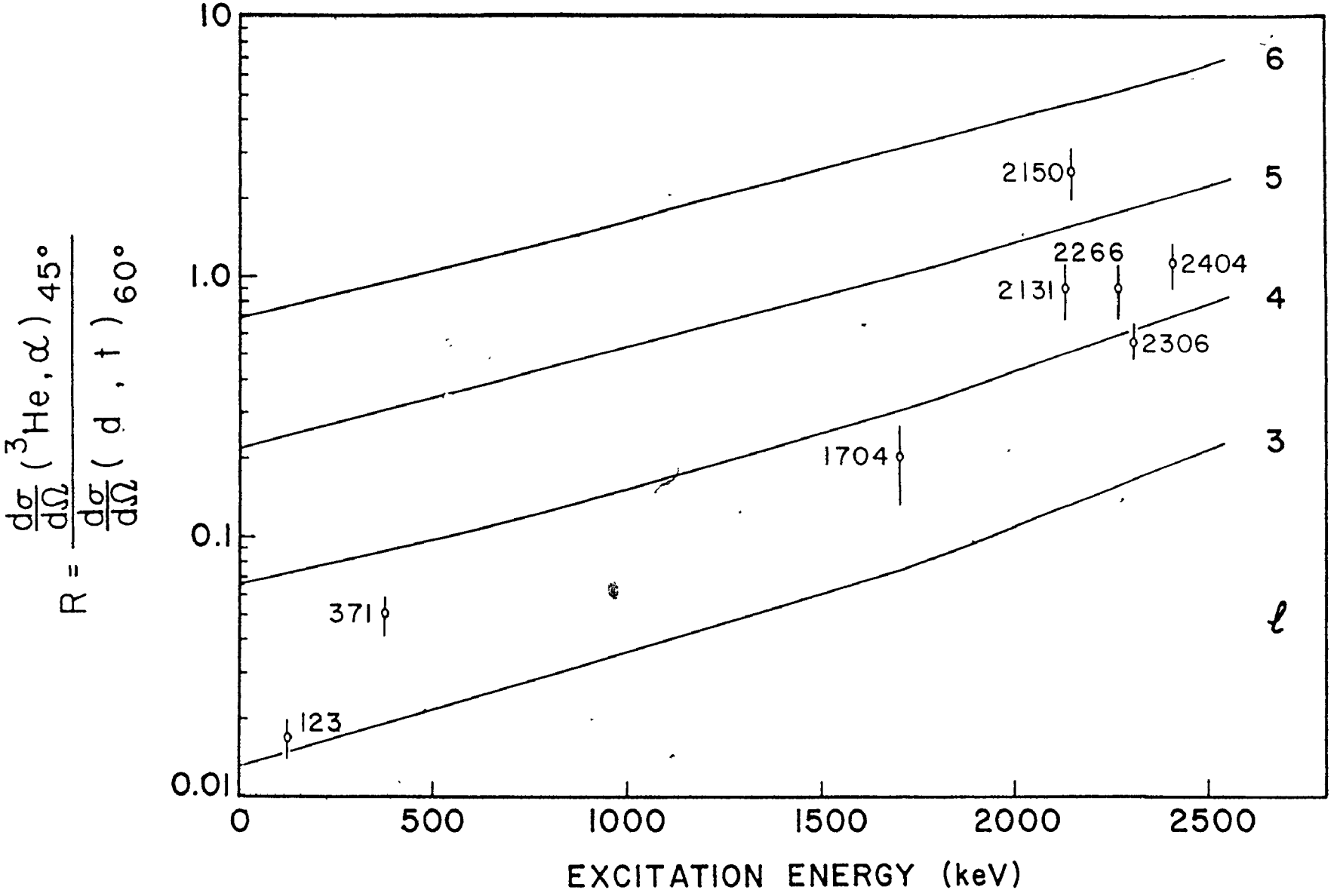
$R = \frac{d\sigma}{d\Omega}(^3He,\alpha)_{45°} / \frac{d\sigma}{d\Omega}(d,t)_{60°}$
10
1.0
0.1
0.01
0
500
1000
1500
2000
2500
EXCITATION ENERGY (keV)
6
5
4
3
ℓ
2150
2266
2404
2131
2306
1704
371
123

Figure 4.2

Ratios of the differential cross sections for the $(^3He,d)_{30°}$ and $(\alpha,t)_{45°}$ reactions as a function of excitation energies in keV. The solid lines represent the predicted ratio for the transfer of a proton with a single ℓ-value. The points are the observed ratios for the levels in ^{154}Gd and the numbers indicate the excitation energies.

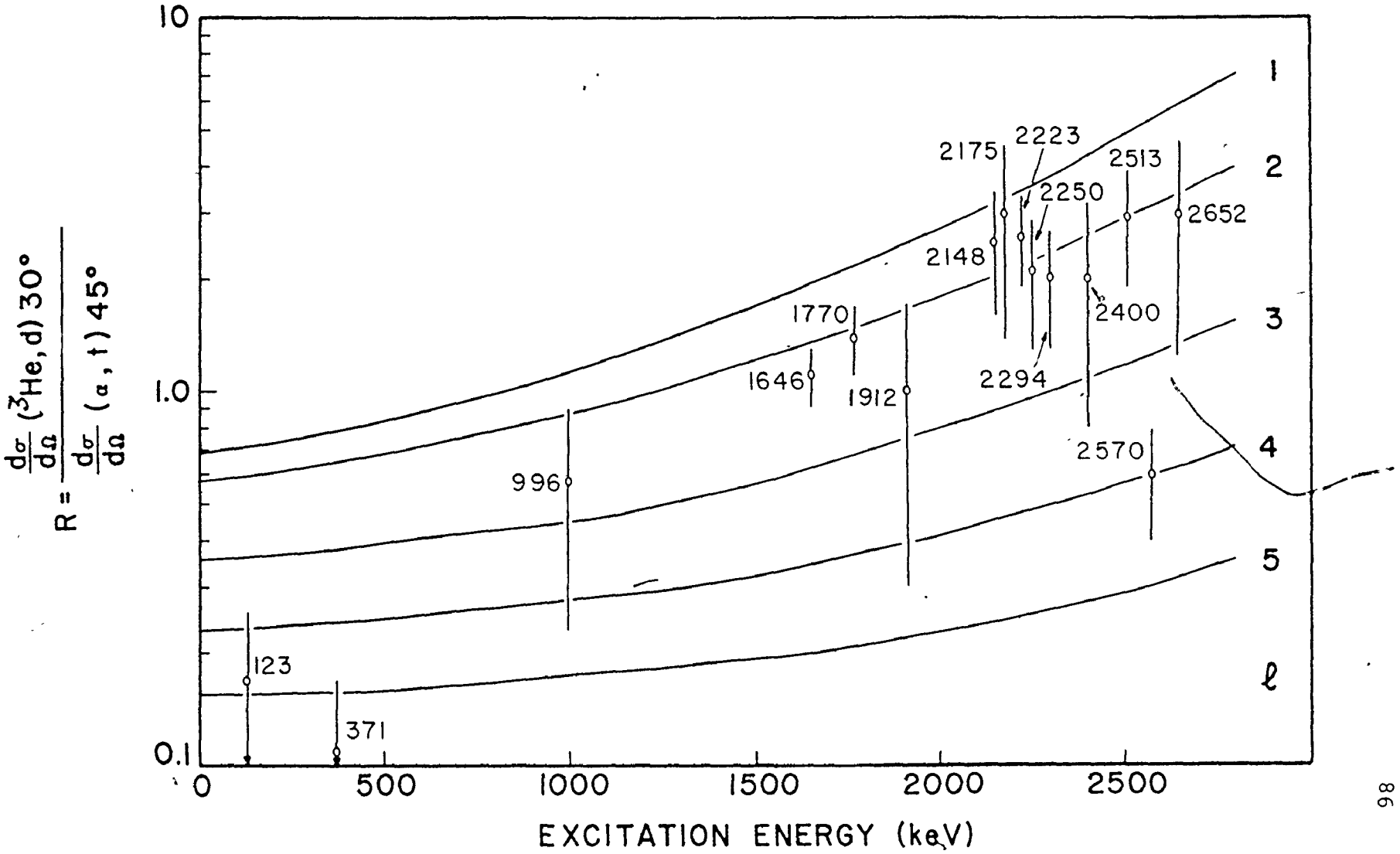
10
1.0
0.1
0
500
1000
1500
2000
2500
EXCITATION ENERGY (keV)
$R = \frac{d\sigma}{d\Omega}(^3He, d)\,30° \Big/ \frac{d\sigma}{d\Omega}(\alpha, t)\,45°$
1
2
3
4
5
ℓ
123
371
996
1646
1770
1912
2148
2175
2223
2250
2294
2400
2513
2570
2652

ℓ-component responsible for the population of a given state.

4.2 Results for ^{152}Eu

i) Q-values measured in the ^{151}Sm(^{3}He,d)^{152}Eu and ^{151}Sm(α,t)^{152}Eu reactions

In the compilation of Meredith and Barber (1972), the proton separation energy for ^{152}Eu is reported to be 5.5971(34) MeV. This value corresponds to ground state Q-values for the (^{3}He,d) and (α,t) reactions on the ^{151}Sm target of 0.1039(34) and -14.2177(34) MeV respectively. These Q-values have been used only as a guide for the approximate location of the ground state of ^{152}Eu in the (^{3}He,d) and (α,t) spectra. The sets of observed energy level differences were then compared with the previously known excitation energies (von Egidy et al., 1975) for ^{152}Eu to find the best correspondence and hence to determine the actual zero of the excitation energy scale in the ^{151}Sm(^{3}He,d)^{152}Eu and ^{151}Sm(α,t)^{152}Eu spectra (figure 3.6).

Table 3.1 shows that ^{152}Sm is a major isotopic impurity (6.84%) in the ^{151}Sm target. The Q-values for the (^{3}He,d) and (α,t) reactions on ^{152}Sm (Tippett, 1972) are about 300 keV more positive than the corresponding values for ^{151}Sm. Consequently peaks due to the levels in ^{153}Eu occurred in the (^{3}He,d) and (α,t) spectra (figure 3.6). From the excitation energy scale as determined above and the measured differences in the energies of the outgoing particle groups due to reactions on ^{151}Sm and ^{152}Sm, the differences in the ground state Q-

vales for two isotopes were obtained. From these differences and the proton separation energy of 5.8963(28) MeV (Meredith and Barber 1972) for ^{153}Eu, the ground state Q-values obtained are 0.112(5) MeV for the ^{151}Sm(^{3}He,d)^{152}Eu reaction and -14.212(4) MeV for the ^{151}Sm(α,t)^{152}Eu reaction (table 3.3). The proton separation energy for ^{152}Eu deduced from these values is 5.604(4) MeV.

ii) Levels in ^{152}Eu

Table 4.3 lists the levels populated in ^{152}Eu in the (^{3}He,α), (^{3}He,d) and (α,t) reactions. In the latter two reactions, the peaks of the reaction product groups were fitted to the previously known levels in ^{152}Eu below 321 keV (von Egidy et al., 1975). Table 4.3 also includes some of the energies and spin values of the levels known from the previous studies (von Egidy et al., 1975).

The cross section ratio plot of the $(^{3}He,d)_{30°}$ and $(\alpha,t)_{60°}$ reactions is shown in figure 4.3. For the (^{3}He,d) reaction the most common value for the normalization constant N = 4.42 has been used, while for the (α,t) reaction the value of the normalization constant has been obtained from the peak labelled 'A' (figure 3.6). This level results from the ^{152}Sm impurity in the target (table 3.1), and has been assigned as the 173 keV level of ^{153}Eu, which is the $5/2^{+}$ member of the $3/2^{+}[411]$ rotational band (Blichert-Toft, et al., 1966, Ungrin et al., 1969). This Nilsson orbital originates from the $2d_{5/2}$ shell model state and the cross section of the

Levels in ^{152}Eu

Previous[a]		(^{3}He,α)				(^{3}He,d)			(α,t)		
		(keV)	(μb/sr)			(keV)	(μb/sr)		(keV)	(μb/sr)	
(keV)	I^π		25°	30°	60°		30°	60°		60°	90°
0	3^-	0	19	30	12						
45.600	0^-					46	4	3	46	2	1
65.297	1^-					65	12	7	65	3	1
77.258	(3^-)					un			77	4	1
89.613	4^-	90	17	23	15						
111.4	(2^-)	111	13	24	9	111	3	3	111	3	
141.825	4^-								142	3	
147.87	8^-	148	57	98	35						
174.938	$(2,3)^-$					175	7	5	175	5	2
196.9	(3^+)	193	28	55	22						
221.453	(2^-)					221	26	16	221	12	3
227.7	$3(4)^+$	227	18	45	12						
246.7	3^-								247	8	3
265.7	$(3)^-$					268	53	37	268	32	10
267.6	$(3,4)$										
		284	27	59	20						
296.3						297	4		297	13	4
321.0	$(2,3)$					321	12	8		un	4
321.8	$(3,4)$										
338.4		338	10	18	11	338	10	9	338	10	3
						367	5	8	367	10	6
		379	15	32	9						
						395	16[c]	14[c]	395	7[c]	6[c]
						431	42	32	431	25	8
						531	18	18	531	9	5
						709	31	20	709	14	

a: von Egidy et al. (1975)

c: contaminated by the 700 keV level in ^{153}Eu

un: unresolved

Figure 4.3

Ratios of the differential cross sections for the $(^3He,d)_{30°}$ and $(\alpha,t)_{60°}$ reactions as a function of excitation energies in keV. The solid lines represent the predicted ratio for the transfer of a proton with a single ℓ-value. The points are the observed ratios for the levels in ^{152}Eu and the numbers indicate the excitation energies. The predicted curves have been normalized to the observed cross-section ratios of the level 'A' which is the 173 keV state in ^{153}Eu.

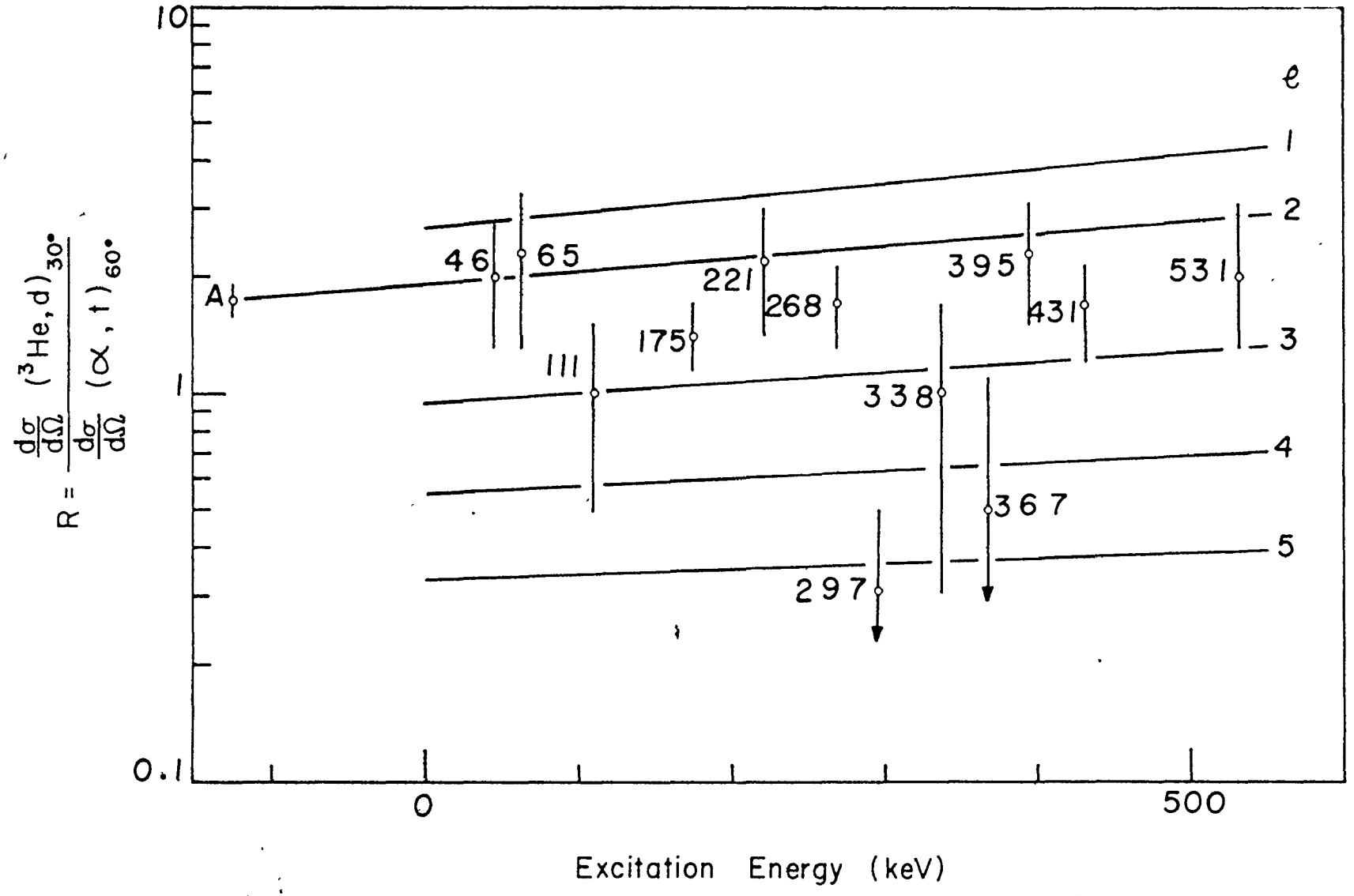
10
1
0.1
$R = \frac{\frac{d\sigma}{d\Omega}(^3He,d)_{30°}}{\frac{d\sigma}{d\Omega}(\alpha,t)_{60°}}$
e
1
2
3
4
5
A
46
65
221
268
395
431
531
175
111
338
367
297
0
500
Excitation Energy (keV)

06

I=5/2 state would be characteristic of an $\ell=2$ transition. Comparing the observed cross section ratio to that calculated with the DWBA program the normalization constant for the (α,t) reaction was found to be 57. This value is very similar to the value obtained from the data of Tippett for ^{153}Eu (1972) and is the same as was found for reactions in ^{154}Gd.

CHAPTER 5

NUCLEAR STRUCTURE OF ^{154}Gd

5.1 The Ground State Band

The ground state band of ^{154}Gd has been studied by many investigators by reaction and decay studies (Bloch et al., 1967, Meyer, 1968, Sousa et al., 1975). The ground state members have been identified up to I=18 in the ^{154}Sm(α,4n)^{154}Gd reaction (Khoo et al., 1973).

In both the neutron and proton transfer reactions the population of the ground state band is restricted to spins 0^+ to 6^+. These members show a rotational pattern corresponding to a rotational parameter of 17.1 keV. This value indicates that probably ^{154}Gd is a transitional nucleus and is not as deformed as the heavier gadolinium nuclei.

The cross sections to the ground state members populated in the single particle transfer reactions are given in table 5.1.

i) Population of the Ground State Band in the Neutron Transfer Reactions

The ground state of the ^{155}Gd target is in the $3/2^-[521]$ neutron Nilsson orbital. The transfer of a $3/2^-[521]$ neutron in the (d,t) and the (^{3}He,α) reactions would allow

Table 5.1

Cross sections (μb/sr) to the ground state band members of ^{154}Gd

Excitation Energy (keV)	I,K^{π}	Neutron Transfer Reactions		Proton Transfer Reactions	
		$(d,t)_{45°}$	$(^3He,\alpha)_{45°}$	$(^3He,d)_{30°}$	$(\alpha,t)_{45°}$
0	$0,0^+$	58	0.2		0.9
123	2,	113	2	5	30
371	4,	77	5	2	18
718	6,	2	1	<0.3	ob

ob: obscured by impurity

population of the 0^+, 2^+, 4^+ and 6^+ members. These have been identified as the ground state, 123, 371 and 718 keV levels respectively of ^{154}Gd.

In these neutron transfer reactions only the ground state (0^+) and the 6^+ members have been populated with a transfer of a pure ℓ value, namely ℓ = 1 and ℓ = 5 respectively. The 2^+ member has been populated with a mixture of ℓ =1 and 3 while the 4^+ by ℓ = 3 and 5. As the (d,t) reaction populates low ℓ values strongly, the first three members have large cross sections. The converse is true for the (^{3}He,α) reaction where high ℓ values are populated strongly.

In these reactions the transferred ℓ values of the ground state members are deduced by two different methods (i) the ratio of the cross sections of the (^{3}He,α) and the (d,t) reactions and (ii) the (d,t) angular distributions. The cross section ratio plot figure 4.1 shows that the 2^+ member has a large ℓ=3 component and the 4^+ member has a weighted average ℓ value higher than 3. The same information in a more quantitative basis is obtained from the (d,t) angular distributions. Figure 5.1 shows the angular distributions of the ground state members. In the same figure, the predicted DWBA angular distributions are also shown. These include the calculated cross sections at various angles using the appropriate nuclear structure factor $\langle I_i j K_i \Delta K | I K \rangle^2 U^2 C^2_{j\ell}$. The $C^2_{j\ell}$ values for the $3/2^-[521]$ orbital were obtained for the well parameters κ = 0.0637, μ = 0.42 and a deformation δ = 0.26 by a procedure outlined in section 2.6. Although the deformation parameter

Figure 5.1

The (d,t) angular distribution for the first four members of the ground state band in ^{154}Gd. The DWBA angular distributions along with the appropriate nuclear structure factor are shown with a solid line. The dashed angular distributions show the effect of using the $C_{j\ell}^2$ values of Tjøm and Elbek (1967) deduced from the study of $^{156}Gd(d,t)^{155}Gd$ (see text for details).

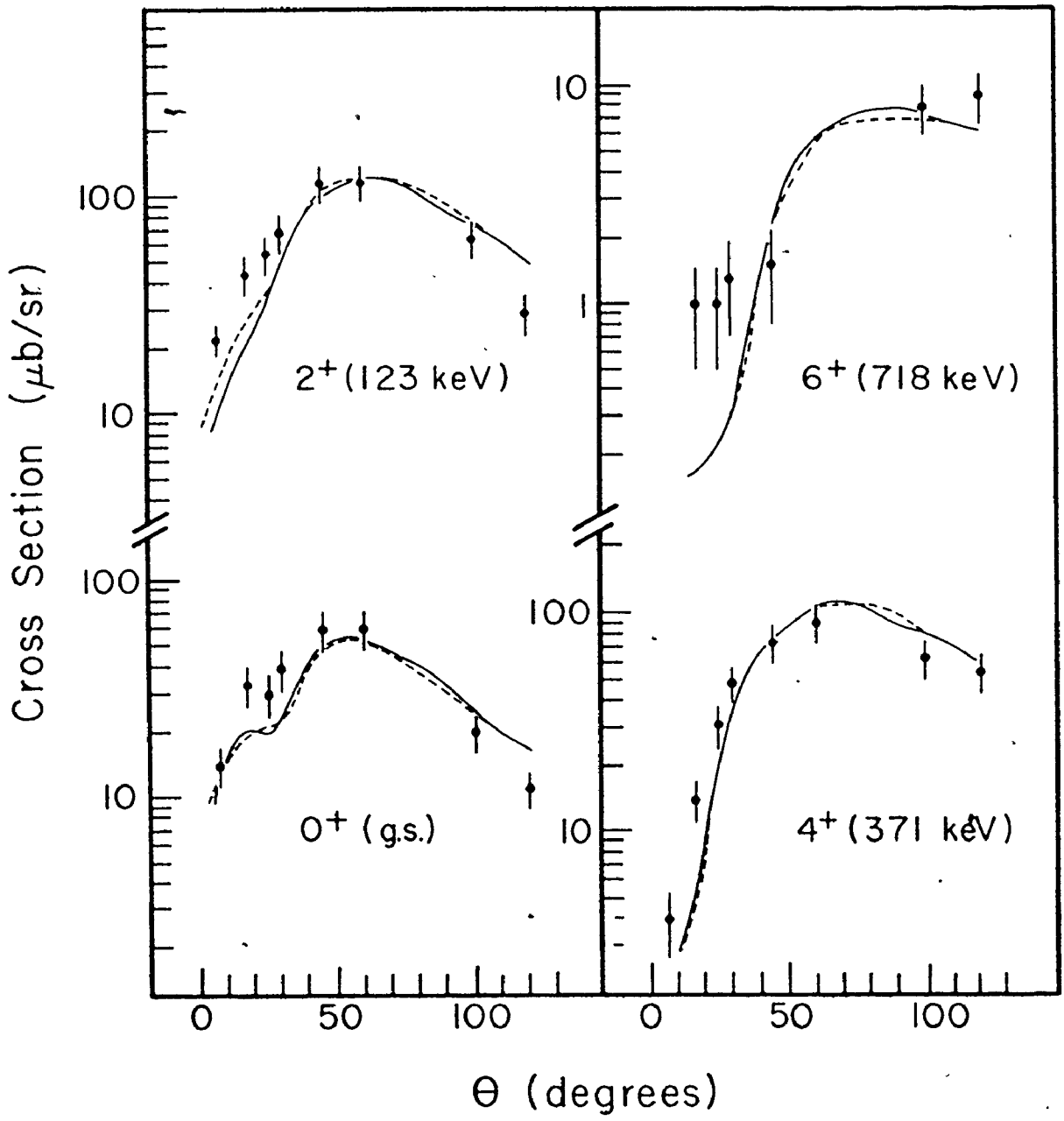
Cross Section (μb/sr)
100
10
2+ (123 keV)
10
1
6+ (718 keV)
100
10
0+ (g.s.)
100
10
4+ (371 keV)
0
50
100
0
50
100
θ (degrees)

was changed from $\delta = 0.18$ to 0.30, no significant change in the angular distributions for the various transitions was predicted. In order to match the calculated cross sections with the observed values, a $U^2 = 0.6$ was used. It can be seen from figure 5.1 that in general the calculated angular distributions fit the experimental data reasonably well. However, for the 6^+ state the agreement is not as good with the calculated cross sections at forward angles.

The effect of using the experimentally deduced $C^2_{j\ell}$ values for the $3/2^-[521]$ orbital on the angular distributions was also investigated. These values (table 5.2) were obtained from the $^{156}Gd(d,t)^{155}Gd$ studies of Tjøm and Elbek (1967). A comparison of the two sets of $C^2_{j\ell}$ values (table 5.2) shows that the agreement is poor for those cases where the magnitudes are small. In figure 5.1, the angular distributions obtained from the $C^2_{j\ell}$ values due to Tjøm and Elbek (1967) are also shown. It can be seen from the figure that the two sets of $C^2_{j\ell}$ values give very similar angular distributions.

ii) Population of the Ground State Band in the Proton Transfer Reactions .

The ground state of the ^{153}Eu target is in the $5/2^+[413]$ proton Nilsson orbital which originates from the $g_{7/2}$ shell model state. The transfer of a $5/2^+[413]$ proton in the $(^3He,d)$ and (α,t) reactions would allow population of the 0^+, 2^+, 4^+ and 6^+ members. All of these members have been populated in the proton transfer reactions (table 5.1).

Table 5.2

The $C_{j\ell}^2$ values for the $3/2^-$[521] neutron orbital

I^π	Calculated[a]	Experimental[b]
$3/2^-$	0.057	0.11
$5/2^-$	0.009	∿0.005
$7/2^-$	0.487	0.54
$9/2^-$	0.396	0.35
$11/2^-$	0.050	-

a: Calculated for well parameters
$\kappa = 0.0637$, $\mu = 0.42$ and $\delta = 0.26$

b: Tjøm and Elbek (1967)

For the $5/2^+[413]$ proton Nilsson orbital, $C^2_{7/2,4} \approx 0.92$. Thus, except for the ground state, all other members are expected to be populated by a predominantly $\ell=4$ transition (figure 4.2). As a result of this, the 2 and 4 members were more strongly populated in the (α,t) reaction than in the $(^3He,d)$ reaction. The distribution of the observed strengths among the ground state members has been shown in figure 5.2. In addition the calculated strengths are shown for the corresponding members assuming a fullness factor $V^2 = 0.65$.

5.2 Excited $K^\pi = 0^+$ Bands

i) The Beta Band

The beta vibrational states are the lowest excited states with $K^\pi = 0^+$. Like the ground state band, the beta band has been investigated by various reaction and decay studies (Bloch et al., 1967, Meyer, 1968, Sousa et al., 1975). Khoo et al. (1973) have identified the beta members up to I=18. The first three members of the beta band, 0^+, 2^+ and 4^+, occur at excitation energies of 681, 816 and 1048 keV respectively. It can be noted that the energy spacings of these members are very similar to those of the corresponding spacings of the ground state band.

In the (d,t) reaction the 0^+, 2^+ and 4^+ states of the beta band were populated. In the $(^3He,\alpha)$ reactions only the 4^+ member has been seen. The cross sections to these members in the (d,t) and the $(^3He,\alpha)$ reactions are very small (table

Figure 5.2

A comparison of the predicted and observed cross sections in the $(\alpha,t)_{45°}$ and $(^3He,d)_{30°}$ reactions for the first four members of the ground state band in ^{154}Gd. The solid lines are the predicted cross sections and arrows show the observed cross sections ($\mu b/sr$).

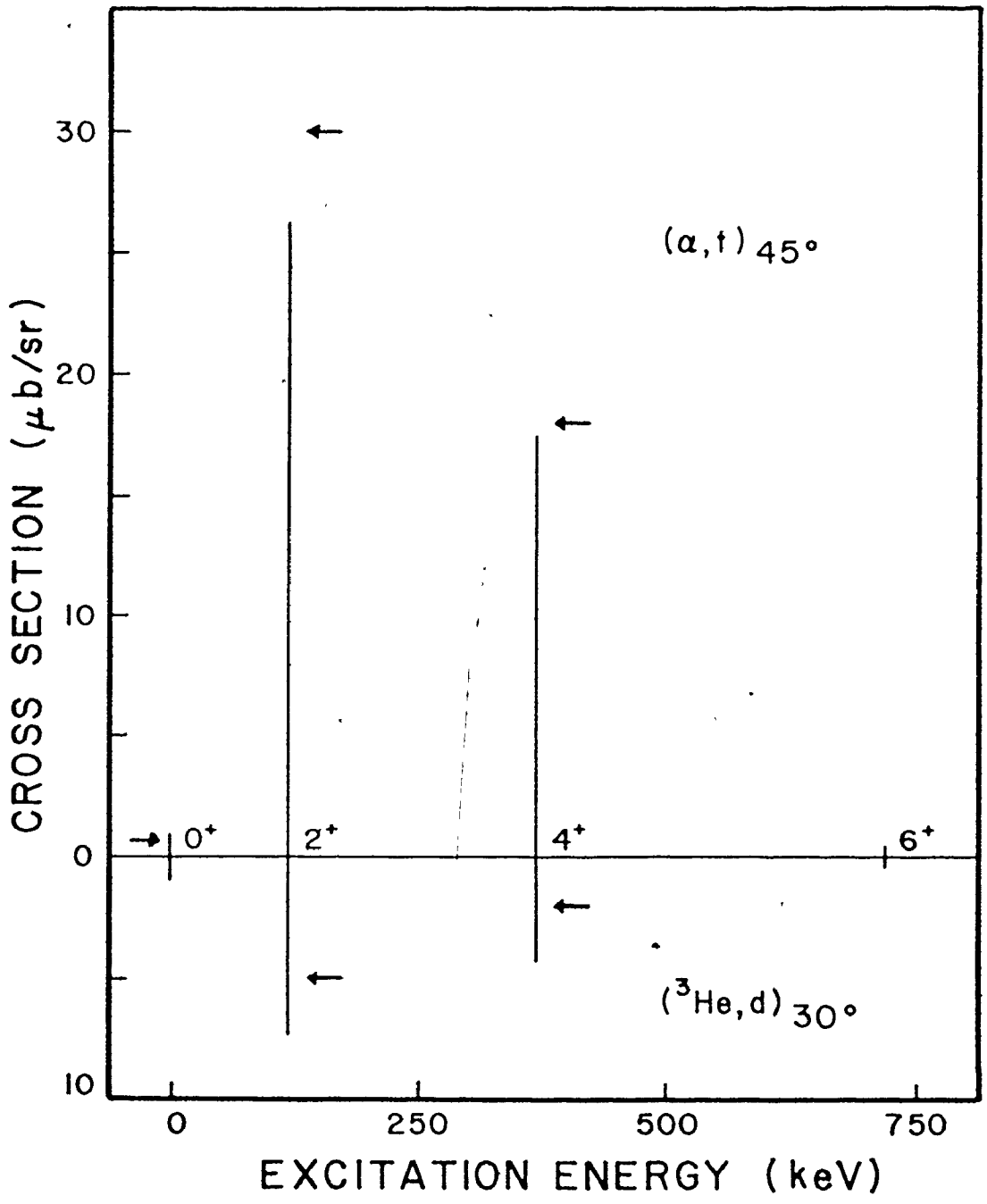
30
20
10
0
10
CROSS SECTION (μb/sr)
(α,t) 45°
0⁺
2⁺
4⁺
6⁺
(³He,d) 30°
0
250
500
750
EXCITATION ENERGY (keV)

4.1). The sum of the cross sections to the beta band was found to be about 25 times smaller than the corresponding figure for the ground state band.

In the (^{3}He,d) and (α,t) reactions only the 2^+ member of the beta band has been observed and its cross section is less than 1 μb/sr (table 4.2).

ii) <u>The $K^\pi = 0^+$ Band at 1296 keV</u>

This $K^\pi = 0^+$ band at 1295.8 keV occurs at about twice the excitation energy of the beta band and is called the two phonon beta vibrational band. The next members, 2^+ and (4^+) are at 1418.3 and 1698.3 keV respectively (Meyer, 1968 and Sousa et al., 1975). In the (d,t) reactions the 0^+ member is barely populated, however the 2^+ member receives an appreciable strength (table 4.1). This level has also been populated weakly in the (^{3}He,α) reaction. Burke and Elbek (1967) have discussed that in the single nucleon transfer reactions the intensity pattern for other $K^\pi = 0^+$ bands are expected to be very much like that of the ground state. The angular distribution for the 1418 keV level is very similar to that for the 2^+ member of the ground state band. Meyer (1968) has tentatively proposed that the 4^+_0 member is at 1698.2 keV. However this member should also have been populated in the (d,t) reaction. The level at 1704 keV is another possibility which might be the 4^+ member of the band.

5.3 The $K^{\pi} = 2^{+}$ Bands

i) The Gamma Vibrational Band

A K^{π} = 2+ band head occurs at an excitation energy of 996 keV in ^{154}Gd. This is the gamma vibrational band and is discussed in detail by Meyer (1968). Spin members up to I=7 are known for this band (West et al., 1976).

ii) Population of the Gamma Band in the Neutron Transfer Reactions

In the (d,t) reactions, the first four members of the gamma band, 2^{+}, 3^{+}, 4^{+} and 5^{+} have been populated at 996, 1128, 1264 and 1432 keV respectively, with a very moderate strength (table 5.3). In the (^{3}He,α) reaction, these gamma band members had only very little strength. The calculations of Soloviev (1965) and Bès et al. (1965) have shown that the $\{3/2^{-}[521] + 1/2^{-}[521]\}_{\nu}$ two-quasiparticle configuration constitutes one of the major components for the gamma vibration in ^{154}Gd.

In the study of the (d,p) reaction, the gamma band in ^{158}Gd is populated strongly and this population is associated with the $\{3/2^{-}[521] + 1/2^{-}[521]\}_{\nu}$ two-quasiparticle configuration (Shelton and Sheline 1971). One might expect a similar situation for the ^{154}Gd nucleus. Calculations show that only 1% of the total strength for the above configuration ($V^2 = 1$) is observed in the (d,t) reaction. This value is considerably

Table 5.3

Cross sections (μb/sr) to the gamma band members of ^{154}Gd

Excitation Energy (keV)	L, K^{π}	Neutron Transfer $(d,t)_{45°}$	Neutron Transfer $(^3He,\alpha)_{45°}$	Proton Transfer $(^3He,d)_{60°}$	Proton Transfer $(\alpha,t)_{45°}$
996	$2, 2^+$	5		2	7
1128	3,	1	0.2	2	6
1264	4,	2	0.4	1	2
1433	5,	0.4	1[d]	un	1

d: doublet

un: unresolved

smaller than the predicted values of 6-7% for the above two-quasi-neutron component by Soloviev (1965) and Bès et al. (1965). This, of course, is probably a result of the fact that the $1/2^-[521]$ orbital is a particle state in ^{155}Gd and thus V^2 is probably considerably less than 1.

The observed intensities in the $(d,t)_{45°}$ reaction for the gamma band members 2^+, 3^+ and 4^+ are 62%, 13% and 25% respectively of the total strength. The calculated strength distributions for the same angle of observation are 75%, 17% and 7% if one assumes that the $1/2^-[521]$ is transferred. It can be seen that the agreement is rather poor, especially for the 4^+ member of the gamma band, for which more than three times the predicted strength is observed. A Coriolis coupling calculation involving the $1/2^-[521]$ and $1/2^-[530]$ orbitals shows that better agreement is possible with a mixed configuration. However, the (d,t) angular distributions for these gamma members do not show any preference either for the pure $1/2^-[521]$ or for the mixed configurations.

iii) Population of the Gamma Band in the Proton Transfer Reactions

In the proton transfer reactions, as in the neutron transfer reactions, only the first four members of the gamma band have been observed (table 5.3). The calculations of Soloviev (1965) and Bès et al. (1965) predict that the $\{5/2^+[413] - 1/2^+[411]\}_\pi$ two-quasiparticle configuration is one of the major components of the gamma vibration in ^{154}Gd.

As the $5/2^+[413]$ orbital is the ground state of the ^{153}Eu target and the $1/2^+[411]$ orbital lies above the Fermi surface, the gamma band members of the above configuration may be populated. The $1/2^+[411]$ Nilsson orbital originates from the $d_{3/2}$ shell model state, the $C^2_{j\ell}$ values are $C^2_{1/2,0} = 0.11$, $C^2_{3/2,2} = 0.55$, $C^2_{5/2,2}=0.19$, $C^2_{7/2,4} = 0.14$ and $C^2_{9/2,4} = 0.01$. Thus the population of the gamma band members would be mainly by $\ell=2$ transfer. This aspect can be seen from the cross section ratio of the $I^\pi = 2^+$ member in the (^{3}He,d) and (α,t) reactions (figure 4.2).

The total strength observed in the gamma band in these reactions is only 16% of the strength for a pure $\{5/2^+[413] - 1/2^+[411]\}_\pi$ two-quasiparticle configuration ($U^2 = 1$). This value is very close to the predictions of 19% by Soloviev (1965).

The observed intensity pattern of the gamma band members in the $(^3\text{He,d})_{60°}$ and $(\alpha,t)_{45°}$ reactions are compared with the calculated pattern based upon the above two-quasiparticle configuration (figure 5.3). Of course the U^2 for the $1/2^+[411]$ orbital is unknown, but the best fit gives $U^2 = 0.16$. It can be seen that the agreement between the calculated and the observed cross sections is very good.

iv) <u>The Second $K^\pi = 2^+$ Band</u>

The 2^+, 3^+ and 4^+ members of this so-called coupled beta-gamma vibrational band are known to be at excitation ener-

Figure 5.3

A comparison of the predicted and observed cross sections in the $(\alpha,t)_{45°}$ and $(^3He,d)_{60°}$ reactions for the first four members of the gamma band in ^{154}Gd. The solid lines are the predicted cross sections and arrows show the observed cross sections (μb/sr).

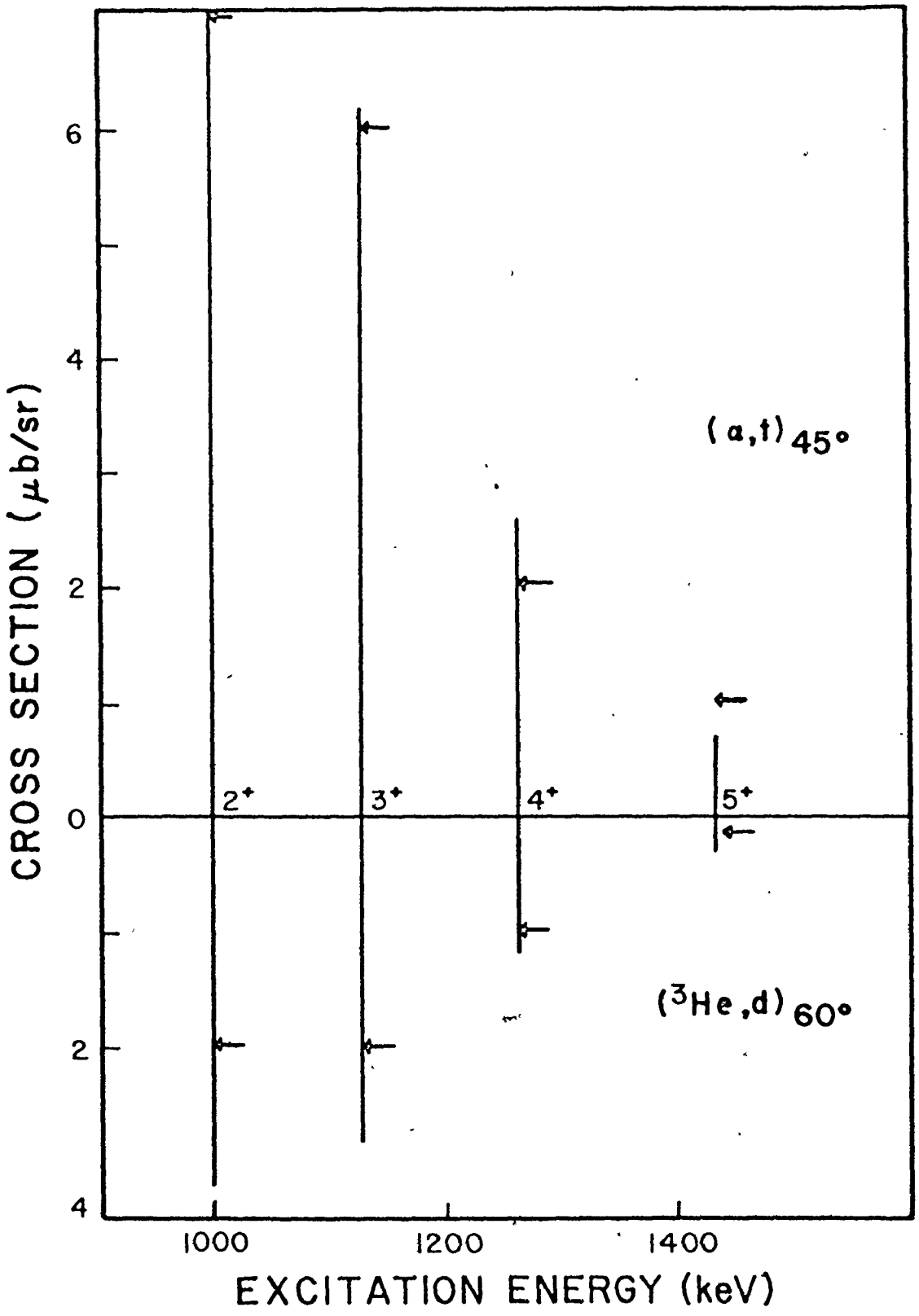
CROSS SECTION (μb/sr)
6
4
2
0
2
4
2+
3+
4+
5+
(α,t)45°
(3He,d)60°
1000
1200
1400
EXCITATION ENERGY (keV)

gies of 1531.3, 1661.1 and 1790.4 keV respectively (Meyer, 1968). The energy spacings of the members of this band are very similar to those of the other $K^{\pi} = 2^{+}$ (gamma) band at 996 keV. The 2^{+} and 3^{+} levels are populated very weakly in the (d,t) reaction at 1532 keV and 1662 keV respectively (table 4.1). In the proton transfer reactions only the 2^{+} member has been observed and even this strength was weak.

5.4 Octupole Vibrational States

From the studies of Meyer (1968) and Sousa et al., (1975), three octupole bands, $K^{\pi} = 0^{-}$, 1^{-} and 2^{-}, are known in ^{154}Gd. These octupole bands are strongly perturbed and in some cases the spin sequences are inverted (table 5.4). In the neutron transfer reactions all three octupole bands are populated very weakly. In the proton transfer reactions, only the $K^{\pi} = 1^{-}$ band has been observed and with very little strength. The octupole bands and their population in the various reactions are summarized in table 5.4.

Population of the octupole bands, like other collective bands in the single nucleon transfer reactions, depend upon two factors which often reduce the cross sections to a great extent. These factors are the percentage of the two-quasi-particle configuration in the octupole band and the U^2 or V^2 associated with the transferred particle. Soloviev (1965) has calculated the two-quasiparticle configuration of the $K^{\pi} = 0^{-}$, 1^{-} and 2^{-} octupole bands for ^{154}Gd. In table 5.5,

Table 5.4

Cross sections (μb/sr) of the octupole vibrational states of ^{154}Gd

Excitation Energy (keV)	I,K^{π} [a]	Neutron Transfer Reactions		Proton Transfer Reactions	
		$(d,t)_{45°}$	$(^3He,\alpha)_{45°}$	$(^3He,d)_{30°}$	$(\alpha,t)_{45°}$
1241	$1,0^-$	2			
1252	3,				
1364	5,				
1398	$2,1^-$	2			
1415	1,			ob	1
1560	4,			ob	1
1617	3,				
1720	$2,2^-$	2			
1796	3,	3			
1864	(4),				
1950	(5) [b]	1	1		

a: Sousa et al. (1975)

b: A state was observed in the $^{154}Gd(d,d')$ reaction at 1950 keV (Bloch et al., 1967). This state is possibly the 5^- member of the K=2 band.

ob: obscured by impurity

Table 5.5

Two-quasiparticle configurations of the octupole bands in ^{154}Gd (Soloviev, 1965)

K^{π}	Two-quasiparticle configurations	%	P^2 [a]
0^-	$\{3/2^-[532]-3/2^+[651]\}_\nu$	23	
	$\{3/2^-[521]-3/2^+[651]\}_\nu$	22	0.70
	$\{5/2^+[413]-5/2^-[532]\}_\pi$	5	0.30
	$\{9/2^+[404]-9/2^-[514]\}_\pi$	4	
	$\{5/2^+[413]-5/2^-[303]\}_\pi$	0.3	
1^-	$\{3/2^+[651]-1/2^-[530]\}_\nu$	8	
	$\{3/2^-[521]-5/2^+[642]\}_\nu$	7	0.19
	$\{3/2^-[532]-1/2^+[660]\}_\nu$	6	
	$\{3/2^-[521]-1/2^+[660]\}_\nu$	2	0.79
	$\{3/2^-[521]-1/2^+[400]\}_\nu$	0.4	0.81
	$\{3/2^+[411]-5/2^-[532]\}_\pi$	58	
	$\{5/2^+[413]-7/2^-[523]\}_\pi$	6	0.81
	$\{5/2^+[413]-3/2^-[541]\}_\pi$	0.4	0.97
2^-	$\{1/2^+[660]+3/2^-[532]\}_\nu$	3	
	$\{5/2^+[642]-1/2^-[530]\}_\nu$	2	
	$\{3/2^-[521]-7/2^+[633]\}_\nu$	0.5	0.07
	$\{3/2^-[521]+1/2^+[660]\}_\nu$	0.5	0.79
	$\{3/2^+[411]-7/2^-[523]\}_\pi$	92	
	$\{5/2^+[413]-1/2^-[301]\}_\pi$	0.04	
	$\{5/2^+[413]-9/2^-[514]\}_\pi$	0.001	

a: $P^2 = V^2$ for neutron orbitals and U^2 for proton orbitals. These values are calculated from the known excitation energies in the target nucleus, otherwise estimated from the Nilsson single particle energies.

the major two-quasiparticle configurations are given with their percentage composition in the octupole bands. This table also lists other components for which the target orbital is one of the two quasiparticles. In order that an octupole band be observed in a single particle transfer reaction, one of the two-quasiparticles must have the same Nilsson configuration as the target. From table 5.5, it can be seen that the octupole bands are not expected to be populated strongly. Since these states are populated so weakly in these reaction studies, it is rather difficult to investigate their microscopic composition in any detail.

The only member of the $K^{\pi} = 0^{-}$ band observed in the (d,t) reaction is at 1242 keV. Table 5.5 suggests that this member might have been populated as a result of a $\{3/2^{-}[521] - 3/2^{+}[651]\}_{\nu}$ component.

The two-quasiparticle configuration $\{3/2^{-}[521] - 5/2^{+}[642]\}_{\nu}$ has been suggested to be a component of the $K^{\pi} = 1^{-}$ octupole band by both Soloviev (1965) and Neergård and Vogel (1970). Probably the level at 1399 keV ($I,K^{\pi} = 2,1^{-}$) might have been populated in the (d,t) reaction as a result of this component. In the proton transfer reactions two other members of this octupole band (I = 1 and 4) have been excited at 1412 and 1559 keV respectively. Table 5.5 suggests that these states might have been populated through the $\{5/2^{+}[413] - 7/2^{-}[523]\}_{\pi}$ component.

The first two members of the $K^{\pi} = 2^{-}$ band have been observed at 1719 and 1797 keV in the neutron transfer reactions. A state at 1950 keV was observed in the $^{154}Gd(d,d')^{154}Gd$ reaction (Bloch et al., 1967). A level at 1950 keV has been populated very weakly in the neutron transfer reactions (table 5.4). It is proposed that this might be the I=5 member of the $K^{\pi} = 2^{-}$ octupole band. The population of these states might be due to the transfer of the $1/2^{+}[660]$ orbital (table 5.5).

5.5 Levels at 1182 and 1576 keV populated weakly in the Neutron Transfer Reactions

Two levels at excitation energies of 1182 and 1576 have been excited very weakly in the (d,t) reaction (table 4.1). These levels have not been observed previously. Before discussing the nature of these levels, it is worthwhile to mention that these peaks are not due to any of the impurities. From the measurements of relative triton energies, made at angles of 7.5° to 120°, it was possible to determine that the nuclei which give rise to these peaks have a mass number of 154, 155 or 156. The Q-values for the (d,t) reactions on ^{154}Gd and ^{156}Gd are at least 2 MeV more negative than that for the reaction on ^{155}Gd. This rules out the possibility that these peaks are due to the isotopic gadolinium impurities in the ^{155}Gd targets.

Since states with spin 0 to 8 and with both parity have been observed in ^{154}Gd (Sousa et al., 1975),

it is rather strange that these levels have not been observed previously in the decay or in the reaction studies. The occurrence of these levels below the energy gap in the ^{154}Gd nucleus is unusual. In the neighbouring isotonic nucleus $^{152}_{62}Sm_{90}$ levels at 1091 keV (0^+) and 1293 keV (2^+) were excited strongly in the (t,p) reaction on the spherical nucleus ^{150}Sm (Hinds et al., 1965). These two levels were interpreted as the 'spherical states' co-existing in the 'deformed' ^{152}Sm nucleus. The levels at 1182 and 1576 keV might have a similar structure and might be spherical 0^+ and 2^+ states in ^{154}Gd. The energy spacing of these levels (395 keV) is slightly larger than the 344 keV spacing of the 0^+ and 2^+ states in the 'spherical' ^{152}Gd nucleus. With this interpretation for these levels of ^{154}Gd, it is possible to explain the (d,t) reaction strength as resulting from a very poor overlap between the deformed target state in ^{155}Gd and the spherical states in the final ^{154}Gd nucleus. Further justification of this interpretation can be sought from (t,p) experiments on the spherical target nucleus ^{152}Gd, but at the moment, such experiments have not been performed on the gadolinium isotopes.

5.6 $K^{\pi} = 1^-$ and 2^- Bands of the $\{3/2^-[521] \mp 1/2^+[400]\}_\nu$ and $\{3/2^-[521] \mp 1/2^+[660]\}_\nu$ Configurations

The (d,t) angular distributions to four levels, 2376, 2443, 2648 and 2683 keV show a forward peaking and a minimum at about 20°, which are characteristic of an $\ell=0$ transition (figures 5.4-5). In order to confirm this fact, the angular distributions will be compared with the experimentally available data for the 367 keV level in ^{155}Gd (Jaskola et al., 1969). This level is known to be populated in the (d,t) reaction by an $\ell=0$ transition and has been assigned as the 1/2, $1/2^+[400]$ state of ^{155}Gd. The deuteron beam energy (12.1 MeV) used in their experiments was similar to that used in the present study (12 MeV) and the Q-values to the levels concerned are also similar. In figures 5.4-5, these angular distributions are compared and may be seen to be in good agreement. It seems quite reasonable to believe that these transitions into ^{154}Gd predominantly have an $\ell=0$ character.

From the spectra (figures 3.3 -4), it can be seen that these levels are excited with large (d,t) strength and the 2683 keV level has the largest cross section of all the levels populated above the energy gap (table 4.1).

At the most, two $\ell=0$ transitions have been observed in the neighbouring odd mass gadolinium nuclei (Tjøm and Elbek, 1967). These transitions are associated with the $1/2^+[400]$ and $1/2^+[660]$ Nilsson orbitals. The $C^2_{j\ell}$ coefficients for the $\ell=0$ transition for the $1/2^+[400]$ orbital is about 0.6 and

Figure 5.4

The (d,t) angular distributions for the members of the K_u = 1 and 2 bands, resulting from the $\Delta N=2$ mixing between the $\{3/2^-[521]\mp 1/2^+[400]\}_\nu$ and $\{3/2^-[521]\mp 1/2^+[660]\}_\nu$ configurations in ^{154}Gd. The solid lines are the single particle cross sections (DWBA) which also include the appropriate structure factors (see text). The dotted lines are the angular distributions for an $\ell=0$ transition in the ^{156}Gd(d,t)^{155}Gd reaction (Jaskola et al., 1969).

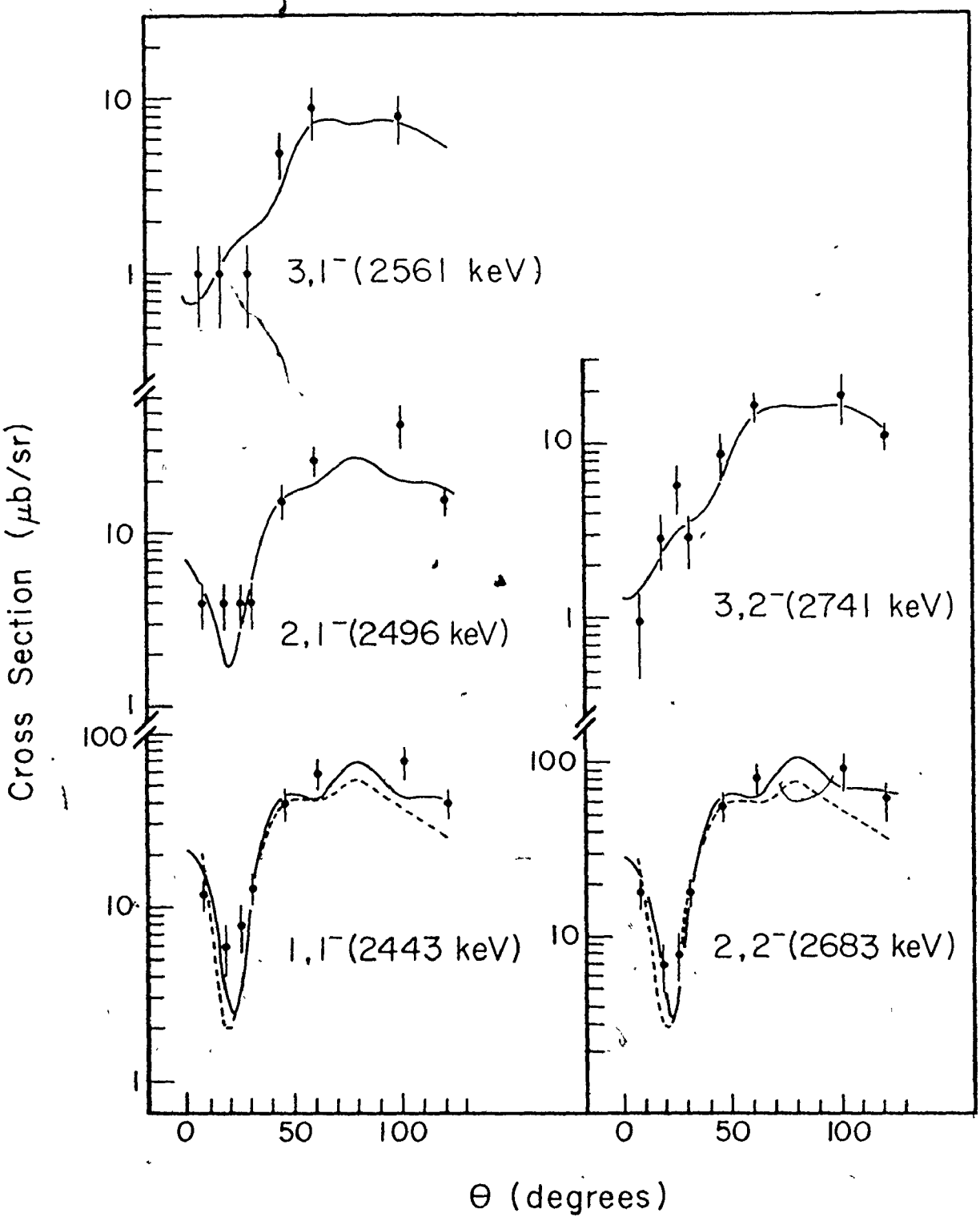
3,1⁻(2561 keV)
2,1⁻(2496 keV)
1,1⁻(2443 keV)
3,2⁻(2741 keV)
2,2⁻(2683 keV)
Cross Section (μb/sr)
Θ (degrees)
10
1
100
0
50
100

Figure 5.5

The (d,t) angular distributions for the members in $K_\ell = 1$ and 2 bands. See caption of figure 5.4.

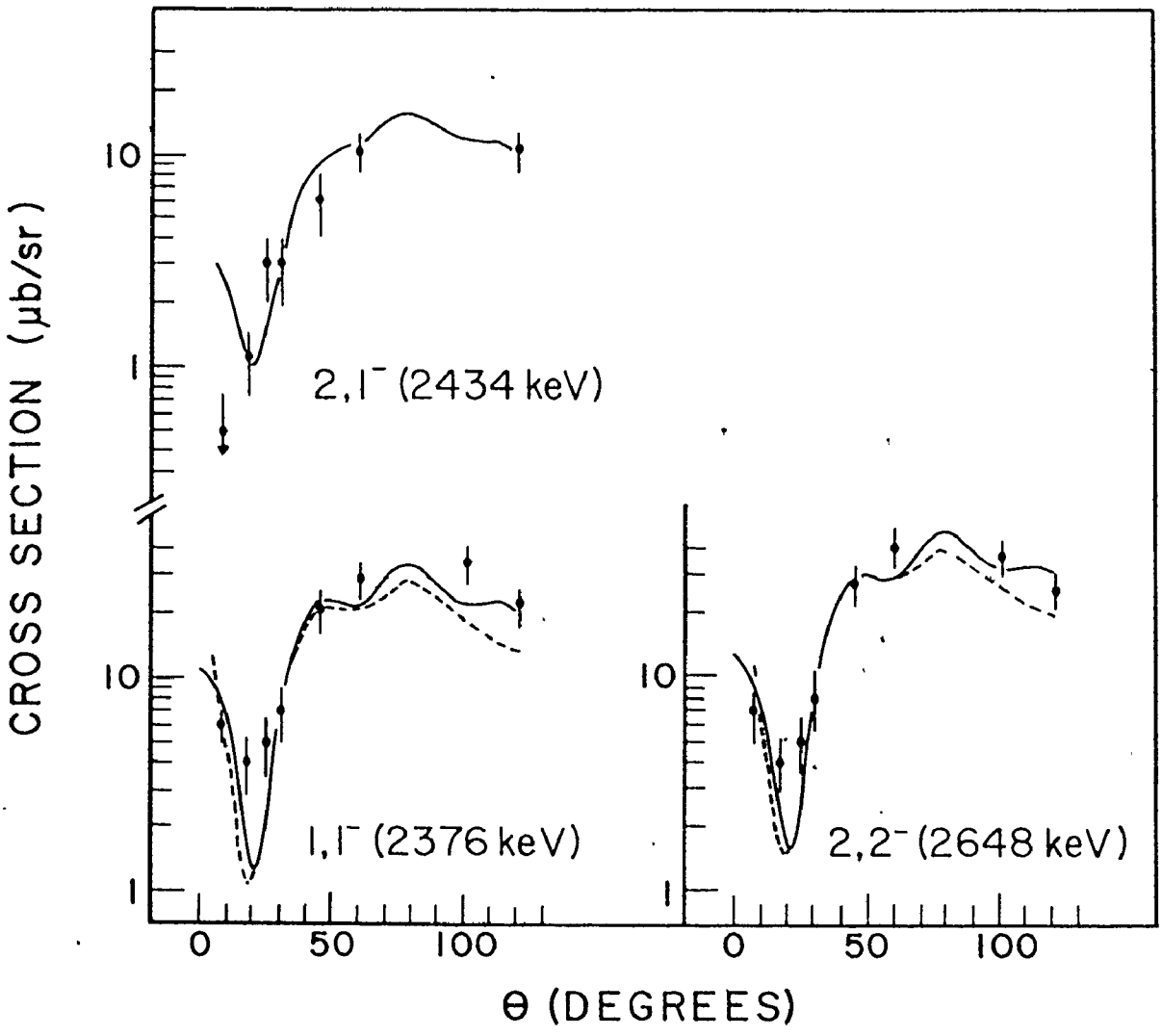
CROSS SECTION (μb/sr)
10
1
2,1⁻ (2434 keV)
10
1
1,1⁻ (2376 keV)
10
1
2,2⁻ (2648 keV)
0
50
100
0
50
100
θ (DEGREES)

the corresponding value for the $1/2^+[660]$ orbital is 500 times smaller. Thus the total $\ell=0$ strength in the (d,t) reaction should be mainly due to the transfer of the $1/2^+[400]$ orbital and only one such $\ell=0$ transition is expected to be populated. The occurrence of more than one $\ell=0$ transition in the odd mass nuclei has been explained on the basis of $\Delta N=2$ coupling between the $1/2^+[400]$ and $1/2^+[660]$ orbitals (Tjøm and Elbek, 1967, Jaskola et al., 1969). This coupling splits the $\ell=0$ strength into two parts and thus two levels have been observed in the single neutron transfer reactions.

In the doubly-even ^{154}Gd nucleus, each of the $1/2^+[400]$ and $1/2^+[660]$ orbitals should couple parallel and anti-parallel to the target ground state, $3/2^-[521]$ and should give rise to a total of four bands. Two of these four bands have $K^\pi = 1^-$ and the other two would have $K^\pi = 2^-$. Furthermore it is expected that the states with $I = 1$ and 2 in the four bands would have large $\ell=0$ component to the transitions.

On this basis, it is proposed that the levels at 2376 and 2443 keV are the $K_\ell = 1$ lower and the $K_u = 1$ upper band heads respectively. Similarly the other two levels at 2648 and 2683 keV are the $K_\ell = 2$ lower and the $K_u = 2$ upper band heads respectively. Another feature of these levels which is quite apparent from table 5.6 is that the level 2443 keV $(I, K_u^\pi = 1, 1^-)$ has a (d,t) cross section about twice as strong

Table 5.6

The (d,t) cross sections to the levels in ^{154}Gd populated by the transfer of the $1/2^+[400]$ and the $1/2^+[660]$ neutron orbitals

Bands	Excitation Energy (keV)	I,K^π	Cross section (μb/sr) $(d,t)_{45°}$	$(d,t)_{60°}$
Lower	2376	$1,1^-$	21	29
	2434	2,	6	10
		Total	27	39
	2648	$2,2^-$	27	40
Upper	2443	$1,1^-$	40	59
	2496	2,	15	26
	2561	3,	5	9
		Total	60	94
	2683	$2,2^-$	57	82
	2741	3,	9	17
		Total	66	99

as that for the 2376 keV ($I,K_\ell^\pi = 1,1^-$) level and a similar ratio is observed for the other two levels corresponding to I=2.

Other members of the $K_u = 1$ band are identified as $I^\pi = 2^-$ and 3^- at excitation energies of 2496 and 2561 keV respectively. While for the $K_\ell = 1$ band only one other member, $I^\pi = 2^-$, at 2434 keV has been identified. For the $K_u = 2$ band only one more member, $I^\pi = 3^-$, is expected to be populated with an appreciable strength. This member has been identified at an excitation energy of 2741 keV. This level scheme is summarized in table 5.6. The energy spacings of the various members in these bands show a well behaved rotational pattern corresponding to the rotational parameter $\tilde{\sim}$ 11 keV.

The angular distributions of all these levels have been shown in figures 5.4-5. The experimental data have been fitted to the single particle cross sections obtained by DWBA calculations, which also include the appropriate nuclear structure factors $\langle I_i jK_i \Delta K | IK\rangle^2 V^2 a^2 C_{j\ell}^2$. In the present calculations, only the $C_{j\ell}^2$ values corresponding to the $1/2^+[400]$ orbital have been considered since the contributions from the $C_{j\ell}^2$ of the $1/2^+[660]$ orbital have found to be negligible. It can be seen from the figures that the shapes of the various angular distributions are very well reproduced by such calculated cross sections. Further, to match the observed strengths at all angles, an average values of V^2a^2 of 0.3 and 0.1 are required for the upper and lower bands, respectively.

The distribution of the strength in the various band members is shown in figure 5.6. The solid lines are the calculated $(d,t)_{45°}$ cross sections and the arrows show the observed cross sections to the various states. The intensity patterns of the K_ℓ and K_u bands are very similar. Thus it can be concluded that the assignments made here to the various levels are correct. The total observed strengths in the K=1 and 2 bands have very nearly the same value. In the $^{156}Gd(d,t)^{155}Gd$ reaction, the total strength for the ℓ=0 transition measured at $\theta = 60°$ was 608 μb/sr. Only about 35% of this value has been observed in the present case.

5.7 $K^\pi = 3^-$ and 0^- Bands of the $\{3/2^-[521] \pm 3/2^+[402]\}_\nu$ and $\{3/2^-[521] \pm 3/2^-[651]\}_\nu$ Configurations

In the neighbouring odd mass nuclei, the $3/2^+[402]$ Nilsson orbital which arises from the $d_{3/2}$ shell model state, is excited strongly in the (d,t) reactions (Tjøm and Elbek, 1967, Nelson et al., 1973, Løvhøiden and Burke, 1973). The parallel and antiparallel coupling of the transferred neutron $3/2^+[402]$ with the $3/2^-[521]$ target ground state should give two bands, $K^\pi = 3^-$ and 0^- respectively. In the $K^\pi = 3^-$ band only one state is expected to be populated strongly. A level at 2336 keV has a fairly large cross section (tables 4.1 and 5.7) and has been assigned as the I=3 member of the $K^\pi = 3^-$ band. For the $K^\pi = 0^-$ band, the (d,t) reaction strength is distributed mainly to the first three states, and the band

Figure 5.6

A comparison of the predicted and observed cross sections in the $(d,t)_{45°}$ reaction for the various members of the K_u and K_ℓ bands resulting from the $\Delta N=2$ mixing between the $\{3/2^-[521]\mp 1/2^+[400]\}_\nu$ and $\{3/2^-[521]\mp 1/2^+[660]\}_\nu$ configurations in ^{154}Gd. The solid lines are the predicted cross sections and arrows show the observed cross sections (μb/sr).

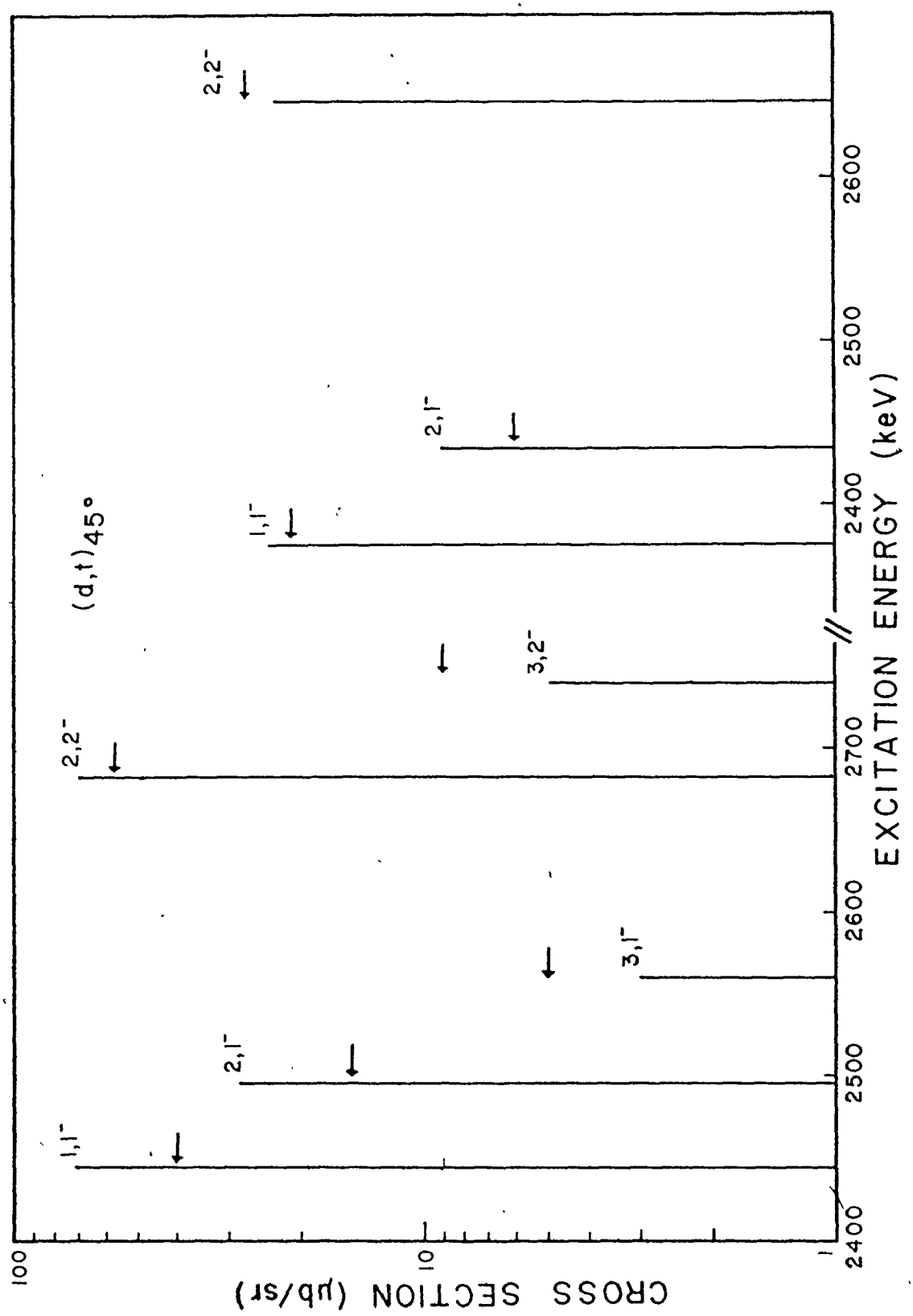
2,2⁻
2,1⁻
1,1⁻
3,2⁻
3,1⁻
(d,t)45°
100
10
1
2400
2500
2600
2700
2400
2500
2600
CROSS SECTION (μb/sr)
EXCITATION ENERGY (keV)

Table 5.7

The (d,t) cross sections to the levels in ^{154}Gd populated by the transfer of the $3/2^{+}[402]$ neutron orbital

Excitation Energy (keV)	I,K^{π}	Cross section (μb/sr) $(d,t)_{45°}$	$(d,t)_{100°}$
2336	$3,3^{-}$	30	65
2536	$0,0^{-}$	9	20
2571	1,	12	29
2632	2,	9	11

members 0^-, 1^- and 2^- have been assigned as the levels at 2536, 2571 and 2632 keV respectively (table 5.7). This arrangement for these two bands agrees with the angular momenta coupling rules for doubly-even nuclei (Gallagher Jr., 1962). The reasons for above assignments will be discussed below.

The Coriolis calculations between the various negative bands discussed so far have shown that the effect of Coriolis mixing is not very serious for the members of the bands arising from the $3/2^+[402]$ Nilsson orbital. This in turn suggests that the rotational structure should not be perturbed and also there is no transfer of strength from one band to any other.

In fact, it can be seen from table 5.7 that the total strength due to the transfer of $3/2^+[402]$ neutron orbital is divided equally between the two bands. Furthermore in the K=0 band, the energy spacings of the first three members are very well described by a rotational parameter of 16 keV.

The $C^2_{j\ell}$ values, for the $3/2^+[402]$ orbit, are such that about 90% of the transition strength is by $\ell=2$. The (d,t) angular distributions, at least to the low spin states should be characteristic of $\ell=2$. However, the higher spin states should have admixtures of $\ell=4$ in their angular distributions. The single particle cross sections for $\ell=2$ and $\ell=4$ are fitted to the experimental data for the various levels mentioned above. Such angular distributions are shown in figure

5.7. The solid lines are the single particle cross sections which also include the appropriate nuclear structure factors such as $\langle I_i j K_i \Delta K | I K \rangle^2 V^2 C^2_{j\ell}$ for a particular state. It can be seen from figure 5.7 that the experimental data, in general, can very well be described by the theoretical predictions. It is also appropriate to compare the observed data for these states in ^{154}Gd to the experimentally observed angular distribution for the 267 keV level populated in the ^{156}Gd(d,t)^{155}Gd (Jaskola et al., 1969). This level has been assigned as the $3/2,3/2^+[402]$ state and the angular distribution is characteristic of an $\ell=2$ transition. It can be seen from figure 5.7 that the angular distributions are similar. The 'finger-print' to the band agrees well with 21% of the calculated cross-sections.

In the neighbouring odd mass gadolinium nuclei, it is known that the $3/2^+[402]$ neutron orbital is mixed with the $3/2^+[651]$ neutron orbital by $\Delta N=2$ interaction (Sheline et al, 1967, Borggreen et al., 1969). Possibly a similar situation might exist in ^{154}Gd. On a simple Nilsson model basis, a state due to $3/2^+[651]$ is not expected to be populated strongly. However the level at 2277 keV has a $(d,t)_{100°}$ cross section of 45 μb/sr and has a (d,t) angular distribution very similar to that of the 2336 keV level. Probably this level at 2277 keV is populated as a result of the $\Delta N=2$ interaction between the $3/2^+[402]$ and $3/2^+[651]$ orbitals. With these arguments, it is proposed that this level at 2277 keV has

Figure 5.7

The (d,t) angular distributions for the members of the $K^{\pi} = 3^{-}$ and 0^{-} bands, resulting from the $\{3/2^{-}[521] \pm 3/2^{+}[402]\}_{\nu}$ configurations. The solid lines are the single particle cross sections (DWBA) which also include the appropriate structure factors (see text). The dotted lines are the angular distribution for a $\ell=2$ transition in the $^{156}Gd(d,t)^{155}Gd$ reaction (Jaskola et al., 1969).

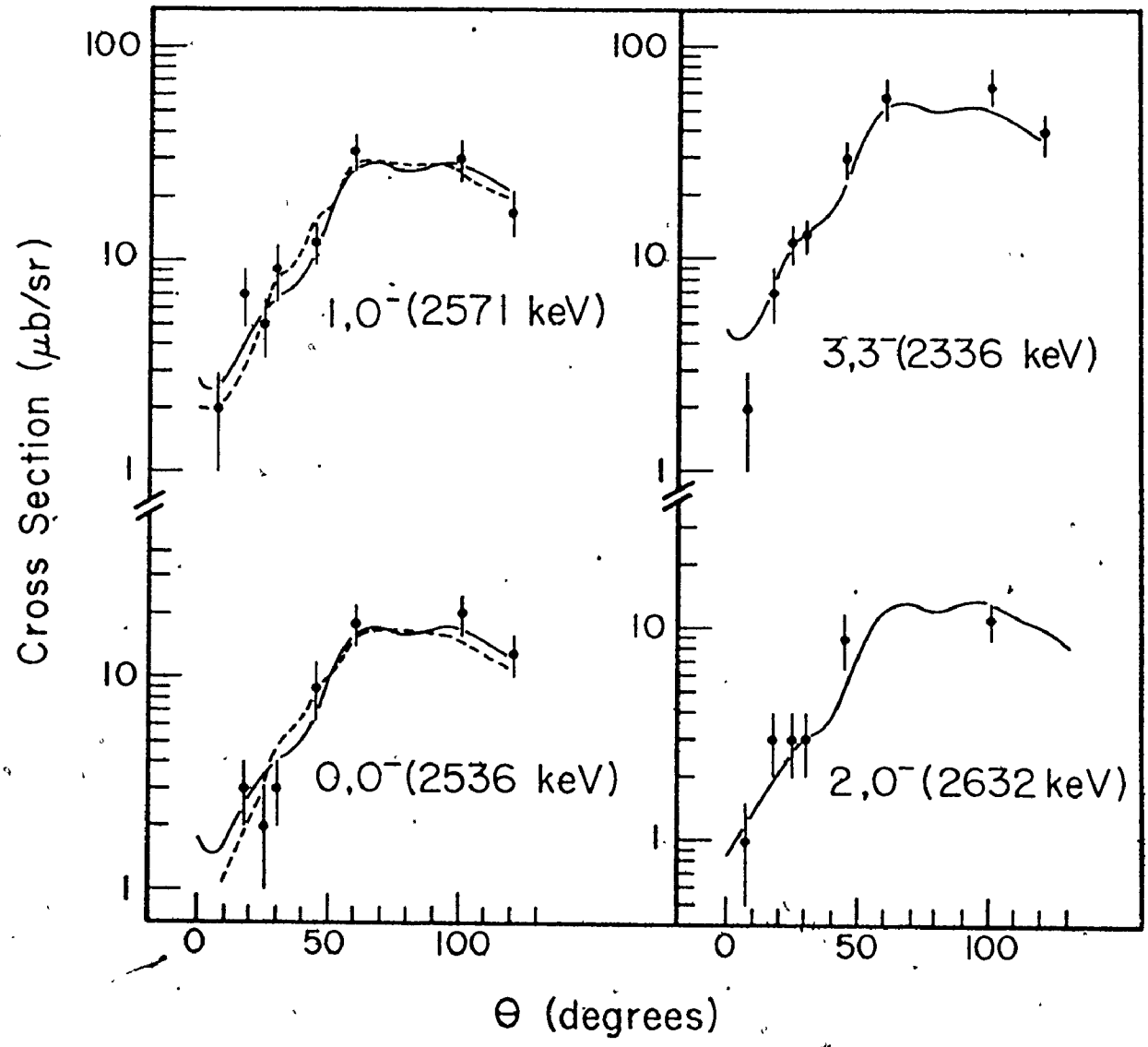
100
10
1
Cross Section (μb/sr)
1,0⁻(2571 keV)
3,3⁻(2336 keV)
0,0⁻(2536 keV)
2,0⁻(2632 keV)
0
50
100
Θ (degrees)

$I,K^{\pi} = 3,3^{-}$.

It is also to be noted that Sousa et al. (1975) have observed two levels at 2277.0 and 2336.1 keV. For both these levels, they have assigned $I^{\pi} = 2^{+}$, 3, 4^{+}. It seems that these two levels are the same ones that were observed in the (d,t) reaction studies.

5.8 ΔN=2 and Coriolis Interactions

In the discussion of the negative parity levels (section 5.6), it has been assumed that the splitting of the $\ell=0$ reaction strength is a result of a simple ΔN=2 coupling between the $1/2^{+}[400]$ and $1/2^{+}[660]$ orbitals. With this assumption it is possible to estimate the magnitude of the ΔN=2 interaction responsible for this splitting. As discussed in section 2.10, two observable quantities, e.g. the energy difference between the two band heads and the ratio of their cross sections are sufficient to calculate the strength of the ΔN=2 interaction. Using expression 2.10.2 for the two $I,K^{\pi} = 1,1^{-}$ band heads at 2376 and 2443 keV one gets $|V_1| = 31$ keV. Similarly for the $I,K^{\pi} = 2,2^{-}$ band heads at 2648 and 2683 keV a value $|V_2| = 16$ keV is obtained. It can be seen that these two values are very different, while for the two $I,K^{\pi} = 3,3^{-}$ bands (section 5.7) at 2277 and 2336 keV, the value of the ΔN=2 matrix element obtained is $|V_3| = 29$ keV. Probably the Coriolis mixing also plays a role with these bands. This is a result of the presence of the other Nilsson orbitals arising from the $i_{13/2}$ shell model

state, which are known to be very strongly Coriolis mixed. In order to investigate this situation it is necessary to carry out calculations involving both the Coriolis and $\Delta N=2$ mixings. The Coriolis matrix elements between the N=6 orbitals are much larger than those between the N=4 orbitals. The following scheme was adopted for these calculations:

1) Only the eight bands, due to the parallel and anti-parallel coupling of the $1/2^+[400]$, $1/2^+[660]$, $3/2^+[402]$ and $3/2^+[651]$ orbitals with the target ground state orbital, $3/2^-[521]$, have been considered.
2) The Fermi surface was assumed to be near the $3/2^+[651]$ orbital.
3) Although the band head energies were adjusted, a constant rotational parameter of 13 keV was used.
4) The Coriolis strength was reduced to 75% of the value obtained from the simple Nilsson model (Løvhøiden et al., 1970).
5) The $\Delta N=2$ matrix elements were adjusted such that the excitation energies and the reaction strengths of the various states were reproduced.

The results of one such calculation are presented in table 5.8. Only one value of the $\Delta N=2$ matrix element, i.e. -35 keV, has been used. The calculated cross sections shown are for $V^2 = 0.37$. This is to get the best correspondence between the observed and calculated values of cross sections. It can be seen from the table that in general the comparison is quite good. Most of the states which are expected to be

Table 5.8

$\Delta N=2$ and Coriolis mixed levels in ^{154}Gd

I,K^{π}	(keV) Calculations	Observed	$(\frac{d\sigma}{d\Omega})(d,t)_{60°}$ (μb/sr) Calculations	Observed
$0,0^-$	2220		<1	
1,	2192		1	
2,	2165		<1	
3,	2145		<1	
$0,0^-$	2552	2536	22	18
1,	2575	2571	39	32
2,	2628	2632	27	un
3,	2709	(2713)	6	14[d]
$1,1^-$	2377	2376	22	29
2,	2428	2434	11	10
3,	2536		4	
$1,1^-$	2444	2443	60	59
2,	2483	2496	35	26
3,	2569	2561	13	9
$2,2^-$	2633	2648	34	40
3,	2850		2	
$2,2^-$	2694	2683	70	82
3,	2749	2741	15	17
$3,3^-$	2335	2336	57	58
$3,3^-$	2276	2277	38	37

un: unresolved

d : doublet

observed in the (d,t) reaction have been identified in the present study. The lower $K^{\pi} = 0^{-}$ band is strongly perturbed and is not expected to be populated strongly in the (d,t) reaction.

The two $K^{\pi} = 2^{-}$ bands show some deviation from the observed values. These two bands are only 35 keV apart, while the calculations predict a somewhat higher splitting (51 keV). The other bands arising from the Nilsson orbitals derived from the $i_{13/2}$ shell model state are not included in these calculations and might be responsible for this discrepancy. The main reason that these bands have not been included is because their position is unknown. If these bands were included the number of the parameters would exceed the number of data values.

However a better agreement was obtained when the values of the $\Delta N=2$ matrix elements were chosen similar to those obtained on the basis of the simple $\Delta N=2$ coupling between the K=1, 2 and 3 bands.

5.9 States Populated by High ℓ in the Neutron Transfer Reactions

In the study of the odd mass gadolinium nuclei, some of the levels were excited very strongly in the $(^{3}He,\alpha)$ reaction (Løvhøiden et al., 1971). These levels were assigned to the $11/2^{-}[505]$ Nilsson orbital and the Coriolis mixed states due to the Nilsson orbitals originating from the $i_{13/2}$ spherical shell model state. It is expected that the reaction

strength to these orbitals will be distributed over many states in ^{154}Gd. Table 5.9 lists the levels strongly excited in the (^{3}He,α) reaction, along with the corresponding (d,t) cross sections. Some indication about the nuclear structure of these levels could be obtained from the cross section ratio plot (figure 4.1) and the (d,t) angular distributions (figure 5.8). The (d,t) cross sections obtained from DWBA calculations do not fit the experimental data for ℓ=5 and 6 transitions very well, especially at the forward angles. The angular distributions to the levels of ^{154}Gd (table 5.9) are fitted to the experimental data of the ^{156}Gd(d,t)^{155}Gd reaction for the 119 (ℓ=5) and 214 keV (ℓ=6) levels (Jaskola et al., 1969).

i) $K^{\pi} = 4^{+}$ and 7^{+} Bands of the $\{3/2^{-}[521] \mp 11/2^{-}[505]\}_{\nu}$ Configurations

Riedinger et al. (1971) have suggested a two-quasiparticle configuration of $\{3/2^{-}[521]+11/2^{-}[505]\}_{\nu}$ for a level at 2459.6 keV in ^{154}Gd. A possible spin of 7 or 8 has been suggested for this level. The spin 7^{+} member of this configuration should have been excited very strongly in the ^{155}Gd(^{3}He,α)^{154}Gd reaction by the transfer of a $11/2^{-}[505]$ neutron. However, it can be seen from the (^{3}He,α) spectra (figure 3.3) and table 4.1 that no levels have been populated very strongly (< 7 μb/sr) in that region. In this section, other possible assignments to the $\{3/2^{-}[521] \pm 11/2^{-}[505]\}_{\nu}$ configurations are discussed. It is

Table 5.9

The (d,t) and (^{3}He,α) cross sections to the levels in ^{154}Gd, populated by ℓ=5 or 6 transitions

Excitation Energy (keV)	Cross section (μb/sr)			
	$(d,t)_{60°}$	$(d,t)_{100°}$	$(^3He,\alpha)_{45°}$	$(^3He,\alpha)_{60°}$
2131	9	6	8	11
2150	14	23	35	17
2266	8	8	7	6
2306	33[c]	36	18	10
2404	32	41	34	20

c: contaminated

Figure 5.8

The (d,t) angular distributions to the levels in ^{154}Gd populated by ℓ=5 or 6 transitions. The angular distributions are fitted to the 119 keV (ℓ=5) and 214 keV (ℓ=6) levels populated in the $^{156}Gd(d,t)^{155}Gd$ reaction (Jaskola et al., 1969).

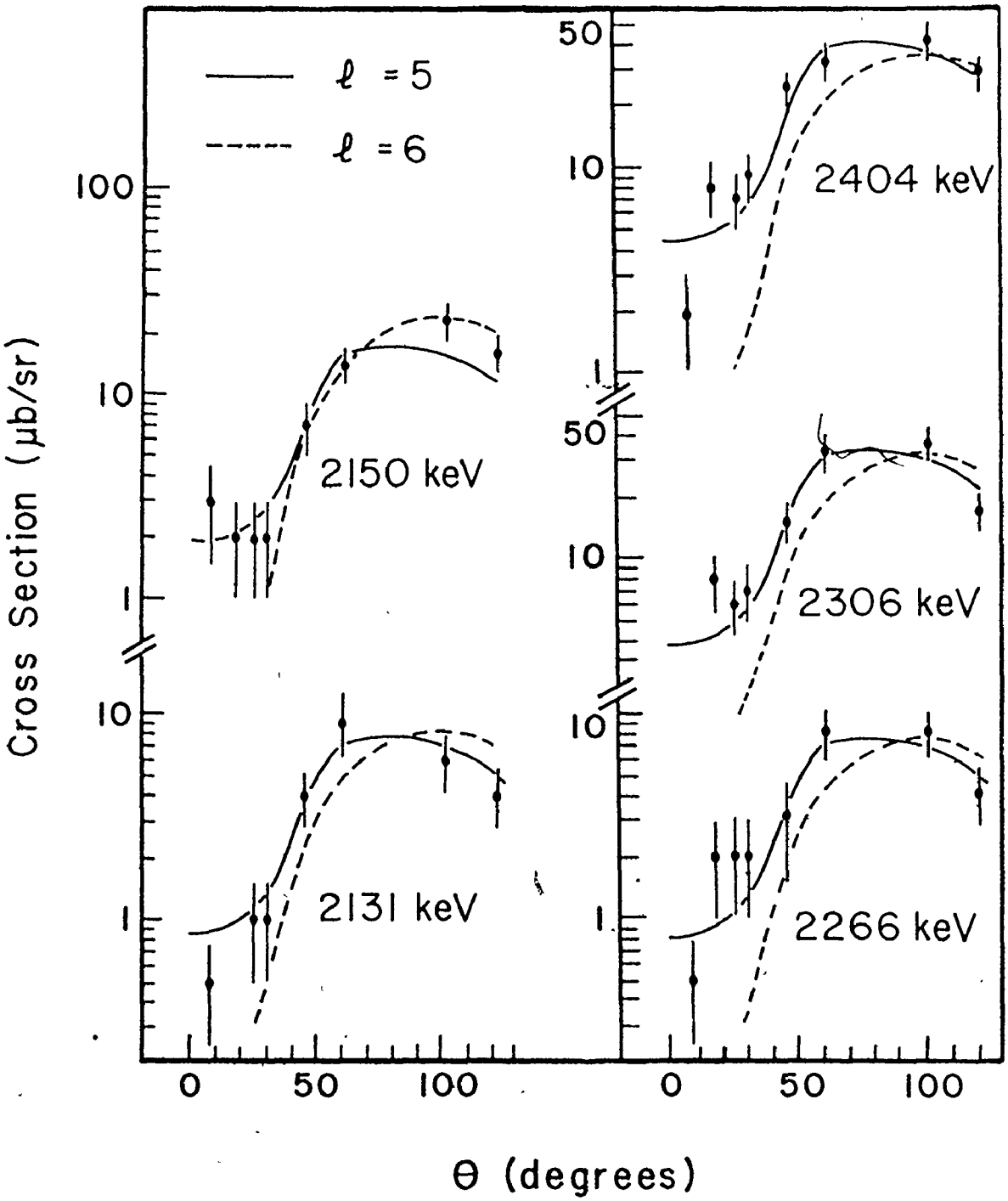
ℓ = 5
ℓ = 6
2150 keV
2131 keV
2404 keV
2306 keV
2266 keV
Cross Section (μb/sr)
Θ (degrees)
100
10
1
50
0
50
100

expected that only one member, $I,K^{\pi} = 7,7^{+}$, of the parallel coupled band should be populated in these reactions. However for the $K^{\pi} = 4^{+}$ band, states from spin values I=4 to 7 could be populated, with most of the spectroscopic strength concentrated in the first member, I=4, of this band.

Tentative assignments of the 2306 and 2404 keV levels to the $I,K^{\pi} = 4,4^{+}$ and $7,7^{+}$ states respectively have been made. These assignments are based upon the (d,t) angular distributions, cross section ratios of the (^{3}He,α) reaction to the (d,t) reaction and also the expected large reaction strength in both the (^{3}He,α) and (d,t) reactions. The observed cross sections to these states agree with the calculated cross sections for a $V^{2} = 0.85$.

It can be noted that the K=4 band with Σ=0 lies lower in energy than the K=7 band for which Σ=1, in agreement with the prediction of Gallagher (1962).

ii) Coriolis Coupled $i_{13/2}$ Nilsson States (Calculations)

The cross section ratio plot (figure 4.1) shows that only the level at 2150 keV lies above the line for ℓ=5. The (d,t) angular distribution for this level along with the experimental angular distributions for ℓ=5 and 6 (Jaskola et al., 1969) are shown in figure 5.8. This level might be associated with the $i_{13/2}$ spherical shell model state, for which the various Nilsson orbitals are very badly Coriolis mixed (Løvhøiden and Kanestrøm, 1972).

Coriolis coupling calculations were performed considering all the Nilsson orbitals arising from the $i_{13/2}$ state coupled to the $3/2^-[521]$ target ground state. The Fermi surface was placed somewhat below the $3/2^+[651]$ orbital and the band head energies were taken from a Nilsson calculation. One feature of these calculations was quite apparent. The amplitudes of the wave functions add up coherently in such a manner that the lowest bands receive most of the reaction strength. These findings were not changed when the number of Nilsson orbitals were restricted to the $1/2^+[660]$, $3/2^+[651]$, $5/2^+[642]$ and $7/2^+[633]$ orbitals. The results, however, were quite different when the Coriolis matrix elements were attenuated. The predicted energies of the yrast spin members I=0 to 8 were found to lie on a parabola for a E versus I plot (figure 5.9). It can be seen from that figure that the apex of the parabola is sensitive to the attenuation factor (η). It moved to higher spin with an increase in η. This feature for the $i_{13/2}$ orbitals was first mentioned by Løvhøiden and Rekstad (1976) for the N=89 odd-A nuclei. It seems to be a general result for the Coriolis mixed $i_{13/2}$ orbitals, including doubly-even nuclei. It was found that the effect of η on the reaction strength was not very drastic. In the (^{3}He,α) reaction, two of the states, $I^\pi = 6^-$ and 7^-, are expected to be populated with very large strengths. Moreover these two states are very close in energy (figure 5.9) for large η. With these theoretical features,

Figure 5.9

Calculated energies of yrast states arising from the $i_{13/2}$ orbitals coupled to the $3/2^-[521]$ orbital for ^{154}Gd.

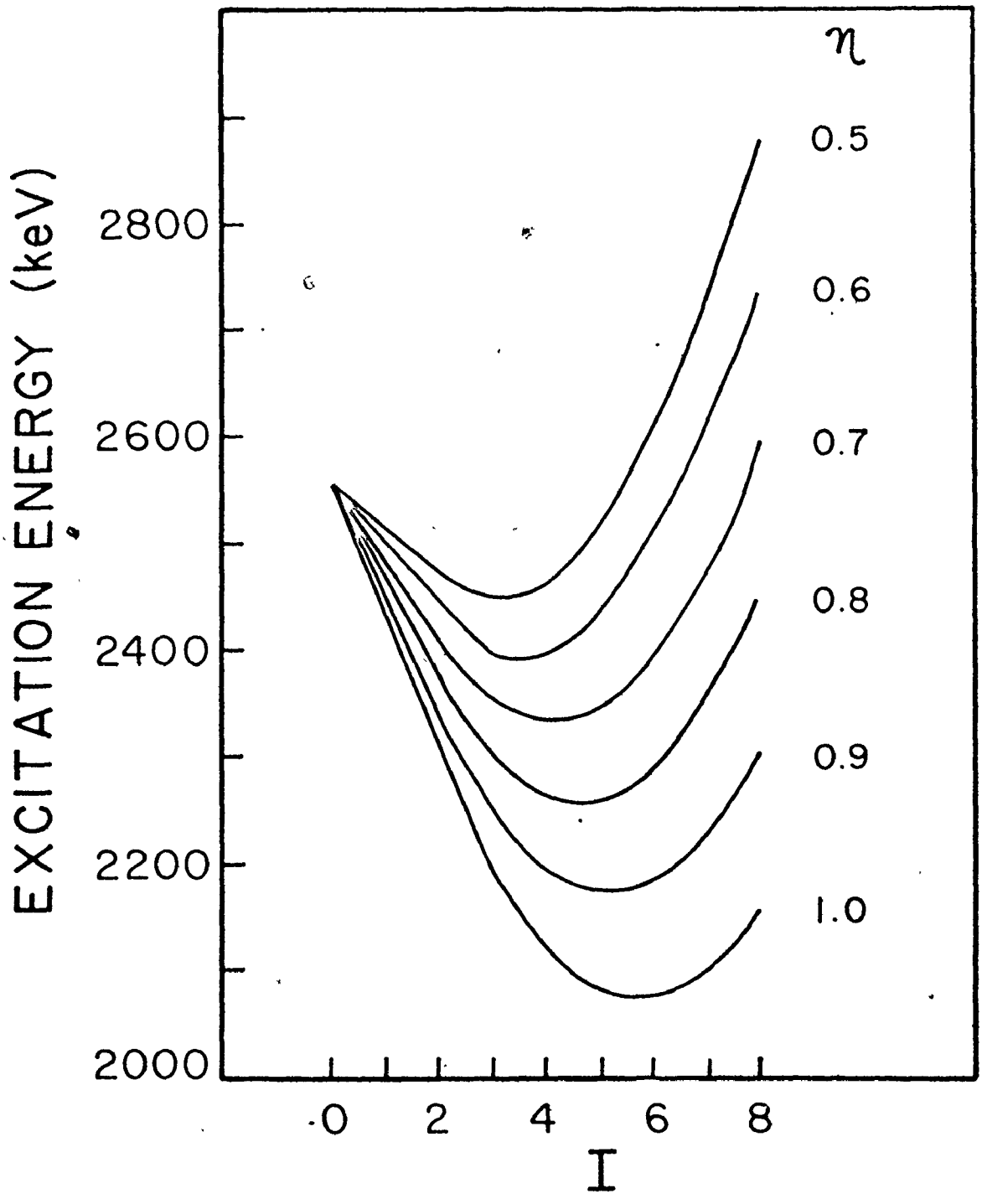
η
0.5
0.6
0.7
0.8
0.9
1.0
EXCITATION ENERGY (keV)
2800
2600
2400
2200
2000
0
2
4
6
8
I

it is suggested that the peak at 2150 keV is composed of these two states.

A similar Coriolis calculation has been extended to higher spin members to describe the phenomenon of 'backbending' in the doubly-even nuclei (Flaum and Cline, 1975).

5.10 The Transfer of the $1/2^-[530]$ Neutron

In the $^{156}Gd(d,t)^{155}Gd$ reaction at 60°, the $3/2,1/2^-[530]$ state is excited at 451 keV with a cross section of 405 μb/sr. It can be expected that the two-quasiparticle states of the $\{3/2^-[521]\pm1/2^-[530]\}_\nu$ configurations in ^{154}Gd, should also be populated in the (d,t) reaction. In this mass region the other negative parity Nilsson orbitals are $1/2^-[510]$, $3/2^-[532]$ and $5/2^-[523]$. The parallel and anti-parallel coupling of these orbitals will generate a large number of bands which would be greatly perturbed by the Coriolis interaction. This makes the identification of the states arising from the $\{3/2^-[521]\pm1/2^-[530]\}_\nu$ configurations very difficult. However, it can be noticed that some of the unassigned levels at 2209, 2417, 2467, 2489 and 2513 keV have been excited strongly in the (d,t) reaction (table 4.1). Possibly these levels might be associated with the transfer of $1/2^-[530]$ neutron.

5.11 The Transfer of the $3/2^+[411]$ Proton

i) The $K^\pi = 4^+$ Band

Three members, I = 4,5,6, of a $K^\pi = 4^+$ band at excitation energies 1645.9, 1770.3 and 1911.7 keV were known

from the ^{154}Tb decay studies (Riedinger et al., 1971, Sousa et al., 1975). Recently, West et al. (1976) have suggested a level at 2117.1 keV as the I=7 member of this band. The rotational character of these levels is described by a rotational parameter value of 12.1 keV. Prior to these results, Meyer (1968) had suggested that the levels at 1645.9 and 1770.3 keV might form a two phonon band in view of the preferential decay to these states to the one phonon vibrational band. Sousa et al., also considered this possibility, but their choice favours a two-quasiproton configuration for these levels. This description will become more transparent in view of the present proton transfer reactions study.

The (^{3}He,d) and (α,t) spectra (figure 3.5) show two peaks at 1646 and 1770 keV populated very strongly in both reactions. These levels have approximately the same reaction cross sections (tables 4.2 and 5.10). The cross section ratios indicate a predominantly ℓ=2 character for these levels (figure 4.2). The level at 1912 keV has been populated with only very little intensity in both the (^{3}He,d) and (α,t) reactions.

In the study of the odd mass europium (Ungrin et al., 1969, Tippett, 1972) and the terbium isotopes (Boyno and Huizenga, 1972, Tippett and Burke, 1972) by proton transfer reactions, the states populated by the transfer of the $3/2^+$[411] orbital have been identified and the I=5/2 members have been excited very strongly. This Nilsson orbital

Table 5.10

Cross section (μb/sr) to the levels in ^{154}Gd populated by the transfer of the $3/2^+[411]$ proton orbital

Excitation Energy (keV)	I,K^π	$(^3He,d)_{30°}$	$(\alpha,t)_{45°}$
1646	$4,4^+$	30	27
1770	5,	39	28
1912	6,	1	1
2175	$1,1^+$	12	4
2223	2,	31	12
2294	3,	16	8
2400	4,	6	3

originates from the $d_{5/2}$ shell model state. The parallel and anti-parallel coupling of the $3/2^+[411]$ proton with the ^{153}Eu target ground state, $5/2^+[413]$, would form two bands, $K^\pi = 4^+$ and 1^+ respectively. Both of these bands are expected to be populated strongly. The expected cross sections to the I=4 to 6 members of the $K^\pi = 4^+$ band have been calculated for the $(^3He,d)_{30°}$ and $(\alpha,t)_{45°}$ for an emptiness factor $U^2 = 0.68$. These cross sections have been compared with the observed cross sections in the same reactions for the 1646, 1770 and 1912 keV levels (figure 5.10) and the comparison shows very good agreement between calculations and experiments. Thus the present study, without any ambiguity, confirms the previous assignments for the known $K^\pi = 4$ band and also establishes the two-quasiparticle configuration as $\{5/2^+[413]+3/2^+[411]\}_\pi$.

ii) <u>The $K^\pi = 1^+$ Band</u>

It can be seen from the $(^3He,d)$ and (α,t) spectra (figure 3.5), that the density of levels above 2000 keV is very large and thus the reaction strength is not concentrated in a few states. However, the levels at 2223 and 2294 keV do have appreciable cross sections in the proton transfer reactions (tables 4.2 and 5.10). The cross section ratios (figure 4.2) are consistent with an $\ell=2$ transition which may be due to the transfer of a $3/2^+[411]$ proton. The calculations for the various members of the $K^\pi = 1^+$ band formed by the anti-parallel coupling of the $3/2^+[411]$ with the $5/2^+[413]$,

Figure 5.10

A comparison of the predicted and observed cross sections in the $(^3He,d)_{30°}$ and $(\alpha,t)_{45°}$ reactions for the members of the $K^\pi = 4^+$ and 1^+ bands of the $\{5/2^+[413] \pm 3/2^+[411]\}_\pi$ configurations in ^{154}Gd. The solid lines are the predicted cross sections and arrows show the observed cross sections (μb/sr).

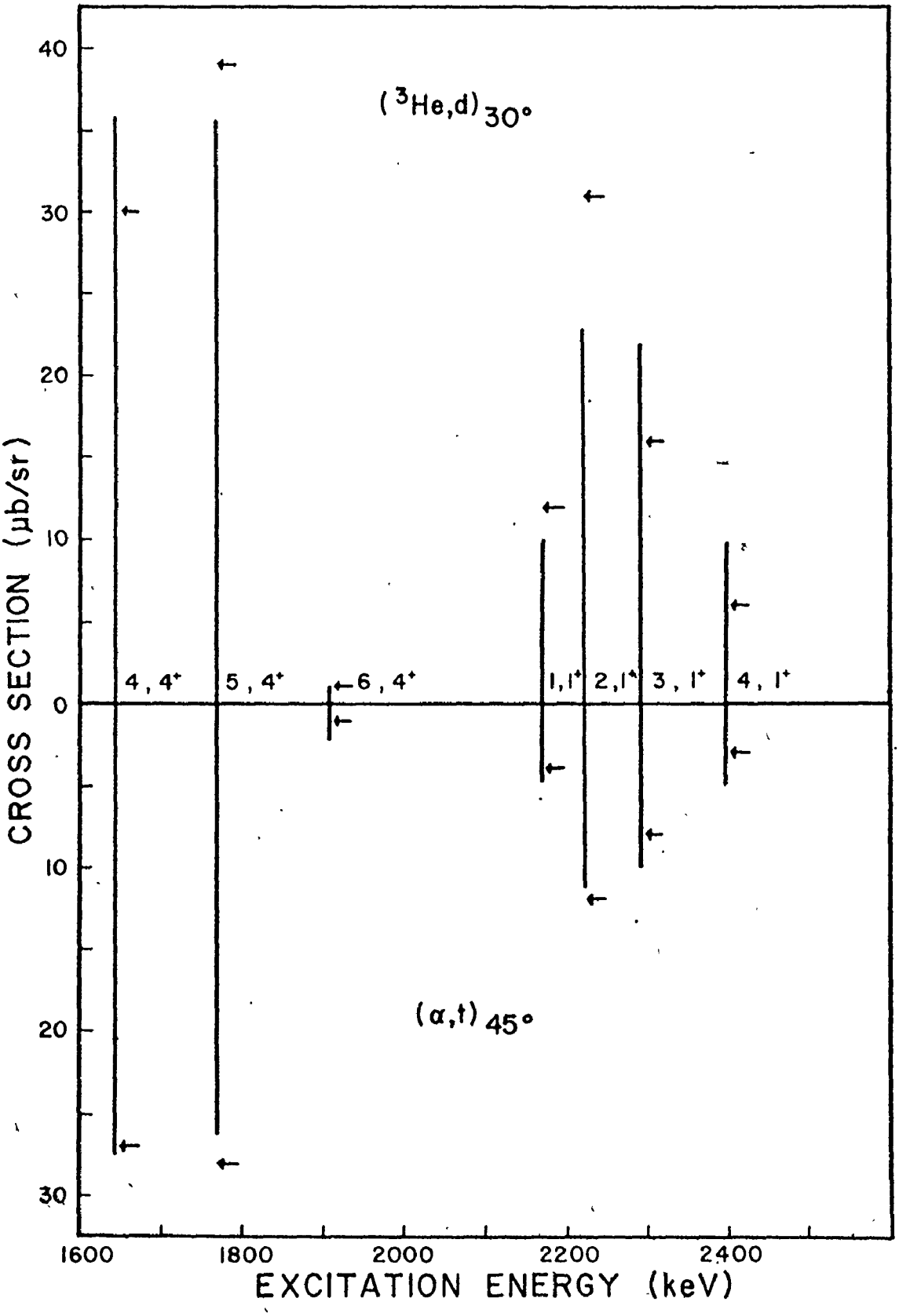
(³He,d)30°
(α,t)45°
4, 4⁺
5, 4⁺
6, 4⁺
1, 1⁺
2, 1⁺
3, 1⁺
4, 1⁺
CROSS SECTION (μb/sr)
EXCITATION ENERGY (keV)
40
30
20
10
0
10
20
30
1600
1800
2000
2200
2400

show that most of the strength is concentrated among the first four members I=1 to 4. The other feature of this calculation is that the spin I=2 and 3 members should have approximately the same intensity. The I=1 and 4 members should have about one half the intensity of the others. Based upon these predictions, it is proposed that the levels at 2223 and 2294 keV are the I=2 and 3 members respectively of the $K^{\pi} = 1^{+}$ band. The other members, I=1 and 4, are assigned to the levels at 2175 and 2400 keV respectively. These levels are also consistent with an ℓ=2 character for their reaction cross sections (figure 4.2). It can be seen from the energy spacings of these four levels, 2175, 2223, 2294 and 2400 keV, that they could be the I=1,2,3 and 4 members of a well-behaved rotational band $K^{\pi} = 1^{+}$. The rotational parameter value for these levels is 12.5 keV which is very close to that of the $K^{\pi} = 4^{+}$ band formed by the same Nilsson configurations.

The distribution of the strength in the $(\alpha,t)_{45°}$ and $(^{3}He,d)_{30°}$ reactions for these levels is shown in figure 5.10. Also included is the predicted strength for the band members for an emptiness factor $U^2 = 0.55$. It can be seen that in general the agreement seems to be quite good. However the results are not as good as in the case of the K=4 band. This is probably because the K=1 band is situated in that region, where the effects of other bands with $\Delta K = \pm 1, 0$ might be important.

The assignments made here for the $K^{\pi} = 1^{+}$ band are not known from the previous decay studies (Meyer, 1968, Sousa et al., 1975).

The Gallagher (1962) rule for the coupling of the angular momenta in doubly-even nuclei predicts that the lower band should have $\Sigma=0$. The present assignments for the two bands, K=4 and 1, discussed above correspond to the two-quasiparticle configurations $\{5/2^{+}[413] \pm 3/2^{+}[411]\}_{\pi}$ which have $\Sigma=0$ for the K=4 band.

5.12 The Transfer of the $1/2^{+}[411]$ Proton

i) The $K^{\pi} = 2^{+}$ Band

The two peaks at 2148 and 2250 keV have been populated with relatively large (^{3}He,d) and (α,t) cross sections (tables 4.2 and 5.11). The cross section ratios of these levels indicate a transition corresponding to $\ell=2$, as was shown to be the case for the gamma band member (figure 4.2). The observed intensity patterns to the 2148, 2250 and 2386 keV levels (figure 5.11) are similar to the gamma band (figure 5.3). Due to these similarities it is proposed that the levels at 2148, 2250 and 2386 keV probably have a two-quasiparticle configuration identical to that component through which the gamma band members have been populated in the proton transfer reactions. These levels are thus assigned as the 2^{+}, 3^{+} and 4^{+} members respectively of the K=2 band of the $\{5/2^{+}[413]-1/2^{+}[411]\}_{\pi}$ configuration. The calculated cross sections for the various band members show

Table 5.11

Cross sections (μb/sr) to the levels in ^{154}Gd populated by the transfer of the $1/2^+[411]$ proton orbital

Excitation Energy (keV)	I,K^π	$(^3He,d)_{30°}$	$(\alpha,t)_{45°}$
2148	$2,2^+$	15	6
2250	3,	17	8
2386	4,		2
2513	$3,3^+$	20	7
2652	4,	6	2

Figure 5.11

A comparison of the predicted and observed cross sections in the $(^3He,d)_{30°}$ and $(\alpha,t)_{45°}$ reactions for the various members of the $K^\pi = 2^+$ and 3^+ bands of the $\{5/2^+[413] \mp 1/2^+[411]\}_\pi$ configurations in ^{154}Gd. The solid lines are the predicted cross sections and arrows show the observed cross sections (μb/sr).

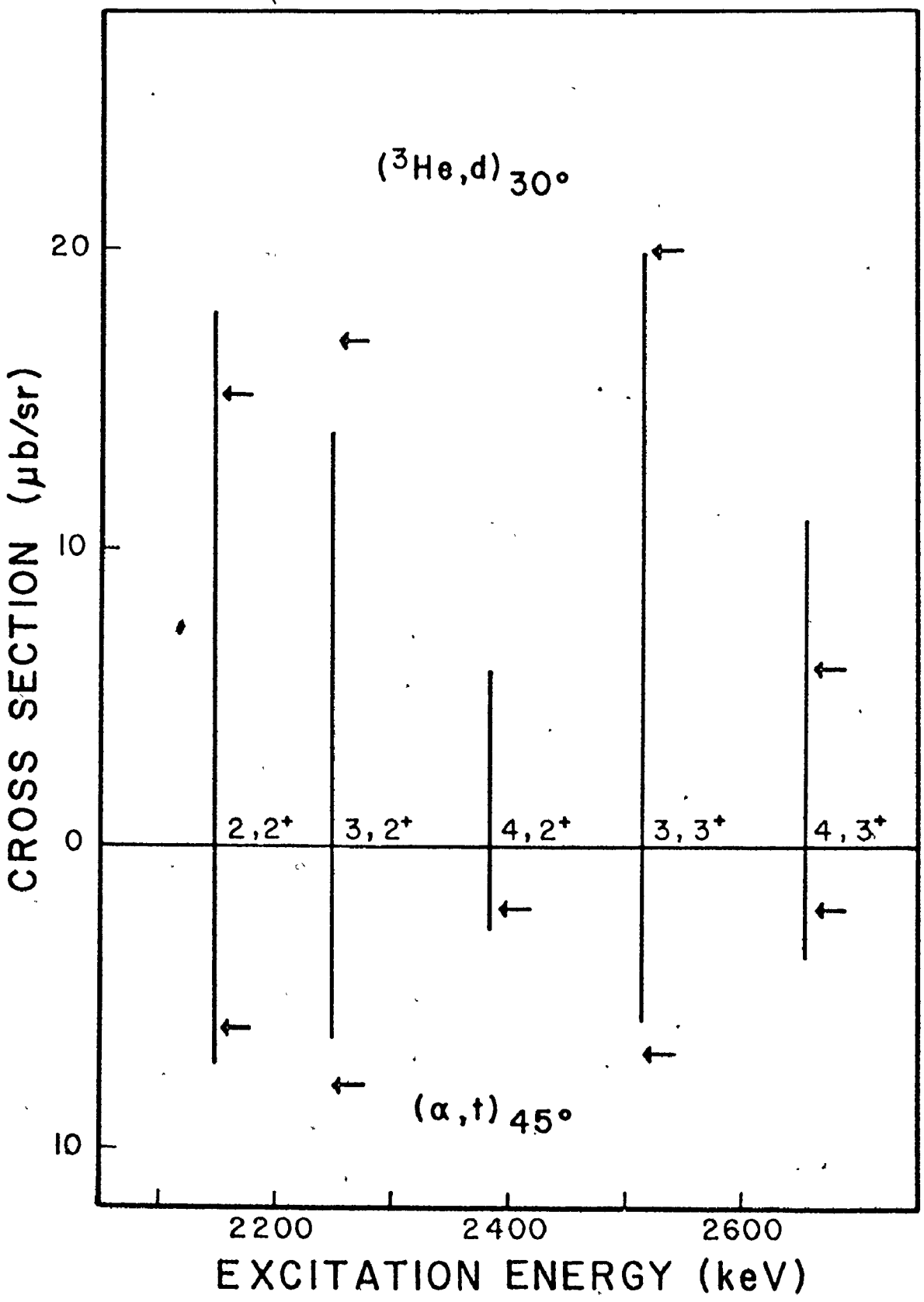
(3He,d)30°
(α,t)45°
20
10
0
10
CROSS SECTION (μb/sr)
2,2+
3,2+
4,2+
3,3+
4,3+
2200
2400
2600
EXCITATION ENERGY (keV)

that most of the spectroscopic strength is contained in the first three members. The predicted cross sections for the 2^+, 3^+ and 4^+ members agree quite well with the observed cross sections in the $(^3He,d)_{30°}$ and $(\alpha,t)_{45°}$ reactions for the levels at 2117, 2250 and 2386 keV respectively when an assumed emptiness factor $U^2 = 0.29$ is used (figure 5.11). A similar correspondence has been found for these levels at the other laboratory angles. The inertial parameter of this $K^\pi = 2^+$ band is 17 keV.

ii) The $K^\pi = 3^+$ Band

Two levels at higher excitation energies, 2513 and 2652 keV (table 5.11) have cross section ratios (figure 4.2) similar to those of the states at 2148 and 2250 keV of the K=2 band discussed in the previous section. These levels might be populated by the transfer of the same $1/2^+[411]$ proton coupled to the $5/2^+[413]$ target ground state. The parallel coupling of the orbitals would yield a $K^\pi = 3^+$ band. The cross sections for the $(^3He,d)$ and (α,t) reactions for the $K^\pi = 3^+$ band members have been calculated for a $U^2 = 0.23$. The calculated cross sections show that most of the spectroscopic strength is contained in the first two members, I=3 and 4. The comparison of the predicted cross sections of the levels populated at excitation energies of 2513 and 2652 keV in the $(^3He,d)_{30°}$ and $(\alpha,t)_{45°}$ reactions is shown in figure 5.11. It can be seen that by and large the agreement is quite good and thus these levels have been as-

signed as the I=3 and 4 members of the $K^{\pi} = 3^{+}$ band of the two-quasiparticle configuration $\{5/2^{+}[413]+1/2^{+}[411]\}_{\pi}$. It should also be noted that the energy difference of 140 keV between these members is very similar to that of the corresponding members in the previously discussed $K^{\pi} = 2^{+}$ band. Further, the $K^{\pi} = 2^{+}$ band is at a lower excitation energy, 2148 keV, than the $K^{\pi} = 3^{+}$ band, 2513 keV, as is predicted by the Gallagher rule (1962) for the doubly-even nucleus.

It is worth mentioning that in the (d,t) reactions, levels at 2150, 2247, 2386, 2514 and 2656 keV (Table 4.1) have also been excited at energies very similar to those discussed above. With the exception of the 2150 keV level, which has also been populated in the (^{3}He,α) reaction, these levels are probably the ones which have been populated in the proton transfer reactions. The neutron component of these might arise from the $1/2^{-}[530]$, $1/2^{-}[510]$, $3/2^{-}[532]$ or $5/2^{-}[523]$ neutron orbitals coupled with the $3/2^{-}[521]$.

5.13 The Coriolis Mixed Negative Parity Band

From table 4.2, it can be seen that there is a large number of levels which have been populated in the (α,t) reactions and have not been observed in the (^{3}He,d) reaction. Such levels should have been populated by a high ℓ-transfer, probably 4 or 5. In the neighbouring odd mass europium (Ungrin et al., 1969) and the terbium isotopes (Boyno and Huizenga, 1972, Tippett and Burke, 1972) ℓ=5 transitions have been observed in the (^{3}He,d) and (α,t) reactions at low

excitation energies. These states are associated with the Coriolis mixed $5/2^-[532]$ and $7/2^-[523]$ Nilsson orbitals from the $h_{11/2}$ shell . In the case of ^{154}Gd, the number of bands due to these orbitals is rather large. This makes it difficult to investigate these states in detail. The Coriolis calculations involving the Nilsson orbitals from the $h_{11/2}$ shell show that of these the lowest $I^\pi = 7^-$ should have the largest cross sections in the (α,t) and $(^3He,d)$ reactions. A peak at 2570 keV in the (α,t) reaction is populated strongly with a $(\alpha,t)_{45°}$ cross section of 15 μb/sr and a corresponding $(^3He,d)_{30°}$ cross section of 9 μb/sr. The cross section ratio plot (figure 4.2) indicates a high ℓ-transfer is involved. Thus it is proposed that this level at 2570 keV has $I^\pi = 7^-$. Two other levels at 2432 and 2739 keV have been observed in the (α,t) reaction with their reaction strengths 8 and 4 μb/sr at a laboratory angle of 45°. The Coriolis calculations mentioned above predict that the $I^\pi = 6^-$ and 8^- states should be at approximately these energies relative to the 7^- state. A similar correspondence in the energy exists in the isotonic nucleus ^{152}Sm for a negative parity state at somewhat lower excitation energy than in ^{154}Gd (Waddington, 1976, Hirning and Burke, 1976). The observed cross sections for the 2739 keV level are much smaller than the predictions (figure 5.12).

Figure 5.12

A comparison of the calculated and observed cross sections in the $(\alpha,t)_{45°}$ and $(^3He,d)_{30°}$ reactions. The solid lines are the predicted cross sections for the $I^\pi = 6^-$, 7^- and 8^- states of the Coriolis mixed bands from the $\{5/2^+[413]+h_{11/2}\}_\pi$ configurations. The arrows show the observed cross sections (μb/sr).

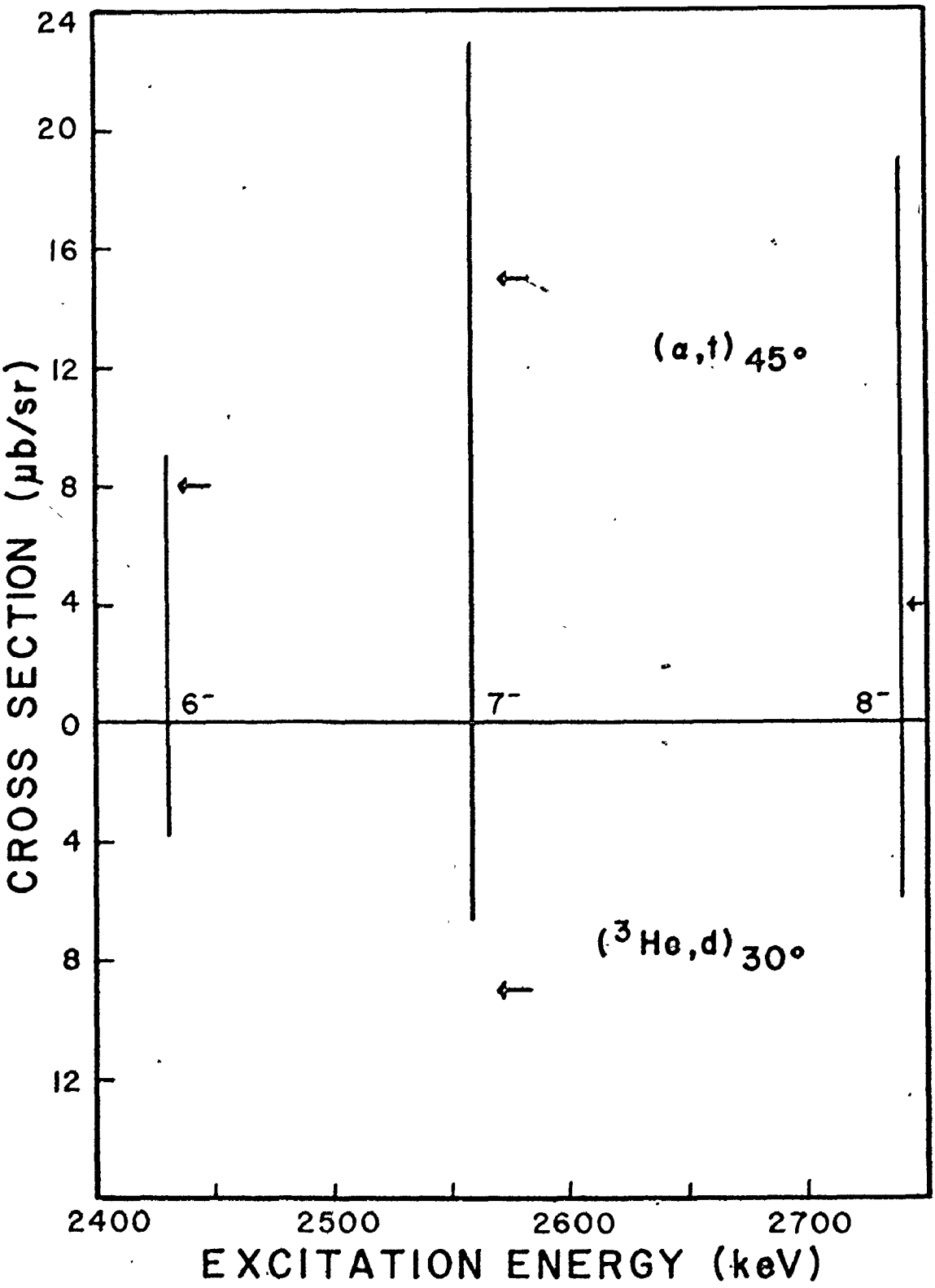
24
20
16
12
8
4
0
4
8
12
CROSS SECTION (μb/sr)
(α,t) 45°
(³He,d) 30°
6⁻
7⁻
8⁻
2400
2500
2600
2700
EXCITATION ENERGY (keV)

5.14 Levels Above the Energy Gap Populated in Reactions and the Decay of ^{154}Tb

Table 5.12 lists those levels which have not been discussed so far and which are populated in the proton and/or the neutron transfer reactions. Furthermore their configuration, wherever it is available from the decay properties of ^{154}Tb (Sousa et al., 1975), is included. It is worthwhile to mention that an agreement in energy might be just a coincidence, because in this region the level density is very high.

5.15 The $K^{\pi} = 1^{+}$ Band at 2187.2 keV

Although Sousa et al. (1975) have determined that the level at 2187.2 keV has $K^{\pi} = 1^{+}$, the spin was only limited to 1 or 2. The other members of this band are also not known. There exists a number of levels for which the possible spin and parity quoted are $I^{\pi} = 2^{+}$, 3 or 4^{+}. There are three of these levels at excitation energies of 2230.0, 2305.8 and 2407 keV which might be the I=2,3 and 4 respectively members of the $K^{\pi} = 1^{+}$ band at 2187.2 keV. These four levels exhibit a rotational pattern corresponding to a rotational parameter of 12.2 keV. It can be seen that there exists a set of levels populated in the (α,t) reaction which falls very close to the excitation energies of the levels observed in the ^{154}Tb decay (Sousa et al., 1975). (table 5.13).

In the (α,t) reaction all four members have very similar reaction strengths. In the (^{3}He,d) reaction only one member ($I^{\pi} = 3^{+}$) at 2304 keV has been populated, while only the first two members, $I^{\pi} = 1^{+}$ and 2^{+} have been observed

Table 5.12

Levels above the energy gap in ^{154}Gd populated in reactions and in the decay of ^{154}Tb

Assignment[a] I^{π},K	^{154}Tb decay keV	(d,t) keV	(d,t) $(\frac{d\sigma}{d\Omega})_{60°}$	(^{3}He,α) keV	(^{3}He,α) $(\frac{d\sigma}{d\Omega})_{45°}$	(α,t) keV	(α,t) $(\frac{d\sigma}{d\Omega})_{45°}$	(^{3}He,d) keV	(^{3}He,d) $(\frac{d\sigma}{d\Omega})_{30°}$
A	2025					2025	1		
B	2081.0	2082	ob						
4^+	2093.8					2089	3	2091	8
$1^+,1$	2119.7	2122	1			2117	12	2116	18
4^-	2186.0	2189	3			2186	6		
$(1^+,2^+),1$	2187.2								
		2209	20[c]			2210	3		
B	2230.0	2230	12			2234	5		
B	2266	2266	8	2267	7	2262	2		
B	2305.8					2304	6	2304	13
A	2342.6					2344	1	2346	5
B	2407					2411	6		
$(3^+,4^+)$	2416.3					2420	10	2424	12
A	2430.5					2432	8		

(continued next page)

Table 5.12 (continued)

Assignment[a] I^{π},K	^{154}Tb decay keV	(d,t) keV	(d,t) $(\frac{d\sigma}{d\Omega})_{60°}$	(^{3}He,α) keV	(^{3}He,α) $(\frac{d\sigma}{d\Omega})_{45°}$	(α,t) keV	(α,t) $(\frac{d\sigma}{d\Omega})_{45°}$	(^{3}He,d) keV	(^{3}He,d) $(\frac{d\sigma}{d\Omega})_{30°}$
(7,8)	2459.6	2461	85[d]						
A	2468	2467				2466	5	2467	10
A	2590	2590	11						
		2595	7			2594	6	2591	9
		2606	un			2605	1		
		2717	14[d]			2718	3		
		2749	10			2749	5	2752	6
		2786	15			2785	7	2782	7

a: Sousa et al. (1975)

A: $(1,2^+)$

B: $(2^+,3,4^+)$

c: contaminated

d: doublet

Table 5.13

$K^{\pi} = 1^{+}$ Band at 2187.2 keV

I,K^{π}	Excitation Energy keV				Cross sections (μb/sr)			
	Previous[a]	(α,t)	(^{3}He,d)	(d,t)	$(\alpha,t)_{45°}$	(^{3}He,d)$_{30°}$	$(d,t)_{60°}$	
$1,1^{+}$	2187.2	2186		2189	6		3	
2,	2230.0	2234		2230	5		12	
3,	2305.8	2304	2304		6	13		
4,	2407	2411			6			

a: Sousa et al. (1975)

at 2189 and 2230 keV respectively in the (d,t) reaction. No corresponding levels were observed in the (^{3}He,α) reaction.

It is interesting to note that this band is situated at an excitation energy about 11 keV higher than the other $K^\pi = 1^+$ band at 2175 keV populated in the proton transfer reactions (section 5.11.ii). This lower $K^\pi = 1$ band was assigned to the two-quasiproton configuration $\{5/2^+[413]-3/2^+[411]\}_\pi$. It might be speculated that a mixed two-quasineutron and proton configuration might be responsible for this band (Khoo et al., 1972). To prove this point it would be required to observe another $K^\pi = 1^+$ band in both the proton and neutron transfer reactions. An explanation of this situation in ^{154}Gd is not possible at this time.

CHAPTER 6

NUCLEAR STRUCTURE OF ^{152}Eu

6.1 The Transfer of the $11/2^-[505]$ Neutron and the Ground State Band

The ground state of ^{152}Eu is known to be $I^\pi = 3^-$ (Takahashi et al., 1965). In the (d,t) studies its configuration was assigned (von Egidy et al., 1975) as the antiparallel coupling of the $5/2^+[413]$ proton from the ^{153}Eu target and the $11/2^-[505]$ transferred neutron corresponding to $K^\pi = 3^-$. This assignment has been confirmed in the present study of the (^{3}He,α) reaction, where high ℓ-values are preferentially populated. Thus the other possibilities suggested by Takahashi et al., (1965), viz. $\{7/2^+[404]\}_\pi - \{1/2^-[530]\}_\nu$ and $\{3/2^+[411]\}_\pi + \{3/2^-[521]\}_\nu$ for the ^{152}Eu ground state are not correct. In the previous study (von Egidy et al., 1975), a level at 89.613 keV was shown to decay to the ground state by an M1 transition. This level has been interpreted as the 4^- member of the ground state band and the 5^- member has been assigned at 200.75 keV (von Egidy et al., 1975). In the (^{3}He,α) reaction a level at 90 keV has been observed which is most likely the second member of the ground state band. It appears that these three members of the ground state band show a well behaved rotational pattern corresponding to

a rotational parameter value of $\sim$ 11 keV.

On the other hand, only the $I,K^{\pi} = 8,8^{-}$ member of the band formed by parallel coupling of the $5/2^{+}[413]$ proton and $11/2^{-}[505]$ neutron can be populated in the (^{3}He,α) reaction. For the $11/2^{-}[505]$ orbital, the $C_{j\ell}^{2}$ value is 1.0 for $j = 11/2$ and all the (^{3}He,α) reaction strength is concentrated in this 8^{-} state. The level at 148 keV (a 96 minute isomer of ^{152}Eu) was populated strongly at all angles and has been assigned as this $I^{\pi} = 8^{-}$ state.

These two bands, $K^{\pi} = 3^{-}$ (ground state) and $K^{\pi} = 8^{-}$ (at 148 keV), agree with the neutron-proton coupling rules for deformed nuclei due to Gallagher and Moszkowski, (1958).

6.2 The Transfer of the $3/2^{+}[411]$ Proton

i) The $K^{\pi} = 4^{-}$ Band

In the (^{3}He,d) and the (α,t) spectra (figure 3.6) there are two distinct peaks at 268 and 431 keV. The cross sections to these levels are large compared to those for other levels populated in ^{152}Eu (table 4.3). The cross section ratios indicate a predominant ℓ=2 transfer to these levels (figure 4.3). In the neighbouring odd-mass nuclei, ^{153}Eu and ^{155}Eu, the most strongly populated low-lying states, are also fed by ℓ=2 transitions (Ungrin et al., 1969, Tippett, 1972).

These levels at 173 keV in ^{153}Eu and 307 keV in ^{155}Eu have been assigned as the 5/2,3/2$^+$[411] states. In ^{152}Eu one would expect to populate strongly two bands with the transfer of a 3/2$^+$[411] proton. Since the target ground state has a large component of K = 5/2, these bands will have K=1 and 4. The strength to the low K band will be spread over about 5 states, but only 2 members (I=4 and 5) of the high K band will be populated appreciably.

The expected cross-sections to the $I^\pi = 4^-$ and 5^- members have been calculated under the assumption that the target ground state has K = 5/2. If the 3/2$^+$[411] orbital has $U^2 = 1.0$ in the target, these cross sections would be 64 and 65 μb/sr in the (^{3}He,d) reaction at 30°. The cross sections to the 268 and 431 keV levels were found to be 53 and 42 μb/sr respectively. Similar agreement is found for the (α,t) reaction. Therefore it is reasonable to assign these two states as the 4^- and 5^- members of the K=4 band formed by coupling a 3/2$^+$[411] proton to the odd neutron in the ground state of ^{151}Sm. Previous information (von Egidy et al., 1975) for the ^{152}Eu nucleus has shown two levels at 265.7 keV and 267.6 keV for which the values for spin and parity quoted are (3^-) and (3,4) respectively . The present study implies that one of these levels (most likely the one at 267.6 keV) has $I^\pi = 4^-$.

ii) <u>The $K^\pi = 1^-$ Band</u>

From table 4.3 it can be seen that the 221 keV level is the lowest strongly populated level (26 μb/sr and 12 μb/sr

in the $(^3He,d)_{30°}$ and the $(\alpha,t)_{60°}$ reaction respectively). The cross section ratio plot, figure 4.3, indicates an $\ell=2$ value for this level. The 321 keV level has also a fairly large cross-section of 12 μb/sr in the $(^3He,d)_{30°}$ reaction but is unresolved in the $(\alpha,t)_{60°}$ spectrum. A comparison of the cross sections at other angles has shown that its population is due to a low value, probably $\ell=2$. Thus these two levels may be populated by the transfer of a $3/2^+[411]$ proton. The calculations for the antiparallel coupling of the $3/2^+[411]$ proton state to a $K^\pi = 1^-$ band indicate the spin 2 and 3 members should have approximately the same intensity. These findings have led to the conclusion that the 221 and 321 levels are the $I^\pi = 2^-$ and 3^- members of the K=1 rotational band. Previous studies (von Egidy et al., 1975) have shown that there are three closely spaced levels at 220.80 keV (3^-), 221.2 keV (3^+, $\{5/2^-[532]\}_\pi - \{11/2^-[505]\}_\nu$) and 221.453 keV ($2^+$). Most probably the latter is the one populated in these proton transfer reactions. Two levels at 321.0 keV (2,3) and 321.8 keV (3,4) are also known (von Egidy et al., 1975). One of these levels might be the 3^- state which is populated in these reactions. Using the I(I+1) interval rule and the energy spacing between the 221 and 321 keV levels, one obtains an inertial parameter of 16.6 keV. This value is amazingly close to that of 16.3 keV obtained for the K=4 band. Other members of the K=1 band do not have large spectroscopic strengths and have not been identified.

The present results indicate that the K=1 band lies lower in energy than the K=4 band. For such a case, the Gallagher-Moszkowski rule (1958) predicts that the K=1 band should correspond to Σ=1, while the K=4 band to the Σ=0. This is possible only if the ^{151}Sm target ground state has $\Omega = \Lambda - \Sigma$ as is the case for the 5/2$^-$[523] orbital. These findings from the present investigation are in accordance with the results of Nelson et al., (1973) for the ^{151}Sm ground state.

6.3 Levels at 65, 111 and 175 keV

In the previous study (von Egidy et al., 1974), it has been suggested that the levels at 65.3 keV (1$^-$), 111.4 keV (2$^-$) and 174.9 keV (3$^-$) might form a rotational band. These levels have been populated in the (d,t) reaction probably by a removal of a 3/2$^-$[521] neutron. If this were so, the component of the wave function populated would have K=1, $\{5/2^+[413]\}_\pi - \{3/2^-[521]\}_\nu$. All of these states were also observed in present proton transfer reactions and the 111 keV state was seen in the (^{3}He,α) reaction. Since the ^{151}Sm ground state contains an admixture of a 3/2$^-$[521] neutron, the above component could be populated by the transfer of a 5/2$^+$[413] proton. However, figure 4.3 shows that ℓ=2 is also involved in the population of the 65 and 175 keV levels. This indicates that the situation is not very simple and probably mixed configurations are responsible for such an effect. The information obtained from these experiments is not sufficient to

determine these mixing amplitudes

6.4 Isomeric State at 46 keV

This 9.3 hour isomer of ^{152}Eu is known (Takahashi et al., 1965) to have $I^{\pi} = 0^-$ and is populated weakly in the (^{3}He,d) and the (α,t) reactions. Takahashi et al. have suggested three possibilities for the configuration of this isomer, viz:

a) $\{5/2^+[413]\}_{\pi} - \{5/2^-[523]\}_{\nu}$,

b) $\{5/2^-[532]\}_{\pi} - \{5/2^+[642]\}_{\nu}$,

c) $\{3/2^+[411]\}_{\pi} - \{3/2^-[521]\}_{\nu}$.

Configuration (b) may not be populated in the proton transfer reactions because the ^{151}Sm ground state has negative parity. The cross section ratio for this level indicated an ℓ-value of 2 which is consistent with the transfer of a $3/2^+[411]$ proton. The calculated cross section for configuration (a) is much smaller than the observed one. However, the small amount of $3/2^-[521]$ admixture in the ^{151}Sm target ground state could result in an observable cross section for the 0^- state if configuration (c) were present in the 46 keV level. The present data are not sufficient to allow a determination of the amplitude of this configuration, as the $3/2^-[521]$ amplitude in the target ground state is not known.

6.5 Other Levels

A number of other levels has been observed which are known from the previous work (von Egidy et al., 1975). Spin and parity assignments for the 142 and 247 keV levels have been made as 4^- and 3^- respectively . These two levels are

populated very weakly in the $(^3He,d)_{30°}$ reaction and with moderate strength in the $(\alpha,t)_{60°}$ reaction.

Since there is no previous information available about a large number of the levels, it was found to be impossible to make assignments for them. Furthermore, the nuclear models available may not be adequate to describe all the levels populated in these reactions.

6.6 Total Reaction Strength

If the low-lying states populated in ^{152}Eu may be thought of as consisting of the Nilsson model orbitals $3/2^+[411]$, $5/2^+[413]$ and $5/2^-[532]$ coupled to the $I^\pi = 5/2^-$ ground state of ^{151}Sm, then the cross sections could be calculated with expression 2.12.1. Table 6.1 gives the total cross sections expected with this assumption. The transfer of $3/2^+[411]$, $5/2^+[413]$ and $5/2^-[532]$ protons is largely by ℓ=2, 4 and 5 respectively.

The target ground state ($I^\pi = 5/2^-$) is not well described as a pure Nilsson model orbital (Nelson et al., 1973). Although it has a large component of $K^\pi = 5/2^-$ (probably $5/2^-[523]$), it may have a small component of $3/2^-[521]$. As a result of this, the reaction strength of table 6.1 is not concentrated in a few states, but is distributed over many levels of ^{152}Eu.

One important piece of information, however, comes from the total observed cross sections of all the levels of

Table 6.1

Expected total strength in the low lying levels of ^{152}Eu. Values are predicted cross-sections (μb/sr) obtained from DWBA calculations for 24 MeV $(^3He,d)_{30°}$ and 27 MeV $(\alpha,t)_{60°}$ Calculations included the $3/2^+[411]$, $5/2^+[413]$ and the $5/2^-[532]$ Nilsson orbitals. U^2 was assumed to be 1.

ℓ-value	Cross sections (μb/sr)	
	$(^3He,d)_{30°}$	$(\alpha,t)_{60°}$
2	270	143
4	46	88
5	30	90

^{152}Eu up to 531 keV. The sum of the cross sections to these levels yields a value of 290 μb/sr for the $(^{3}He,d)_{30°}$ reaction. This agrees very well with the cross section observed in the $^{152}Sm(^{3}He,d)^{153}Eu$ reaction summed to 570 keV (Tippett, 1972). This indicates that most of the levels populated in ^{152}Eu may be thought of as mixtures of $3/2^{+}[411]$, $5/2^{+}[413]$ and $5/2^{-}[532]$ protons coupled to the ground state of ^{151}Sm.

CHAPTER 7

SUMMARY

Various single nucleon transfer reactions have been employed to probe the nuclear structure of two transitional nuclei, $^{154}_{64}Gd_{90}$ and $^{152}_{63}Eu$. At least some of the levels in these nuclei showed a rotational nature and can be described within the framework of the unified model. Many of the states populated in these reactions have been described as the two-quasiparticle configurations of the two unpaired Nilsson orbitals. It was also found necessary to incorporate other effects such as pairing, Coriolis and $\Delta N=2$ interactions. For the doubly-even nucleus $^{154}_{64}Gd_{90}$, the microscopic nature of the collective states was also described in terms of two-quasiparticle configurations.

7.1 ^{154}Gd

The level structure and possible two-quasiparticle configurations in ^{154}Gd are summarized in table 7.1. In this table, for comparison's sake, the results of previous investigators are also shown. The same level scheme arranged in various rotational bands has been shown in figures 7.1-3. In figure 7.1 the collective bands known from the previous studies (Sousa et al., 1975 and West et al., 1976) have also been in-

Table 7.1

Level structure of ^{154}Gd

Excitation Energies (keV)							Assignments		Configuration
^{154}Tb [a] decay	^{154}Eu [b] decay	(d,d') [c]	(d,t)	(^{3}He,α)	(α,t)	(^{3}He,d)	Previous I,K^π	Present I,K^π	
0	0	0	0	0	0	0	$0,0^+$	$0,0^+$	ground state band
123.1	123.14	123	123	122	123	123	$2,0^+$	$2,0^+$	ground state band
371.2	371.18	371	371	371	371	371	$4,0^+$	$4,0^+$	ground state band
680.7	680.71	679	680				$0,0^+$	$0,0^+$	beta band
717.9	717.96	718	718	721	718	718	$6,0^+$	$6,0^+$	ground state band
815.5	815.55	816	816		815	816	$2,0^+$	$2,0^+$	beta band
996.3	996.32	998	996		997	996	$2,2^+$	$2,2^+$	gamma band
1047.7	1047.65	1048	1049	1052			$4,0^+$	$4,0^+$	beta band
1127.9	1127.90		1128	1128	1128	1128	$3,2^+$	$3,2^+$	gamma band
	1136.07								
1144.7							$8,0^+$		ground state band
			1182					$(0,0^+)$	
1241.3	1241.34	1242	1242				$1,0^-$	$1,0^-$	octupole band
1251.7	1251.48	1253					$3,0^-$		octupole band
1263.9	1263.94	1265	1264	1260	1263	1264	$4,2^+$	$4,2^+$	gamma band

(continued next page)

Table 7.1 (continued)

Excitation Energies (keV)							Assignments		
^{154}Tb[a] decay	^{154}Eu[b] decay	(d,d')[c]	(d,t)	(^{3}He,α)	(α,t)	(^{3}He,d)	Previous I,K^π	Present I,K^π	Configuration
	1277,6								
1295.8	1292.75		1295				$0,0^+$	$0,0^+$	
	1364.2	1365					$5,0^-$		octupole band
1366							$6,0^+$		beta band
1397.6	1397.53		1399				$2,1^-$	$2,1^-$	octupole band
1414.5	1415.60				1412	1415	$1,1^-$	$1,1^-$	octupole band
1418.3	1418.36		1417	1425			$2,0^+$	$2,0^+$	
1432.5			1432		1429	1429	$5,2^+$	$5,2^+$	gamma band
	1509.1						$1,1^-$		octupole band
1531.3	1531.39	1534	1532		1533	1531	$2,2^+$	$2,2^+$	
1559.7	1559.68				1599	1560	$4,1^-$	$4,1^-$	octupole band
			1576					$(2,0^+)$	
1606.8							$6,2^+$		gamma band
1617.3	1616.72	1618					$3,1^-$		octupole band
1645.9	1645.93				1645	1646	$4,4^+$	$4,4^+$	$\{5/2^+[413]+3/2^+[411]\}$
1661.1	1660.94		1662	1677(?)			$3,2^+$	$3,2^+$	
	1698.26	1700					$(4,0^+)$		
			1704	1705				$(4,0^+)$	

(continued on next page)

Table 7.1 (continued)

Excitation Energies (keV)							Assignments		
^{154}Tb[a] decay	^{154}Eu[b] decay	(d,d')[c]	(d,t)	(^{3}He,α)	(α,t)	(^{3}He,d)	Previous I,K^π	Present I,K^π	Configuration
1719.9	1719.62		1719				$2,2^-$	$2,2^-$	octupole band
1770.3	1770.3				1770	1770	$5,4^+$	$5,4^+$	$\{5/2^+[413]+3/2^+[411]\}_\pi$
			1777	1785					
	1790.4						$(4,2^+)$		
1796.4	1796.78	1794	1797				$3,2^-$	$3,2^-$	octupole band
1810.3[d]							$7,2^+$		gamma band
	1838.						$2,^+$		
	1861.4						$(4,2^-)$		octupole band
	1894.69						$2,^+$		
1911.7					1913	1912	$6,4^+$	$6,4^+$	$\{5/2^+[413]+3/2^+[411]\}_\pi$
		1950	1950	1949				$(5,2^-)$	octupole band
			1988	1991					
2025					2025		A		
2081.0			2082				B		

(continued next page)

Table 7.1 (continued)

Excitation Energies (keV)							Assignments		
^{154}Tb [a] decay	^{154}Eu [b] decay	(d,d') [c]	(d;t)	(^{3}He,α)	(α,t)	(^{3}He,d)	Previous I,K^π	Present I,K^π	Configuration
2093.8					2089	2091	$4,^+$		
		2101							
2119.7					2117	2116	$1,1^+$		
			2122						
			2131	2135					
2137.8							$7,7^-$		
			2150	2153	2148	2146		$2,2^+$	$\{5/2^+[413]-1/2^+[411]\}_\pi$
			2169						
					2175	2177		$1,1^-$	$\{5/2^+[413]-3/2^+[411]\}_\pi$
2186.0							$4,^-$		
2187.2			2189		2186		$(1,2),1^+$	$(1,1^+)$	
			2209		2210				
					2223	2224		$2,1^+$	$\{5/2^+[413]-3/2^+[411]\}_\pi$
2230.0			2230		2234		B	$(2,1^+)$	
		2247							
			2247		2250	2250	B	$3,2^+$	$\{5/2^+[413]-1/2^+[411]\}_\pi$
					2262				

(continued next page)

Table 7.1 (continued)

Excitation Energies (keV)							Assignments		Configuration
^{154}Tb [a] decay	^{154}Eu [b] decay	(d,d') [c]	(d,t)	(^{3}He,α)	(α,t)	(^{3}He,d)	Previous I,K^π	Present I,K^π	
2266			2266	2267			B		
2277.0			2277				B	$3,3^-$	$\{3/2^-[521]-3/2^+[651]\}_\nu$
					2294	2293		$3,1^+$	$\{5/2^+[413]-3/2^+[411]\}_\pi$
			2299						
2305.8					2304	2304	B	$(3,1^+)$	
			2306	2310				$(4,4^+)$	$\{3/2^-[521]-11/2^-[505]\}$
2309.9							$8,^-$		
					2317				
			2322						
2336.1			2336				B	$3,3^-$	$\{3/2^-[521]+3/2^+[402]\}_\nu$
2342.6					2344	2346	A		
			2349						
2368.8							B		
					2373				
			2376					$1,1^-$	$\{3/2^-[521]-1/2^+[660]\}$
			2386		2386			$4,2^+$	$\{5/2^+[413]-1/2^+[411]\}$
					2400	2403		$4,1^+$	$\{5/2^+[413]-3/2^+[411]\}$

(continued next page)

Table 7.1 (continued)

Excitation Energies (keV)							Assignments		
^{154}Tb [a] decay	^{154}Eu [b] decay	(d,d') [c]	(d,t)	(^{3}He,α)	(α,t)	(^{3}He,d)	Previous I,K^{π}	Present I,K^{π}	Configuration
2402							A		
2405.5							$(8,^-)$		
			2404	2406				$(7,7^+)$	$\{3/2^-[521]+11/2^-[505]\}_\nu$
2407					2411		B	$(4,1^+)$	
2416.3			2417				$(3,4),^+$		
					2420	2424			
2430.5							A		
					2432			$6,^-$	$\{5/2^+[413]+h_{11/2}\}_\pi$
			2434					$2,1^-$	$\{3/2^-[521]-1/2^+[660]\}_\nu$
			2443					$1,1^-$	$\{3/2^-[521]-1/2^+[400]\}_\nu$
2459.6							(7,8)		
			2461						
2468			2467		2466	2467	A		
2486.3							A		
			2489						
2496							$2,^+$		
			2496					$2,1^-$	$\{3/2^-[521]-1/2^+[400]\}_\nu$
2500							A		
			2503						

(continued next page)

Table 7.1 (continued)

Excitation Energies (keV)							Assignments		Configuration
^{154}Tb [a] decay	^{154}Eu [b] decay	(d,d') [c]	(d,t)	(^{3}He,α)	(α,t)	(^{3}He,d)	Previous I,K^π	Present I,K^π	
			2514		2513	2512		$3,3^+$	$\{5/2^+[413]+1/2^+[411]\}$
					2531	2535			
			2536					$0,0^-$	$\{3/2^-[521]-3/2^+[402]\}$
					2541				
			2561					$3,1^-$	$\{3/2^-[521]-1/2^+[400]\}$
					2570	2566		$7,^-$	$\{5/2^+[413]+h_{11/2}\}_\pi$
			2571					$1,0^-$	$\{3/2^-[521]-3/2^+[402]\}$
					2578				
2590			2590				A		
			2595		2594	2591			
			2606		2605				
			2618		2622				
			2632					$2,0^-$	$\{3/2^-[521]-3/2^+[402]\}$
			2648					$2,2^-$	$\{3/2^-[521]+1/2^+[660]\}$
			2656		2652	2649		$4,3^+$	$\{5/2^+[413]+1/2^+[411]\}$
2655							$2,^+$		
			2669						
			2683					$2,2^-$	$\{3/2^-[521]+1/2^+[400]\}$

(continued next page)

Table 7.1

Excitation Energies (keV)							Assignments		Configuration
^{154}Tb [a] decay	^{154}Eu [b] decay	(d,d') [c]	(d,t)	(^{3}He,α)	(α,t)	(^{3}He,d)	Previous I,K^π	Present I,K^π	
			2691						
			2699						
					2707	2703			
			2713						
			2717		2718				
2722.6							A		
2734							A		
					2739			$8,^-$	$\{5/2^+[413]+h_{11/2}\}_\pi$
			2741					$3,2^-$	$\{3/2^-[521]+1/2^+[400]\}_\nu$
			2749		2749	2752			
			2757						
			2768		2773				
			2780						
			2786		2785	2782			
2789.1							A		
					2797				

a: Sousa et al. (1975) and Riedinger et al. (1971)
b: Meyer (1968)
c: Bloch et al. (1967)
d: West et al. (1976) (Observed in the $^{152}Sm(\alpha,2n\gamma)^{154}Gd$ reaction).
e: Observed by Meyer (1968) in the decay of ^{154}Tb, see reference Sousa et al. (1975)
A: $I^\pi = 1,2^+$
B: $I^\pi = 2^+,3,4^+$

Figure 7.1

Various bands in ^{154}Gd, below 2000 keV. Levels shown with triangles on the left side were observed in the neutron transfer reactions and those with triangles on the right side were observed in the proton transfer reactions. Circles in the centre are on states reported in references (Sousa et al., 1975, West et al., 1976). Assignments shown in parentheses are uncertain.

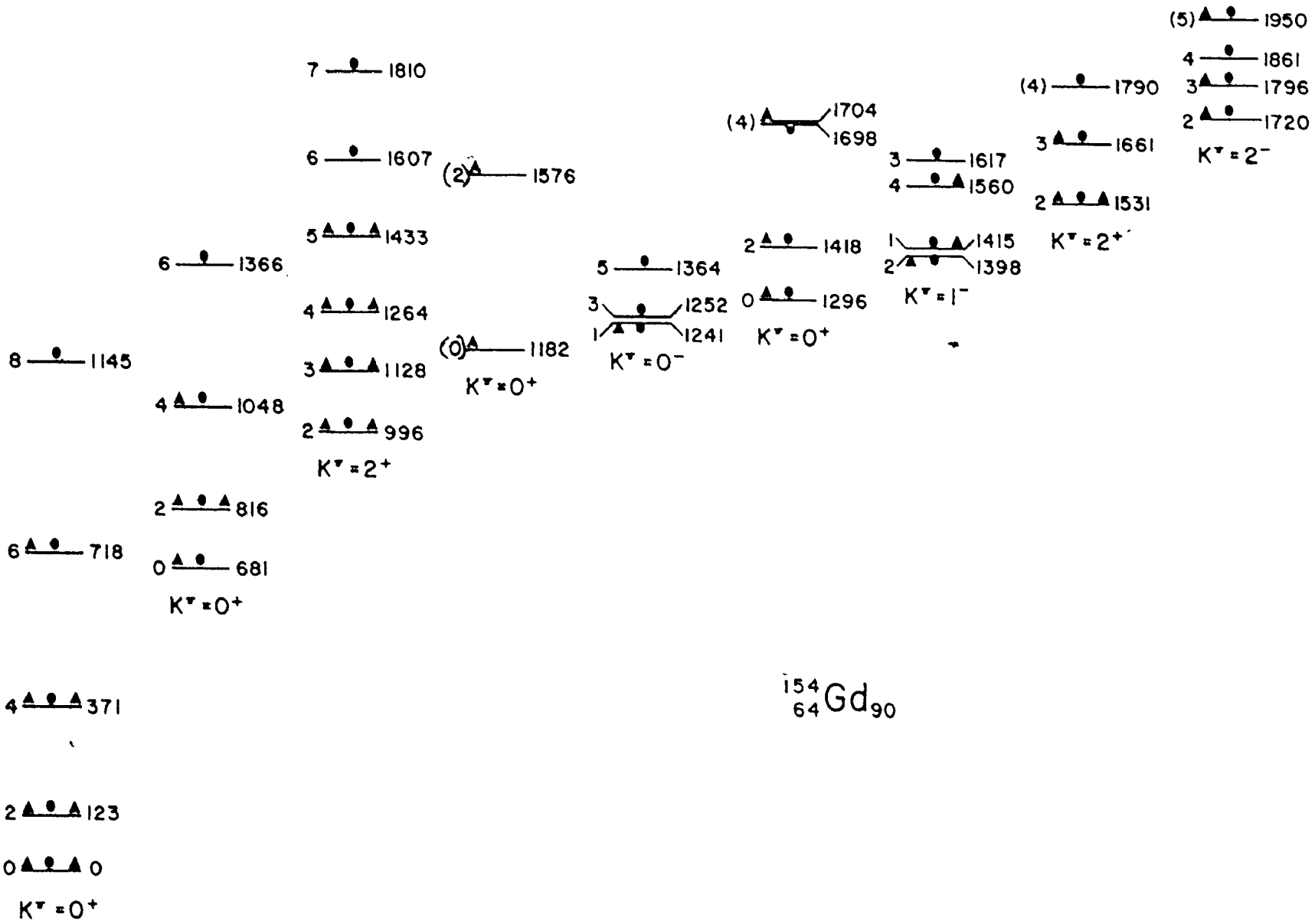
(5) 1950
4 1861
(4) 1790
3 1796
3 1661
2 1720
K^π = 2^-
2 1531
K^π = 2^+
(4) 1704
1698
3 1617
4 1560
2 1418
1 1415
2 1398
K^π = 1^-
5 1364
3 1252
1 1241
0 1296
K^π = 0^+
K^π = 0^-
7 1810
6 1607
(2) 1576
5 1433
6 1366
4 1264
(0) 1182
8 1145
3 1128
K^π = 0^+
4 1048
2 996
K^π = 2^+
2 816
6 718
0 681
K^π = 0^+
4 371
2 123
0 0
K^π = 0^+
154 64 Gd 90

Figure 7.2

Various bands in ^{154}Gd above 2000 keV, populated in neutron transfer reactions. The bands are designated by the main component of the two quasineutron configurations. See caption for figure 7.1 for the meaning of various symbols.

$^{154}_{64}Gd_{90}$
$\{K\}_\nu = \{\frac{3}{2}^-[521]\}_\nu$
$\{K\}_c + \{\frac{1}{2}^+[651]\}_c$
$\{K\}_c \pm \{\frac{1}{2}^-[505]\}_c$
$\{K\}_c \pm \{\frac{3}{2}^+[402]\}_c$
$\{K\}_c \pm \{\frac{1}{2}^+[660]\}_c$
$\{K\}_c \pm \{\frac{1}{2}^+[400]\}_c$
$K^\pi = 3^-$
$K^\pi = 4^+$
$K^\pi = 7^+$
$K^\pi = 0^-$
$K^\pi = 3^-$
$K^\pi = 1^-$
$K^\pi = 2^-$
$K^\pi = 2^-$
$K^\pi = 1^-$
3 2277
(4) 2306
(7) 2404
2 2632
1 2571
0 2536
3 2336
2 2434
1 2376
2 2648
2 2683
3 2741
3 2561
2 2496
1 2443

Figure 7.3

Various bands in ^{154}Gd, populated mainly in proton transfer reactions. The bands are designated by two-quasiproton configurations. See caption for figure 7.1 for the meaning of various symbols.

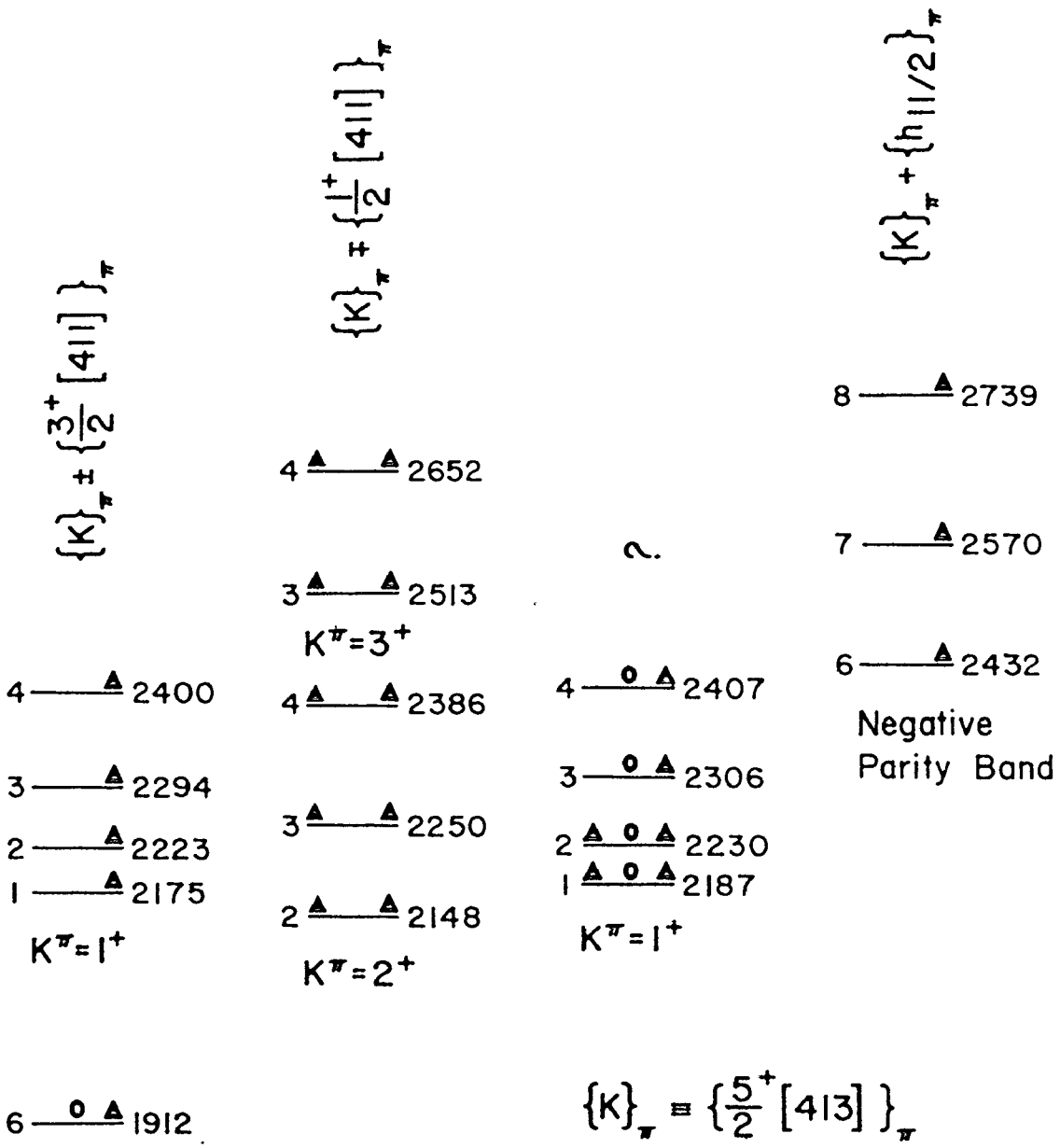
{K}π = {3/2+ [411]}π
4 2400
3 2294
2 2223
1 2175
Kπ=1+
{K}π = {1/2+ [411]}π
4 2652
3 2513
Kπ=3+
4 2386
3 2250
2 2148
Kπ=2+
4 2407
3 2306
2 2230
1 2187
Kπ=1+
{K}π = {h11/2}π
8 2739
7 2570
6 2432
Negative Parity Band
6 1912
5 1770
4 1646
Kπ=4+
{K}π = {5/2+ [413]}π

$^{154}_{64}Gd_{90}$

cluded. The states populated in the neutron and proton transfer reactions have been indicated separately. Most of the states below the energy gap in ^{154}Gd were known previously, with the exception of the levels at 1182 and 1576 keV. These levels have been tentatively assigned as the 0^+ and 2^+ members of a spherical band.

Figure 7.2 presents the two-quasineutron states in ^{154}Gd. It can be seen that most of the states described are of negative parity, formed as a result of the parallel and antiparallel coupling of the $1/2^+[400]$, $1/2^+[600]$, $3/2^+[402]$ and $3/2^+[651]$ Nilsson orbitals with the target ground state $3/2^-[521]$ orbital.

Apart from these states, there are many other levels populated in the (d,t) reaction which remain unassigned. Their excitation energies and cross sections have been measured and are given in table 4.1. Their (d,t) angular distributions show that most of the levels populated are the result of transfer of low ℓ-values. The results of the (^{3}He,α) reactions were not very conclusive. Above 2100 keV, only a few of the states had an appreciable (^{3}He,α) reaction strength and beyond 2450 keV no single level was strongly populated. Although the ℓ=5 and 6 transitions corresponding to the Nilsson orbitals arising from $h_{11/2}$ and $i_{13/2}$ states respectively have been observed in the neighbouring odd mass nuclei (Borggreen et al., 1969, Løvhøiden and Burke, (1973), it has not been possible to definitely identify them in ^{154}Gd. Two positive parity bands at 2306 keV ($K^\pi = 4^+$) and 2406 keV ($K^\pi = 7^+$) have been tentatively proposed as the two-quasineutron configurations $\{3/2^-[521]+$

$11/2^-[505]\}_\nu$. The Coriolis calculations involving the Nilsson orbitals arising from the $i_{13/2}$ state show a very general result: the yrast states of these Coriolis mixed bands receive most of the reaction strength and their excitation energies lie on a parabola (a curve obtained as a function of E(I) versus I).

The two-quasiproton states are shown in figure 7.3. A $K^\pi = 4^+$ band at 1645.9 keV proposed by Riedinger et al. (1970) to the $\{5/2^+[413]+3/2^+[411]\}_\pi$ configuration has been confirmed in the present study. The first three band members of this configuration have been populated both in the (^{3}He,d) and (α,t) reactions. The $K^\pi = 1^+$ band formed by the anti-parallel coupling of the above Nilsson configurations is at 2175 keV. The first four members of this band have been identified. Another possible $K^\pi = 1^+$ band is found at 2187 keV. The first four members of this band lie about 10 keV higher than the lower $K^\pi = 1^+$ band. All these four members of the upper $K^\pi = 1^+$ band have been observed in the decay of ^{154}Tb (Sousa et al., 1975). In the neutron transfer reactions, the first two members have been populated. Because of this complexity, no definite configuration was proposed.

Two other positive parity bands, $K^\pi = 2^+$ and 3^+ at 2148 and 2513 keV respectively, have been identified. For these two bands, the two-quasiproton configurations are $\{5/2^+[413]\mp 1/2^+[411]\}_\pi$ respectively. Although these band members have also been populated in the neutron transfer reactions, no

definite two-quasineutron configurations were established. An additional component of the $K^{\pi} = 2^{+}$ band of the $\{5/2^{+}[413]-1/2^{+}[411]\}_{\pi}$ configuration has been populated in the proton transfer reactions as part of the gamma band at 996 keV.

Only three negative parity two-quasiproton states, $I^{\pi} = 6^{-}$, 7^{-} and 8^{-}, have been observed. These states are assigned to the Coriolis mixed bands of the $\{5/2^{+}[413]+h_{11/2}\}_{\pi}$ configurations.

In both the neutron and proton transfer reactions, the observed strength was rather small for many of the transferred orbitals. The experimental values of U^2 and V^2 are deduced from the total observed strengths of the orbitals and compared to the total calculated strength of the transferred orbitals. The calculated values are obtained from the expressions for U^2 and V^2 given in section 2.7. Instead of the single particle energies of the transferred orbitals, the values of the excitation energies of the orbitals in the target nucleus have been used in these calculations. It can be seen that the experimental values of U^2 and V^2 are in many cases quite small compared to the calculated ones (table 7.2).

7.2 ^{152}Eu

$^{152}_{63}Eu_{89}$ lies in a region where the deformation is changing rapidly with neutron number. The present study has shown that the level structure of this transitional nucleus is very complex. However, some of the low lying levels

Table 7.2

Theoretical and Experimental Values of U^2 and V^2 (^{154}Gd)

Transferred Orbitals	Theoretical	Experimental
Proton	U^2	
$5/2^+[413]$	0.50	0.35
$3/2^+[411]$	0.70	0.68[a], 0.55[b]
$1/2^+[411]$	0.89	0.23[a], 0.45[b]
$5/2^-[532]$	0.30	
$7/2^-[523]$	0.81	
Neutron	V^2	
$3/2^-[521]$	0.50	0.40
$11/2^-[505]$	0.71	0.85[c]
$1/2^+[400]$	0.83	0.40
$3/2^+[402]$	0.79	0.30
$1/2^+[660]$	0.79	
$3/2^+[651]$	0.70	

a: for the parallel coupling of this orbital with the target ground state $5/2^+[413]$

b: for the anti-parallel coupling of this orbital with the target ground state $5/2^+[413]$

c: tentative assignments

exhibit the rotational structure which is typical of a deformed nucleus. A large number of levels in ^{152}Eu has been populated in both the proton and neutron transfer reactions (table 4.3). The unpublished results of von Egidy et al. (1975) for this nucleus have made it possible to identify many of these levels. The ^{153}Eu(^{3}He,α)^{152}Eu reaction has confirmed the $I,K^{\pi} = 3,3^{-},\{5/2^{+}[413]\}_{\pi} - 11/2^{-}[505]\}_{\nu}$ configuration for the ground state of ^{152}Eu. Another member of the ground state band, $I^{\pi} = 4^{-}$, at 90 keV has also been identified. A 96 min isomer of ^{152}Eu at 148 keV ($I^{\pi} = 8^{-}$) has been confirmed as the $\{5/2^{+}[413]\}_{\pi} + 11/2^{-}[505]\}_{\nu}$ configuration. There are many other levels populated in the ^{153}Eu(^{3}He,α)^{152}Eu reaction, for which no two-quasiparticle assignments are given. It is suspected that some of the levels might have positive parity and a complex structure due to the Coriolis and $\Delta N=2$ interactions between various bands formed by $1/2^{+}[400]$, $1/2^{+}[660]$, $3/2^{+}[402]$, $3/2^{+}[651]$ and $5/2^{+}[642]$ neutron Nilsson orbitals. It has been found in the study of ^{154}Gd that the (^{3}He,α) reaction alone is not good enough to sort out these bands. Probably a detailed study of the ^{153}Eu(d,t)^{152}Eu reaction (von Egidy et al., 1975) along with the ^{153}Eu(^{3}He,α)^{152}Eu reaction might further reveal the structure of this nucleus.

From the proton transfer reaction studies, two bands for the $\{3/2^{+}[411]\}_{\pi} \pm \{5/2^{-}[523]\}_{\nu}$ configuration has been established. These assignments have shed further light on

the ground state structure of ^{151}Sm. The present study suggests that the $5/2^-[523]$ neutron orbital is one of the major components in the ^{151}Sm ground state. This finding is in accordance with the results of Nelson et al., (1973).

Five rotational bands in ^{152}Eu, with their possible two-quasiparticle configurations, are summarized in figure 7.4.

7.3 Splitting Energies

Thirteen bands in ^{154}Gd and four bands in ^{152}Eu have been assigned to two-quasiparticle configurations. From the observed band head energies belonging to the same Nilsson orbital configurations, the values of splitting energies could be obtained by subtracting the rotational contribution $\hbar^2/2\mathcal{J}\ (K_1-K_2)$. For the cases where the Coriolis and $\Delta N=2$ mixing are involved, the contribution from these interactions must also be taken into account. The experimental values of the splitting energies thus deduced in ^{154}Gd and ^{152}Eu are given in the last column of table 7.3. For the $\{3/2^-[521]\mp 11/2^-[505]\}_\nu$ configurations, the assignments are tentative so the deduced value for the splitting energy should be taken with some caution. The splitting energies have been calculated (section 2.11) using the parameters given by different authors. Pyatov (1963) has used parameters $\alpha = 0.1$ and $W = 2.4$ MeV for the calculations of the splitting energies for both doubly-odd and even nuclei. In the calculations for doubly-odd

Figure 7.4

Five bands in ^{152}Eu with their possible two-quasiparticle configurations. Levels shown with triangles on the left side were observed in the neutron transfer reaction and those with triangles on the right side were observed in the proton transfer reactions. Circles in the centre are from the reference (von Egidy et al., 1975).

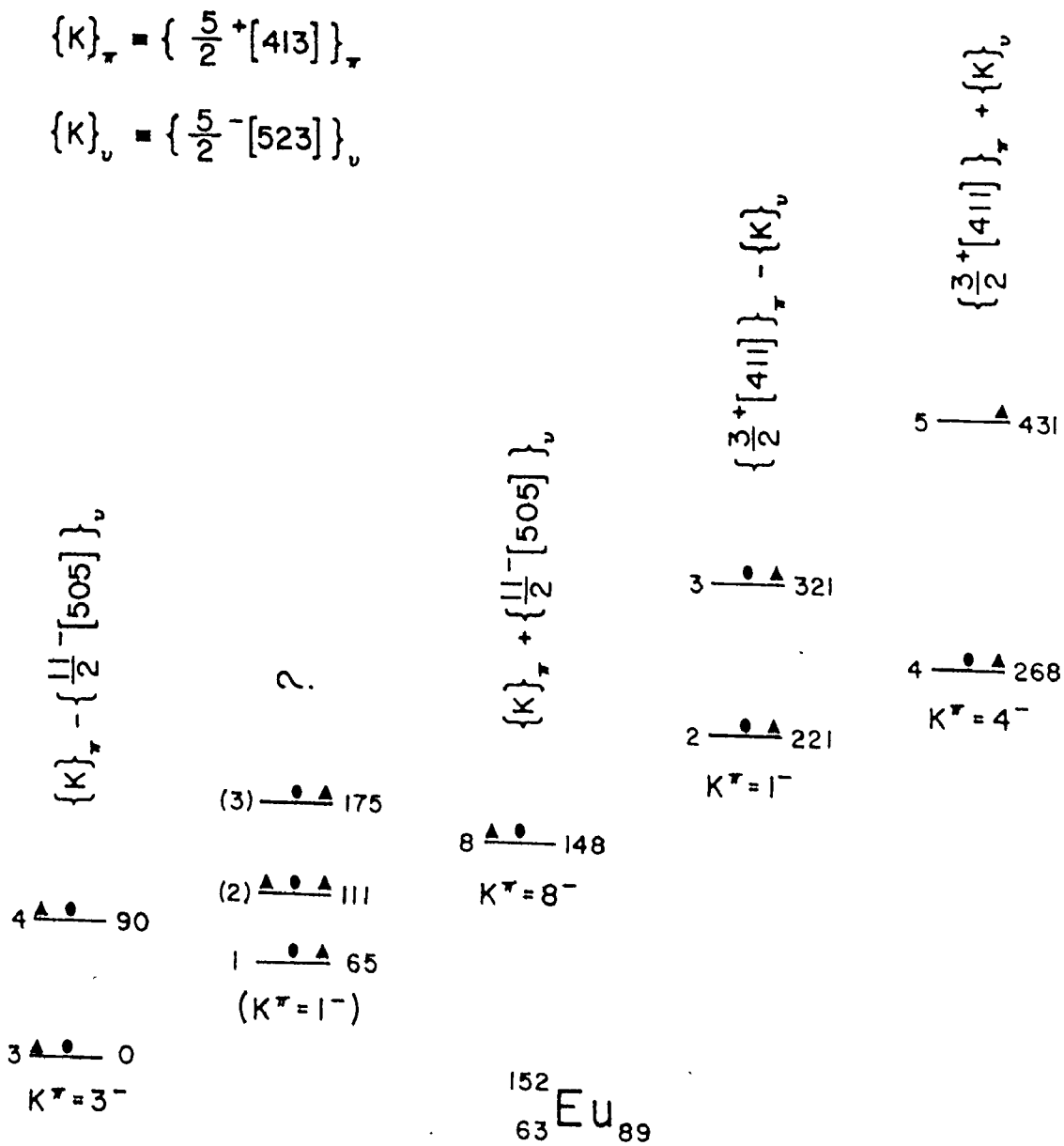

$\{K\}_\pi = \{\frac{5}{2}^+[413]\}_\pi$
$\{K\}_\nu = \{\frac{5}{2}^-[523]\}_\nu$
$\{K\}_\pi - \{\frac{11}{2}^-[505]\}_\nu$
4 90
3 0
$K^\pi = 3^-$
?
(3) 175
(2) 111
1 65
$(K^\pi = 1^-)$
$\{K\}_\pi + \{\frac{11}{2}^-[505]\}_\nu$
8 148
$K^\pi = 8^-$
$\{\frac{3}{2}^+[411]\}_\pi - \{K\}_\nu$
3 321
2 221
$K^\pi = 1^-$
$\{\frac{3}{2}^+[411]\}_\pi + \{K\}_\nu$
5 431
4 268
$K^\pi = 4^-$
$^{152}_{63}Eu_{89}$

Table 7.3

Theoretical and Experimental Splitting Energies (keV)

Nucleus	Configuration	K_1, K_2	Theoretical			Experimental
			$\alpha=0.1$ W=2.4 MeV $\alpha W=0.24$[a]	$\alpha=0.146$ W=5.82 MeV $\alpha W=0.85$[b]	$\alpha=0.11$ W=7.7 MeV $\alpha W=0.85$[c]	
$^{154}_{64}Gd_{90}$	$\{5/2^+[413]\mp 3/2^+[411]\}_\pi$	1,4	155	261	484	567
	$\{3/2^-[521]\mp 3/2^+[402]\}_\nu$	0,3	57	96	178	281
	$\{3/2^-[521]\mp 11/2^-[505]\}_\nu$	4,7	- 51	- 85	-158	- 65[d]
	$\{3/2^-[521]\mp 3/2^+[651]\}_\nu$	0;3	- 10	- 16	- 30	- 73[e]
	$\{3/2^-[521]\mp 1/2^+[660]\}_\nu$	1,2	- 4	- 6	- 11	-208
	$\{3/2^-[521]\mp 1/2^+[400]\}_\nu$	1,2	- 41	- 68	-127	-233
	$\{5/2^+[413]\mp 1/2^+[411]\}_\pi$	2,3	-159	-268	-498	-348
$^{152}_{63}Eu_{89}$	$\{3/2^+[411]\}_\pi \mp \{5/2^-[523]\}_\nu$	1,4	- 31	-109	-109	- 63
	$\{5/2^+[413]\}_\pi \mp \{11/2^-[505]\}_\nu$	3,8	- 40	-142	-142	-137

a: Pyatov (1963)
b: Khoo et al. (1975), Khoo (1976) private communication
c: These values of α and W gave the best fit
d: Assignments for these configurations are tentative
e: $K_1=0$ band unobserved (estimated value)

nuclei only a single parameter, αW, is required. Jones et al. (1971) have chosen an $\alpha W = 0.85$ to fit the data for a large number of doubly-odd nuclei. However, for a doubly-even nucleus, separate values of α and W are required. Khoo et al. (1975,1976) have used $\alpha = 0.146$ and $W = 5.82$ MeV corresponding to $\alpha W = 0.85$, the same value as used by Jones et al. (1971). The calculated values of the splitting energy for these parameters are given in table 7.3. The qualitative features of the experimental results are well reproduced by the calculations, i.e. the signs of the splitting energies are correct in all the cases. However, it should be noticed that the values of the splitting energies calculated from Pyatov's parameters are consistently smaller in magnitude than the experimental values for both ^{154}Gd and ^{152}Eu. However, for the value of $\alpha W = 0.85$ (Jones et al., 1971), the ^{152}Eu results are in good agreement with the experimental values.

In the ^{154}Gd case, the effect of α and W for a fixed value of $\alpha W = 0.85$ has been investigated. In figure 7.5, the splitting energies for various configurations as a function of $(1-4\alpha)W$ are shown. From table 7.3 and figure 7.5, it can be noticed that for the $\{3/2^-[521]\mp 1/2^+[660]\}_\nu$ and $\{3/2^-[521]\mp 3/2^+[651]\}$ configurations, the experimental values of the splitting energies are much larger in magnitude than the calculated ones. This discrepancy is probably due to the Coriolis interaction between the various states arising

Figure 7.5

The splitting energies as a function of $(1-4\alpha)W$ for two-quasiparticle configurations in ^{154}Gd.

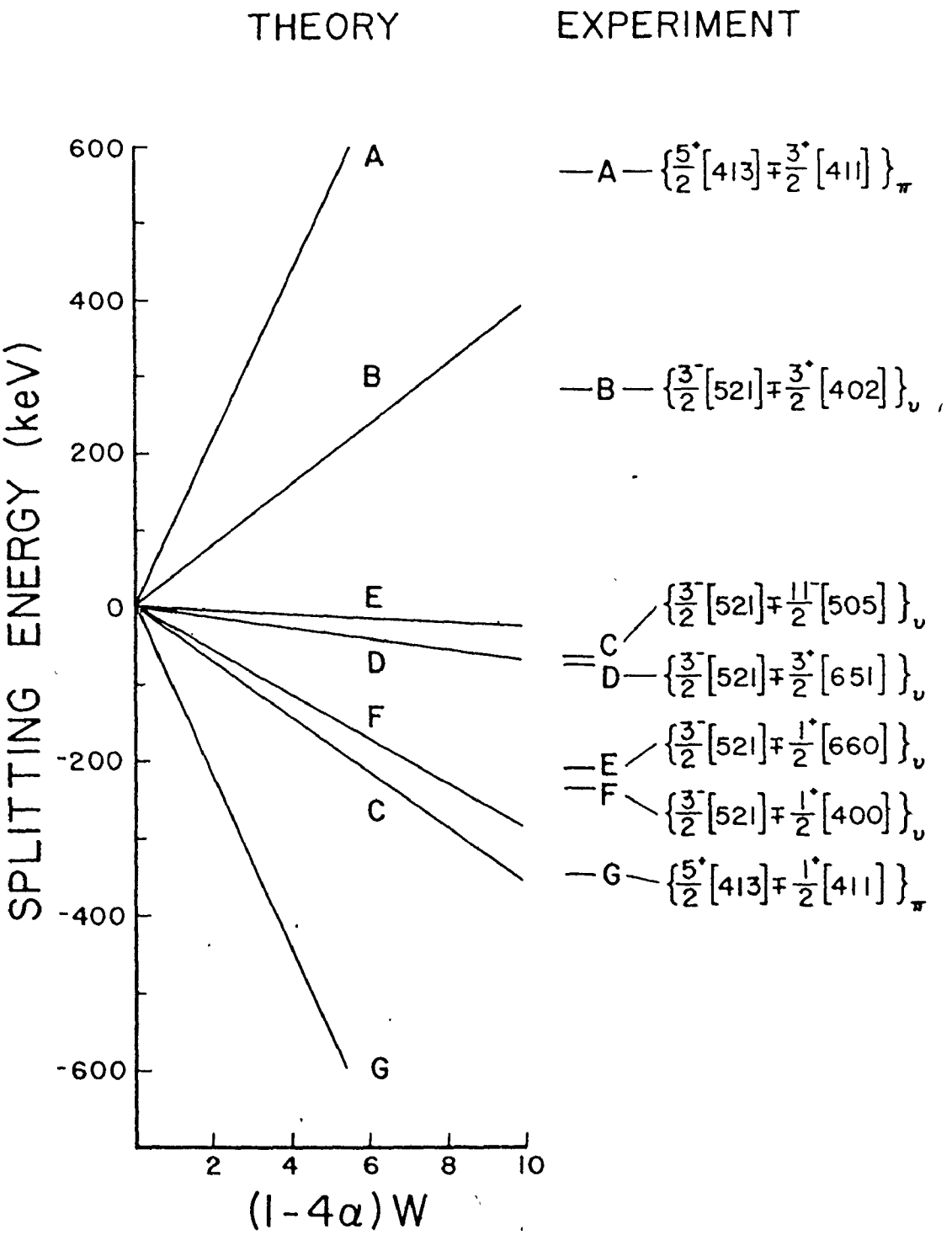
THEORY
EXPERIMENT
SPLITTING ENERGY (keV)
600
400
200
0
-200
-400
-600
2
4
6
8
10
(1-4α)W
A
B
E
D
F
C
G
—A— $\{\frac{5^+}{2}[413]\mp\frac{3^+}{2}[411]\}_\pi$
—B— $\{\frac{3^-}{2}[521]\mp\frac{3^+}{2}[402]\}_\nu$
C $\{\frac{3^-}{2}[521]\mp\frac{11^-}{2}[505]\}_\nu$
D— $\{\frac{3^-}{2}[521]\mp\frac{3^+}{2}[651]\}_\nu$
E $\{\frac{3^-}{2}[521]\mp\frac{1^+}{2}[660]\}_\nu$
F $\{\frac{3^-}{2}[521]\mp\frac{1^+}{2}[400]\}_\nu$
—G— $\{\frac{5^+}{2}[413]\mp\frac{1^+}{2}[411]\}_\pi$

from the $\{3/2^-[521]+i_{13/2}\}_\nu$ configurations.

The value of $(1-4\alpha)W$ has been obtained which gives the best fit to the experimental splitting energies in ^{154}Gd. From this value of $(1-4\alpha)W$ and $\chi W = 0.85$, the deduced values of α and W are 0.11 and 7.7 MeV respectively. For these values, the splitting energies are calculated and are shown in table 7.3. It can be seen that these values give better agreement to the splitting energies in ^{154}Gd than the values used by previous authors (Pyatov, 1963 and Khoo et al., 1975, 1976).

In summary, it can be concluded that the zero range interaction (equation 2.11.1) describes reasonably well the splitting energies for both the doubly-even nucleus ($^{154}_{64}Gd_{90}$) and doubly-odd nucleus ($^{152}_{63}Eu_{89}$). This means, of course, that the observed band head energies are in agreement with the empirical rules laid down by Gallagher and Moszkowski (1958) for doubly-odd nuclei and Gallagher (1962) for doubly-even nuclei.

7.4 Concluding Remarks

The present study has shown that in general the level structure of the transitional ^{154}Gd and ^{152}Eu nuclei could be described within the framework of the unified models. There still remains a large number of levels which are unassigned. In the neutron transfer reactions leading to the final nucleus ^{154}Gd, some of these levels could be populated by the transfer of $1/2^-[530]$, $1/2^-[521]$, $3/2^-[532]$ and $5/2^-[523]$

neutrons. The parallel and antiparallel coupling of these orbitals with the $3/2^-[521]$ ground state would give a large number of bands. Calculations show that these states are greatly perturbed due to Coriolis interaction. As a result of this many of the levels would not show well behaved rotational structure and identification has remained impossible. The (^{3}He,α) reaction was not found to be very successful in identifying states in ^{154}Gd. Probably recent in-beam γ-ray spectroscopy experiments of ^{154}Gd using the (α,2n) reaction (West et al., 1976) will bring some further insight into this situation. Although it has been shown that most of the levels in ^{154}Gd show a rotational structure which is typical of a deformed nucleus, there may be two 'spherical' states at 1182 keV (0^+) and 1576 (2^+) which probably show the transitional nature of ^{154}Gd. In order to check this aspect for these states, further experiments like the (t,p) reaction on the spherical target nucleus ^{152}Gd are required. In this reaction, these states, if they do exist in ^{154}Gd, would be excited very strongly.

The present study for the doubly-odd ^{152}Eu nucleus has shown that the level structure of low lying levels could be described in terms of the two-quasiparticle Nilsson states. There is a number of levels which still remain unassigned. It is hoped that the joint efforts by the team of twenty-eight investigators (von Egidy et al., 1975) in seven different laboratories should bring some more insight about the nature of this very exciting nucleus, $^{152}_{63}Eu_{89}$.

REFERENCES

Andersen, B. L., 1968. Nucl. Phys. A112, 443.

Ascuitto, R.J., King, C. H. and McVay, L.J., 1972. Phys. Rev. Lett. 29, 1106.

Bardeen, J., Cooper, L.N. and Schrieffer, J.R., 1957. Phys. Rev. 106, 162.

Bès, D.R., Federman, P., Maqueda, E. and Zuker, A., 1965. Nucl. Phys. 65, 1.

Blichert-Toft, P.H., Funk, E.G. and Mihelich, J.W., 1966. Nucl. Phys. 79, 12.

Bloch, R., Elbek, B. and Tjøm, P. O., 1967. Nucl. Phys. A91, 576.

Bohr, A., 1952. Mat. Fys. Medd. Dan. Vid. Selsk. 26, #14.

Bohr, A. and Mottelson, B.R., 1953. Mat. Fys. Medd. Dan. Vid. Selsk. 27, 16.

Bohr, N., 1936. Nature, 137, 344.

Borggreen, G., Løvhøiden, G. and Waddington, J. C., 1969. Nucl. Phys. A131, 241.

Boyno, J.S. and Huizenga, J.R., 1972. Phys. Rev. 6, 1411.

Breitig, D., Kane, W.R. and Casten, R. F., 1973. Bull. Am. Phys. Soc. 18, 36.

Brockmeier, R.T., Wahlborn, S., Seppi, E.J. and Boehm, F., 1965. Nucl. Phys. 63, 102.

Burke, D.G. and Elbek, B., 1967. Mat.Fys.Medd.Dan.Vid. Selsk. 36, #6.

Burke, D. G., Alford, W.P. and O'Neil, R.A., 1971. Nucl. Phys. A161, 129.

Burke, D.G. and Waddington, J.C., 1972. Nucl. Phys. A193, 271.

Burke, D.G., Waddington, J.C., Nelson, D.E. and Buckley, J., 1973. Can. J. Phys. 51, 455.

Cairns, J.E., 1973. McMaster University, M.Sc. thesis.

Cheung, H.C., 1975. McMaster University computer program SPLIT, unpublished.

Chi, B. E., 1967. State University of New York, Department of Physics, preprint. Corrected from Chi, B.E. 1966. Nucl. Phys. 83, 97,

Christensen, P.R., Berinde, A., Neamu, I. and Scentai, N., 1969. Nucl. Phys. A129, 337.

Edmonds, A.R., 1957. Angular Momentum in Quantum Mechanics, Princeton University Press, Princeton, N.J.

Elbek, B. and Tjøm, P. O., 1969. Advances in Nuclear Physics, 3, 259. Ed. M. Baranger and E. Vogt, Plenum Press, New York.

Enge. H.A., 1966. Introduction to Nuclear Physics, Addison-Wesley (Canada) Limited, Don Mills, Ontario.

Flaum, C. and Cline, D., 1975. The University of Rochester, Nuclear Structure Research Laboratory, UR-NSRL-103.

Gadsby, R.D., Burke, D.G. and Waddington, J.C., 1973. Can. J. Phys. 51, 203.

Gallagher, C.J. Jr. and Moszkowski, S. A., 1958. Phys. Rev. 111, 1282.

Gallagher, C.J. Jr., 1962. Phys. Rev. 126, 1525.

Hinds, S., Bjerregaard, J.H., Hansen, O. and Nathan, O., 1965, Phys. Lett. 14, 48.

Hirning, C.R. and Burke, D.G., 1976. Phys. in Canada 32, 53.

Jaskola, M., Tjøm, P. O. and Elbek, B., 1969. Nucl. Phys. A133, 65.

Jones, H.D., 1969. The Florida State University. #70-3820, University Microfilms, Inc., Ann Arbor, Michigan, Ph.D. dissertation.

Jones, H. D., Onishi, N., Hess, T. and Sheline, R.K., 1971. Phys. Rev. C3, 529.

Kanestrøm, I., Tjøm, P. O. and Bang, J., 1971. Nucl. Phys. A164, 664.

Kayser, D. C. and Johnson, W.H., Jr., 1975. Phys. Rev. 12C, 1054.

Khoo, T.L., Waddington, J.C., O'Neil, R.A.,Preibisz, Z., Burke, D.G. and Johns, M.W., 1972. Phys. Rev. Lett. 28, 1717.

Khoo, T. L., Bernthal, F.M., Boyno, J.S. and Warner, R.A., 1973. Phys. Rev. Lett. 31, 1146.

Khoo, T.L., Bernthal, F.M., Warner, R.A., Bertsch, G.F. and Hamilton, G., 1975. Phys. Rev. Lett. 35, 1256.

Khoo, T. L., 1976. Private communication.

Kunz, P.D., 1969. University of Colorado, computer program DWUCK and write up thereof, unpublished.

Lamm, I-L., 1969. Nucl. Phys. A125, 504.

Løvhøiden, G., Waddington, J.C., Hagemann, K.A., Hjorth, S.A. and Ryde, H. 1970. Nucl. Phys. A148, 657.

Løvhøiden, G., Waddington, J.C., Ellegaard, C. and Tjøm, P.O., 1971. Nucl. Phys. A160, 305.

Løvhøiden, G. and Kanestrøm, I., 1972. Phys. Norv. 6, 33.

Løvhøiden, G., Burke, D.G. and Waddington, J.C., 1973. Can. J. Phys. 51, 1369.

Løvhøiden, G. and Burke, D.G.,1973. Can. J. Phys. 51, 2354.

Løvhøiden, G., Rekstad, J., 1976. Phys. Lett., 60B, 335.

Mayer,M.G.and Jensen, J.H.D., 1955. Elementary Theory of Nuclear Shell Structure, John Wiley and Sons, Inc., (New York).

Meredith, J.O. and Barber, R.C., 1972. Can. J. Phys. 50, 1195.

Meyer, R.A., 1968, Phys. Rev. 170, 1089.

Meyer, R.A., 1968. Phys. Rev. 174, 1478.

Meyer, R.A., Griffioen, R.D. and Gunnink, R., 1968. Bull. Am. Phys. Soc. 13, 64.

Nathan, O. and Nilsson, S.G., 1965. Alpha Beta and Gamma Ray Spectroscopy, 601. ed. K. Siegbahn, North Holland Publishing Co., Amsterdam.

Neergård, K. and Vogel, P., 1970. Nucl. Phys. A145, 33.

Nelson, D.E., 1972. McMaster University, Ph.D. thesis.

Nelson, D.E., Burke, D.G., Waddington, J.C. and Cook, W.B., 1973. Can. J. Phys. 51, 2000.

Nilsson, S.G., 1955. Mat. Fys. Medd. Dan. Vid. Selsk. 29, #16.

Nilsson, S.G., 1961. Mat. Fys. Medd. Dan. Vid. Selsk. 32, #16.

O'Neil, R.A., Burke, D.G. and Alford, W.P., 1971. Nucl. Phys. A167, 481.

O'Neil, R.A. and Burke, D.G., 1972. Nucl. Phys. A182, 342.

O'Neil, R.A., 1972. McMaster University, computer programs GREATER and SPECTR, unpublished.

O'Neil, R.A., 1972. McMaster University, Ph.D. thesis.

Pyatov, N.I., 1963. Ivz. Akad, Nauk,SSSR Ser. Fiz. 27. 1436 (Trans. Bull. Acad. Sci. USSR Phys. Ser. 27, 1409).

Rainwater, J., 1950. Phys. Rev. 79, 432.

Riedinger, L.L., Eichler, E., Fuglsang, J., Hagemann, G.B. and Herskind, B., 1969. Proc. Fifth Int. Conf. on Nuclear Reactions Induced by Heavy Ions, Heidelberg,Germany, Ed. Bock, R. and Hering, W.R. 1970. North Holland, Amsterdam.

Riedinger, L. L. and Johnson, N.R., 1970. Phys. Rev. 2C, 2358.

Riedinger, L. L., Sousa, D.C., Funk, E.G. and Mihelich, J.W., 1971. Phys. Rev. C4, 1352.

Sheline, R.K., Bennett, M.J., Dawson, J.W. and Shida, Y., 1967. Phys. Lett. 26B, 14.

Shelton, W.N. and Sheline, R.K., 1971. Z. Physik 242, 368.

Soloviev, V.G., 1965. Dubna preprint #D-2157.

Sousa, D.C., Riedinger, L.L., Funk, E.G. and Mihelich, J.W., 1975. Nucl. Phys. A238, 365.

Spencer, J.E. and Enge, H.E., 1967. Nucl. Inst.and Meth. 49, 181.

Struble, G.L. and Rasmussen, J.O., 1965. Phys. Lett. 17, 283.

Takahashi, K., McKeown, M. and Scharff-Goldhaber, G., 1965. Phys. Rev. 137, B763.

Talmi, I., 1952. Helv. Phys. 25, 182.

Tippett, J.C., 1972. McMaster University, Ph.D. thesis.

Tippett, J.C. and Burke, D.G., 1972. Can. J. Phys. 50, 3152.

Tjøm, P. O. and Elbek, B., 1967. Mat. Fys. Medd. Dan.Vid. Selsk, 36, #8.

Ungrin, J., Burke, D.G., Johns, M. W. and Alford, W.P., 1969. Nucl. Phys. A132, 322.

von Egidy, T., Kaiser, W., Mampe, W., Lanier, R.G., Mühlbauer, K., Schult, O.W.B., Koch, H.R., Baader, H.A., Breitig, D., Mlekodaj, R., Sheline, R.K., Shera, E.B., Ungrin, J., Prokofjev, P. T., Simonova, L. I., Seyfarth, H., Delang, W. and Göttel, P., 1971. "Colloquium on Intermediate Nuclei", Orsay, France, 235.

von Egidy, T., Kaiser, W., Mampe, W., Lanier, R.G., Mühlbauer, K., Schult, O.W.B., Koch, H.R., Baader, H.A., Mlekodaj, R. L., Sheline R.K., Shera, E.B., Ungrin, J., Prokofjev, P.T., Simonova, L.I., Seyfarth, H., Kardon,B., Delang, W., Göttel, P., Breitig, D., Kane, W.R., Casten, R.F., Scheerer, H.J., Glässl, P., Huenges, E., Löffler, M., Rösler, H., Vonach, H.K. and Rabenstein, D., 1974. "Second International Symposium on Neutron Capture Gamma Ray Spectroscopy and Related Topics", Petten, The Netherlands, 241 and 1975. Private communication.

Vylov, Ts., Gromova, I.I., Kuznetsov, V.V., Nedovesov, V.G., Fominykh, V. I., Khol'nov, Yu. V. and Shchukin, G.E., 1972. Bull. Acad. Sci. USSR (Phys. Ser.) 36, 649.

Waddington, J.C., 1976. Private Communication.

West, R.L., Funk, E.G. and Mihelich, J.W., 1976. Bull. Am. Phys. Soc. 21, 657.

Westgaard, L. and Bjørnholm, S., 1966. Nucl. Instr. and Meth. 42, 77.

Yoshizawa, Y., Elbek, B., Herskind, B. and Olesen, M.C., 1966. Nucl. Phys. 86, 471.